CHAPTER

POROSITY

7

7.1 SHRINKAGE POROSITY

There are so many ways to obtain porosity in a casting. Mainly, the porosity in castings seems to be entrained air bubbles, although sometimes is a more uniform dispersion of bifilms partly or fully inflated with a gas from solution in the melt. At other times, what appears to be shrinkage porosity is most often not shrinkage at all, but is a mass of oxides generated by the entrainment of the oxide surface in the turbulence of pouring. Finally some porosity is the result of mould or core blows, or even 'micro-blows' fired into the casting from microscopic pockets of volatile binder trapped in recesses in mould particles.

As should become clear, as a result of founders generally knowing how to feed castings, shrinkage porosity is rather rare in castings. On my travels around the foundries of the world, I rarely see shrinkage problems. Foundry people are aghast to hear such blasphemies because everyone knows that most casting scrap is assigned as 'shrinkage'. This is a mistake; a mis-identification. When viewing regions of apparent shrinkage porosity on a radiograph, I recommend that all foundry people should never say the words 'it is shrinkage' but should learn by heart and always use the phrase 'it *appears* to be shrinkage' adding for good measure 'but probably is not'. The mistaken identity arises from the scrambled mess of oxide bifilms and air bubbles which has a convincing appearance of shrinkage, but is not the result of lack of feeding, but the result of a poor filling technique. Entrainment defects constitute the world's most common foundry defect, perhaps accounting for 80–90% of all scrap.

Nevertheless, we need to discuss shrinkage here to highlight some of the conceptual problems of shrinkage conditions which can lead to reduced or negative pressures that can initiate pores. These concepts are, frankly, complicated to explain. I shall do my best.

7.1.1 GENERAL SHRINKAGE BEHAVIOUR

The molten metal in the furnace occupies considerably more volume than the solidified castings that are eventually produced, giving rise to several problems for the founder. The metal contracts at three quite different rates when cooling from the liquid state to room temperature, as Figure 7.1 illustrates.

1. As the temperature reduces, the first contraction to be experienced is that in the liquid state. This is the normal thermal contraction observed by everyone as a mercury thermometer cools; the volume of the liquid metal reduces almost exactly linearly with falling temperature.
   When making castings, the shrinkage of the liquid metal is usually not troublesome; the extra liquid metal required to compensate for this small reduction in volume is provided without difficulty. It is usually not even noticed, being merely a slight extension to the pouring time if freezing is occurring while the mould is being filled. Alternatively, it is met by a slight fall in level in the feeder.
2. The contraction on solidification is quite another matter, however. This contraction occurs at the freezing point, because (in general) of the greater density of the solid compared with that of the liquid. Contractions associated with freezing for several metals are given in Table 7.1. The contraction causes several problems. These include (1) the requirement for 'feeding', which is defined here as any process that will allow for the compensation

Complete Casting Handbook. http://dx.doi.org/10.1016/B978-0-444-63509-9.00007-8

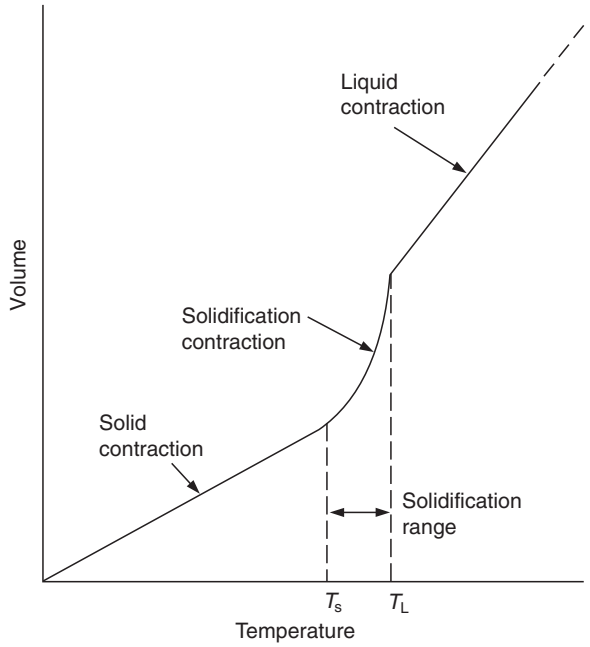

FIGURE 7.1

Schematic illustration of three shrinkage regimes: (i) in the liquid; (ii) during freezing and (iii) in the solid.

of solidification contraction by the movement of either liquid or solid, and (2) 'shrinkage porosity', which is the result of failure of feeding to operate effectively. These issues are dealt with at length in this chapter.

3. The final stages of shrinkage in the solid state can cause a separate series of problems. As cooling progresses, and the solidified casting attempts to reduce its size in consequence, it is rarely free to contract as it wishes. It usually finds itself constrained to some extent either by the mould, or often by other parts of the casting that have solidified and cooled already. These constraints always lead to the casting being somewhat larger than would be expected from free contraction alone. This is because of a certain amount of plastic stretching that the casting necessarily suffers. It leads to difficulties in predicting the size of the pattern because the degree to which the pattern is made oversize (the 'contraction allowance' or 'patternmaker's allowance') is not easy to quantify. The mould constraint during the solid-state contraction can also lead to more localised problems such as hot tearing or cracking of the casting. The conditions for the generation of these defects are discussed in Chapter 8.

7.1.2 SOLIDIFICATION SHRINKAGE

In general, liquids contract on freezing because of the rearrangement of atoms in the liquid structure changes from a rather open 'random close-packed' arrangement to a regular crystalline array of significantly denser packing in the solid.

The densest solids are those that have close-packed (face centred cubic (fcc) and hexagonal close packed (hcp)) symmetry. Thus the greatest values for contraction on solidification are seen for these metals. Table 7.1 shows the contractions to be in the range of 3.2–7.2%. The solidification shrinkage for the less closely packed body-centred cubic (bcc) lattice is in the range 2–3.2%. Other materials that are less dense in the solid state contract by even smaller amounts on freezing.

Table 7.1 Solidification Shrinkage for Some Metals

Metal	Crystal Structure	Melting Point °C	Liquid Density (kgm^{-3})	Solid Density (kgm^{-3})	Volume Change (%)	References
Al	fcc	660	2368	2550	7.14	1
Au	fcc	1063	17,380	18,280	5.47	1
Co	fcc	1495	7750	8180	5.26	1
Cu	fcc	1083	7938	8382	5.30	1
Ni	fcc	1453	7790	8210	5.11	1
Pb	fcc	327	10,665	11,020	3.22	1
Fe	bcc	1536	7035	7265	3.16	1
Li	bcc	181	528	–	2.74	4, 5
Na	bcc	97	927	–	2.6	4, 5
K	bcc	64	827	–	2.54	4, 5
Rb	bcc	303	11,200	–	2.2	2
Cd	hcp	321	7998	–	4.00	2
Mg	hcp	651	1590	1655	4.10	3
Zn	hcp	420	6577	–	4.08	2
Ce	bcc	787	6668	6646	−0.33	1
In	tetrag	156	7017	–	1.98	2
Sn	tetrag	232	6986	7166	2.51	1
Bi	rhomb	271	10,034	9701	−3.32	1
Sb	rhomb	631	6493	6535	0.64	1
Si	diamond	1410	2525	–	−2.9	2

fcc, face centered cubic; bcc, body centered cubic; hcp, hexagonal close packed; tetrag, tetragonal; rhomb, rhombic.
References: 1, Wray (1976); 2, Lucas (quoted by Wray, 1976); 3, This book; 4, Lida and Guthrie (1988); 5, Critical review by J. Campbell in Brandes (1983).

The exceptions to this general pattern are those materials that expand on freezing. These include water, silicon and bismuth (Table 7.1), and, of course, perhaps the most important alloy of all, cast iron.

Remember the ice cubes are always stuck fast, having expanded in the ice tray. Analogously, the success of 'type metal', a bismuth alloy used for casting type for printing, derives some of its ability to take up fine detail required for lettering because of its expansion on freezing. Graphitic cast irons with carbon equivalent above approximately 3.6 (Figure 7.2) similarly expand because of the precipitation of the low-density phase, graphite. The non-feeding requirements of grey irons are in sharp contrast to other cast irons that solidify 'white', i.e. containing the non-equilibrium carbide phase in place of graphite. The white irons in general have solidification contractions similar to those of steels.

For the majority of materials that do contract on freezing, it is important to have a clear idea of what happens in a poorly fed casting. As an ideal case of an unfed casting, it is instructive to consider the freezing of a sphere. We shall assume that the sphere has been fed via an ingate of negligibly small size up to the stage at which a solid shell has formed of thickness x (Figure 7.3). The source of supply of feed metal is then frozen off. Now as solidification continues with the freezing of the following onion layer of thickness dx, the reduced volume occupied by the layer dx compared with that of the original liquid means that either a pore has to form, or the liquid has to expand a little, and the surrounding solid correspondingly has to contract a little. If we assume for the moment that there is no favourable nucleus available for the creation of a pore, then the liquid has to accommodate this by expanding, creating a state of tension, or negative pressure. At the same time, of course, the liquid is in mechanical equilibrium with the enclosing solid shell, effectively sucking it

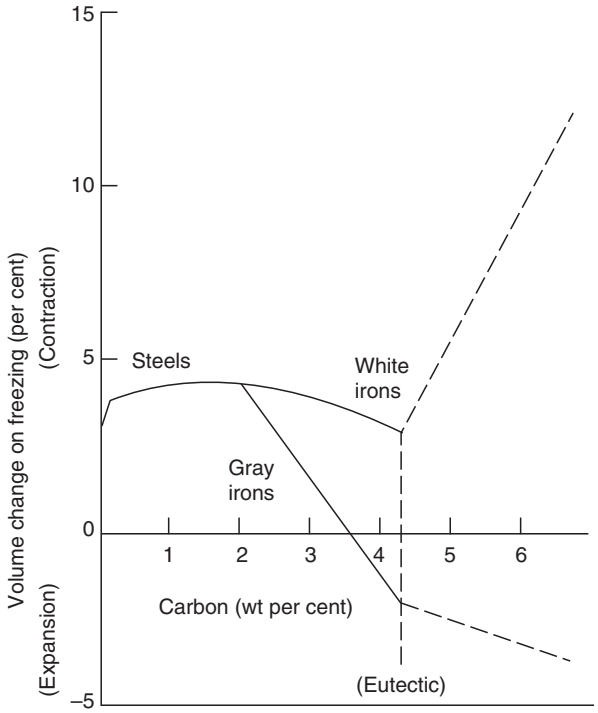

FIGURE 7.2

Volume change on freezing of Fe-C alloys. The relations up to 4.3% carbon are due to Wray (1976); higher carbon values are estimated by the author.

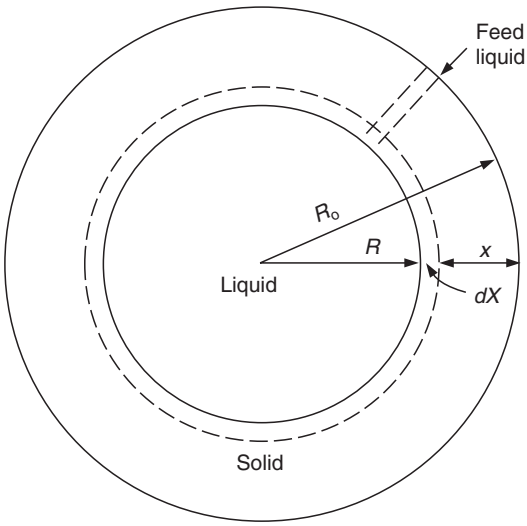

FIGURE 7.3

Solidification model for an unfed sphere.

inwards. As more onion layers form, so the tension in the liquid increases, the liquid expands and the solid shell is drawn inwards, initially suffering only elastic deformation, but as the stress rises, finally suffers inward plastic contraction.

The reader may find the solidifying sphere model easier to visualise by thinking of the exact converse situation of a material that expands on solidification: in this case, the formation of solid squeezes the remaining liquid into a smaller volume. The compressed liquid therefore experiences a positive pressure. The internal positive pressure then clearly acts on the liquid to compress it. In turn, the liquid acts on the solid shell to expand it. It is an instructive exercise to go back and reverse this logic to ensure that the concept of negative pressure, or hydrostatic tension, in the liquid is fully understood before proceeding further with this chapter. However, if the reader finds this challenging, further examples to clarify the concept of negative pressures in liquids are presented in Section 7.1.2.1.

Calculations based on a solidifying sphere model were first carried out by the author (Campbell, 1967, 1968) that show the high tensile stresses in the residual liquid cause the solid to collapse plastically by a creep process. This inward movement of the solid greatly reduces the tension in the liquid, but negative pressures of −100 to −1000 atm (10–100 MPa tensile stress) may be expected under ideal conditions. However, in conditions in which rapid cooling leads to temperature gradients which cause the outside of the casting to shrink, Susumu Oki (1969) estimates that these maximum values can be greatly reduced. Later researchers (Forgac, 1981; Ohsasa et al., 1988) provide further refinements in confirmation of the development of tensile stresses in the residual liquid of a spherical casting. The liquid itself is easily able to withstand such stresses because the tensile strength of liquid metals is in the range of −50,000 to −500,000 atm (5–50 GPa). Incidentally, the liquid–solid interface (whether planar or dendritic is immaterial) is also easily able to withstand the stress, because it is not a favourable site for failure by the nucleation of a cavity (see Section 7.1.5.3).

Even in situations that remain connected to feed metal, it can be shown that the resistance to viscous flow of the residual liquid through a pasty zone can cause the hydrostatic tension to build up, eventually becoming large enough for the casting to collapse by plastic or creep flow. This condition is described more fully later in the sections on inter-dendritic feeding and shrinkage porosity.

Thus, in many casting situations, the pressure in the solidifying metal can fall to low, zero or negative values. The negative values correspond to a hydrostatic stress that powers the formation of shrinkage porosity. However, at the same time, of course, the pressure gradient between the outside and inside of the casting is also the driving force for the various feeding mechanisms that help to reduce porosity.

Whether the driving force for pore formation wins over the driving force for feeding will depend on whether nuclei for pore formation exist. If not (i.e. if the metal is clean), then no pores will nucleate, and feeding is forced to continue until the casting is completely frozen and completely sound. If favourable nuclei are present, then pores will be created at an early stage before the development of any significant hydrostatic stress, with the result that little feeding will occur, and the casting will develop its full percentage of porosity as defined by the physics of the phase change (as given, for instance, in Table 7.1). In most cases, the real situation is somewhere between these extremes, with castings displaying some evidence for partially successful liquid feeding in the form of feeder heads which have drawn down somewhat, and parts of the casting displaying evidence of some solid feeding (Figure 7.4) because of some surface sinks, but the interior exhibiting some porosity. Clearly, in such cases, feeding has continued under increasing pressure differentials until the development of a critical internal stress at which some particular nuclei, or surface puncture, can be activated at one or more points in the casting. Feeding is then stopped at such a locality and pore growth starts.

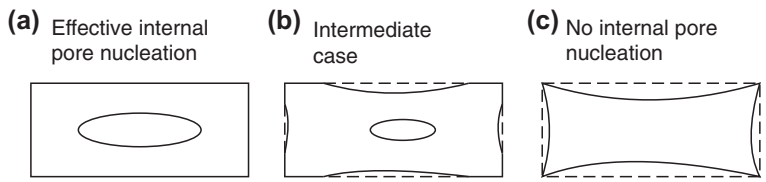

FIGURE 7.4

The three forms of shrinkage porosity: (a) internal; (b) mixed; and (c) external shrinkage porosity.

In those cases in which a pore does form at an early stage of solidification, a freezing contraction of perhaps 3% does not at first sight appear to be of any great significance. However, the reader can easily confirm that in a 100 mm diameter sphere the corresponding cavity will be 31 mm in diameter. For an aluminium casting at 7% contraction, the cavity would be 41 mm in diameter. These considerable cavities require a dedicated effort to ensure that they do not appear in castings. This is especially difficult when it realised that on occasions a substantial casting might be scrapped if it is found to contain a defect of only approximately 1 mm in size. (The scrapping of castings because of the imposition of unreasonably high inspection standards is a widespread injustice that would benefit from the injection of common sense.)

For the vast majority of cast materials, therefore, shrinkage porosity is one of the most important threats to a casting. Paradoxically, this even includes grey cast irons because of the effect of mould dilation. The problem of mould dilation occurs if the mould is weak, allowing the benefits of the expansion of the graphite phase to be wasted on outwards expansion of the casting, rather than being used on inwards compression of cavities.

The serious consequences of the porosity occurring on the inside of the casting, where it causes a disproportionally large hole, contrasts with the occurrence of porosity on the outside of the casting. If our 100 mm diameter sphere had a common solidification contraction in the region of 3% and had no internal nuclei for the initiation of porosity, no pores would form here and the solid would therefore be forced to collapse. The final casting would be slightly smaller by approximately 0.5 mm over its whole surface. This 1% reduction in diameter is sufficiently small to be not noticeable in most situations. If it were to be important for a casting requiring special accuracy, this small adjustment could be added to the patternmaker's shrinkage allowance. Thus the elimination of internal porosity and its displacement to the outside of the casting is a powerful technique that is strongly recommended.

Although shrinkage porosity can be reduced by improvements to the cleanness of the metal as mentioned previously, this chapter deals later with the other major approach to this problem, the design and provision of good feeding, ensuring good conditions for easy accommodation of the volume change during freezing. The special case of provision of good liquid feeding, the usual way to deal with a feeding problem, is dealt with as a 'methoding' issue in Chapter 10 rule 6 'Avoid shrinkage porosity'.

In the meantime, understanding negative pressure (hydrostatic tension) in castings is sufficiently critical to an appreciation of casting behaviour that it will be valuable to divert to discuss examples before proceeding further.

7.1.2.1 Hydrostatic tensions in liquids

In the original book 'Castings 1991', this section was to have been an appendix. However, it proved to be so interesting and so central to the understanding of defect generation in castings that the subject was included as part of the main text. The reader will understand why the subject is included here even though few of the examples described in this section are metal castings. Most relate to water or other organic systems but the principles will be seen to apply perfectly to metals.

Liquids have been known to be able to withstand tension for many years. Mercury is an interesting case. In a clean glass barometer freshly filled with clean mercury, the liquid would adhere to the glass, 'hanging up', supporting the weight of the long length of the heavy liquid like a rope in tension. If the glass was tapped sharply, breaking the liquid away from the glass, the liquid would fall, opening up a vacuum above it. It would settle at the height at which it could be supported by the pressure of 1 atm acting at its base. This height is approximately 760 mm: the barometric height. The so-called vacuum is of course not perfect. A tiny pressure from the vapour pressure of mercury would operate, pushing the upper surface down about 1 μm at room temperature which we shall ignore. Actually, if the glass and the metal had been really clean, in principle the mercury column could have hung from a height somewhere in the stratosphere, because the tensile strength of the liquid is extremely high.

The very high tensile strengths of liquid metals should not be a surprise. The interatomic distances in liquid metals, as random close-packed atomic structures, are only a few percent larger than the distances in solid metals, which have more regular close-packed structures. Thus the strengths would be expected to be similar, which is the case.

In 1850, Berthelot cooled various organic liquids in sealed glass tubes, watching until cavitation occurred as a shower of small bubbles. The number of bubbles was subsequently explained by Lewis (1961), who observed that the rupture was always associated with the sudden appearance and collapse of a single bubble, which was immediately followed by the formation of a large number of tiny bubbles along the length of the tube. The asymmetric collapse of the primary bubble would form an impacting jet and create a series of shock waves. These would be ideal conditions for the formation

of additional bubbles. This simple experiment is of special interest because it is analogous to the solidifying casting, with the internal solidifying liquid progressively occupying less volume, and with the surrounding solid gradually being pulled inwards, its elastic and plastic resistance to deformation steadily increasing, building up the tensile stress in the liquid, to the point at which the liquid fractures.

Berthelot's experiment has been repeated many times in different ways. For instance, Vincent and Simmons (1943) sealed their tube by freezing the liquid in the mouth of the capillary. They found that water would withstand −157 atm and a mineral oil would withstand −119 atm. This is a fascinating observation because it indicates that the freezing interface will withstand high tensions; it is not necessarily a good nucleation site for pores, as has been confirmed theoretically (Section 7.1.5). The facts reveal the error of those assumptions, widely presumed in the solidification literature, of ease of pore nucleation at the solidification front.

For a liquid sealed in a tube, Scott et al. (1948) calculated the build-up of tensile stress ΔP as the liquid cools an amount ΔT, using the coefficient of thermal expansion of the liquid α and the glass σ, together with the modulus of rigidity G and the coefficient of compressibility β of the glass tube:

$$\Delta P = [(\alpha - \sigma)/(\beta - (1/G))]\Delta T$$

They also checked their results by measuring the length of the liquid columns after fracture. This work emphasises the elastic strains built up in the liquid and the surrounding solid during the experiment.

Lewis (1961) found tensile strengths in water and carbon tetrachloride in excess of −60 atm. Also, when water and carbon tetrachloride were introduced into the same tube, the two liquids separated at a clear interface. Fracture was not observed to occur at the interface. The liquid–liquid interface seems as poor a nucleation site as the liquid–solid interface discussed previously. These observations confirm the expectations from classical nucleation theory as presented in Section 7.1.5.

Tyndall (1872) carried out experiments on the internal melting of ice by shining light through the ice. The light was absorbed by particles frozen inside. The heated particles then melted a small surrounding region of the shape of a snowflake (known now as a Tyndall figure, or, occasionally, a negative crystal). However, because ice reduces in volume on melting, the liquid volume created in this way was under tension. As melting progressed, the tensile stress became so great that the liquid fractured with an audible click. The melted region was then observed to contain a small bubble. Kaiser (1966) demonstrated that the critical pressure for fracture was in excess of −150 atm. Tyndall proved that the bubble was a vapour cavity containing practically no air by carefully melting the ice towards the figure using warm water. As soon as a link was established with the bubble, it collapsed and disappeared; no air bubble rose to the surface. The Tyndall figures are analogous to the isolated regions of metal castings, where vapour cavities are expected to be formed at critical stresses during solidification.

Briggs (1950) centrifuged water in a capillary tube, spinning it at increasing speed to stretch the water until it was observed to snap at a tensile stress of −280 atm.

The early work on the determination of the tensile strengths of liquids held in various containers such as a Berthelot tube gave notoriously scattered results. This was probably to be expected from the different degrees of cleanness of the container, and any microscopic imperfections it may have had on its walls. Experiments to test the liquid away from the influence of walls have been carried out using ultrasonic waves focused in the centre of a volume of liquid. The rarefaction (tensile) half of the vibration cycle can cause cavitation in the liquid. These experiments have been moderately successful in increasing the limits, but impurities in the liquid have tended to obscure results.

More recently, Carlson (1975) has reflected shock waves through a thin film of mercury and recorded strengths of up to −30,000 atm. This result is one of the first to give a strength value of the same order as that predicted by various theoretical approaches. Despite the dynamic nature of the test method, the result is not particularly sensitive to the length of the duration of the stress (varying only from −25,000 to −30,000 atm as the time decreased from 1 s to 10^{-7} s). This again is to be expected because nucleation is a process involving the rearrangement of atoms, where the atoms are vibrating about their mean positions at a rate of approximately 10^{13} times per second.

An attempt to measure negative pressures in solidifying aluminium ingots directly was made by Ohsasa et al. (1988a,b). They immersed a stainless steel disc into the top of a solidifying metal to almost fill the top of the crucible in which the metal was held. When the solidification front reached the disc, a volume of liquid was effectively trapped

Table 7.2 Fracture Pressures of Liquids

Liquid	Surface Tension, Nm^{-1}	Atom Diameter, nm	ΔP From Eqn (7.6) GPa	ΔP From Eqn (7.6) atm	ΔP From Fisher GPa	ΔP From Fisher atm	Critical Embryo (No. of Vacancies)	ΔP Complex Inclusion MPa	ΔP Complex Inclusion atm
Water	0.072	–	–	–	0.13	1320	–	1.6	16
Mercury	0.5	0.30	1.67	16,700	2.23	22,300	14	20	200
Aluminium	0.9	0.29	3.10	31,000	3.00	30,000	52	36	360
Copper	1.3	0.26	5.00	50,000	5.00	50,000	72	60	600
Iron	1.9	0.25	7.6	76,000	7.00	70,000	72	85	850

underneath. As this volume solidified, the stress in the liquid was measured by a transducer connected to the disc. Stresses needed to cause pore formation were typically only about −0.1 atm. However, occasionally stresses of up to −2.5 atm were recorded. On these occasions, the walls of the ingot were observed to suffer some inward collapse. Clearly, in this work, the stresses were limited by the nucleation of cavities against the surface of the stainless steel disc. This would be poorly wetted as a result of the presence of the Cr-rich oxide on the steel. At the higher stresses that were measured, these were in turn limited by the inward plastic collapse of the solidified casting.

In general, therefore, it seems that the various attempts to measure the strengths of mercury and the organic liquids have achieved results intermediate between the minimum predicted for a complex inclusion (potentially the weakest point in a liquid metal as explained in Section 7.1.5.3) and the maximum set for the prediction of homogeneous nucleation (Table 7.2). This is probably as good a result as can be expected. However, the one high result by Carlson is reassuring, suggesting that the physics seems basically correct, and really does apply to liquid metals.

7.1.3 FEEDING CRITERIA

Because the first half of this book is concerned with the metallurgy of cast metals, the practical aspects of feeding is taken up later, becoming an important feature from Chapter 10 onwards. However, it is desirable to indicate some central concepts, and some small amount of repetition will do no harm.

To allow for the fact that extra metal needs to be fed to the solidifying casting to compensate for the contraction on freezing, it is normal to provide a separate reservoir of metal. We shall call this reservoir a *feeder* because its action is to *feed* the casting (i.e. to compensate for the solidification shrinkage). The American term *riser* is not recommended. It is not descriptive in a helpful way and could lead to confusion with other features of the *rigging* such as vents, up which metal also rises. However, the American term *rigging* is helpful. It is a general word for the various appendages of runners, gates and feeders etc. No equivalent term exists in UK English.

The provision of a feeder can be complicated to get right. There are seven rules that the author has used to help in the systematic approach to a solution. Readers of the book 'Castings 1991' will note this is one more rule than before. The additional rule was cited in 'Castings' but not elevated to the status of a rule. The reader will appreciate that the new Rule 1 'Do not feed' has a valuable place in the new listing. Chapter 10, Section 6.4, explains that the rule is not as perverse as it first seems.

More recently, Tiryakioglu (2001) has further simplified the Seven Rules as is noted in at the end of this section, but is described in more detail in Chapter 10, Section 6.5.

7.1.3.1 The seven feeding rules

Rule 1. The main question relating to the provision of a feeder on a casting is 'Should we have a feeder at all?' This is a question well worth asking, and constitutes Rule 1 '*Do not feed (unless absolutely necessary)*'.

The avoidance of feeding is to be greatly encouraged, in contrast to the teaching in most traditional foundry texts. There are several reasons to avoid the placing of feeders on castings. The obvious one is cost. Feeders cost money to put on and money to take off. In addition, many castings are actually impaired by the inappropriate placing of a feeder. This is especially true for thin-walled castings, where the filling of the feeder diverts metal from the filling of the casting, with the creation of a misrun casting. Probably half of the small and medium-sized Al alloy castings made today do not need to be fed. Sometimes the casting suffers delayed cooling, impaired properties and even segregation problems as a result of the presence of a feeder. Finally, it is easy to make an error in the estimation of the appropriate feeder size, with the result that the casting can be more defective than if no feeder were used at all.

However, there is one potential major problem if a feeder is not used, but where a feeding problem remains in the casting. The feeding problem will show itself as a region of reduced pressure in the casting at a late stage of freezing. The reduced pressure will act to open bifilms as in the reduced pressure test (RPT) used for nonferrous alloys. Thus in an aluminium alloy casting with medium thickness sections, enhanced size and number of internal microshrinkage pores will be experienced if the sections are unfed. Whether this is important or not depends on the specification of microstructure and properties that the casting is required to meet. If the casting is required to have good elongation properties in a tensile test it is likely that feeding to maintain pressure during solidification (and thus keep the bifilms closed) will be needed to achieve this.

Just for the moment, we shall assume that a feeder is required. The next question is 'How large should it be?'

There is of course an optimum size. Figure 7.5 shows the results of Rao et al. (1975), who investigated an increasing feeder size on the feeding of a plate casting in the Al-12Si alloy. Interestingly, when the data are extrapolated to zero feeder size, the porosity is indicated to be approximately 8%, which is close to the theoretical 7.14% solidification

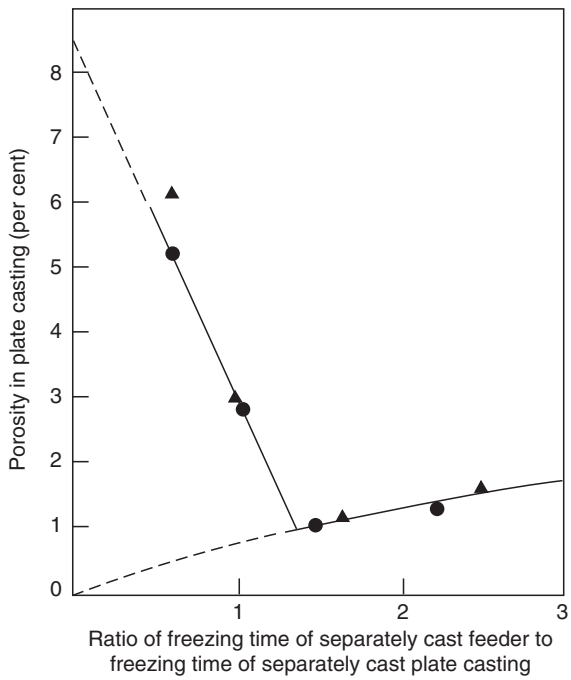

FIGURE 7.5

Effect of increasing feeder solidification time on the soundness of a plate casting in Al-12Si alloy.

Data from Rao et al. (1975).

shrinkage for pure aluminium (Table 7.1). At a feeder modulus of around 1.2 times the modulus of the casting, the casting is at its most sound. The residual 1% porosity is probably dispersed gas porosity. As the feeder size is increased, further the solidification of the casting is now progressively delayed by the nearby mass of metal in the feeder. Thus, although this excessive feeder is no disadvantage in itself, the delay to solidification of the whole casting increases the time available for further precipitation of hydrogen as gas porosity and the unfolding of bifilms. However, it is clear from this work that an undersized feeder will result in very serious porosity, whilst an oversize feeder causes less of a problem. Considering the economics, a slightly oversize feeder may be a good investment to reduce the threat of the total loss of the casting because of porosity.

The previous work illustrates that it is more important to deal with the shrinkage problems than with gas problems in castings. (This conclusion might raise the eyebrows of practised foundry people. It needs to be kept in mind that most of what previously has been generally described as 'gas' in castings has actually been turbulently entrained *air bubbles* introduced by our poor filling systems. In general, good eyesight is needed to see true gas porosity. We shall deal with entrained air bubbles by the provision of non-entraining filling system designs.)

There is a vast amount of literature on the subject of providing adequate-sized feeders for the feeding of castings. It is mainly concerned with two feeding rules. Numbering onwards from Rule 1 mentioned previously, the conventional rules are as follows.

Rule 2. The feeder must solidify at the same time as, or later than, the casting. This is the heat-transfer criterion, attributed to Chvorinov.

Rule 3. The feeder must contain sufficient liquid to meet the volume-contraction requirements of the casting. This is usually known as the volume criterion.

However, there are additional rules which are also often overlooked, but which define additional thermal, geometrical and pressure criteria that are absolutely necessary conditions for the casting to freeze soundly:

Rule 4. The junction between the casting and the feeder should not create a hot spot, i.e. have a freezing time greater than either the feeder or the casting. This is a problem that, if not avoided, leads to '*underfeeder shrinkage porosity*'. The junction problem is a widely overlooked requirement. The use of Chvorinov's equation systematically gives the wrong answer for this reason, so the junction requirement is often found to override Chvorinov (Rule 2).

Rule 5. There must be a path to allow feed metal to reach those regions that require it. The reader can see why this criterion has been often overlooked as a separate rule; the communication criterion appears self-evident! It is, nevertheless, often violated.

Rule 6. There must be sufficient pressure differential to cause the feed material to flow, and the flow needs to be in the correct direction, towards the region requiring the additional liquid (no apologies for spelling out the glaringly obvious—it is surprising how often these rules are broken and the casting scrapped).

Rule 7. There must be sufficient pressure at all points in the casting to suppress the formation and growth of porosity. In Section 9, we shall see that the action of pressure also retains the good mechanical properties of the casting by suppressing the opening of bifilms. The bifilms often constitute a low background level of porosity (that may or may not be just visible) that is highly effective in reducing strength and ductility of castings.

It is essential to understand that *all* the rules must be fulfilled if truly sound castings are to be produced. The reader must not underestimate the scale of this problem. The breaking of only one of the rules may result in ineffective feeding, and a porous casting. The wide prevalence of porosity in castings is a sobering reminder that solutions are often not straightforward.

Because the calculation of the optimum feeder size is therefore so fraught with complications, is dangerous if calculated wrongly, and costs money and effort, the casting engineer is strongly recommended to consider whether a feeder is really necessary at all. This is Rule 1. You can see how valuable it is.

Of the remainder of castings that do suffer feeding demand, many could avoid the use of a feeder by the judicious application of chills and/or cooling fins or pins.

This leaves only those castings that have heavy sections, isolated heavy bosses or other features that *do* need to be fed with the correct size of feeder.

Finally, in a recent development of the concepts of feeding, it is worth drawing attention to the work of Tiryakioglu (2001). He has demonstrated that Rules 2, 3 and 4 can be gathered together under only one new criterion 'The thermal

centre of the total casting (i.e. the casting + feeder combination) should be in the feeder'. This deceptively straightforward statement has been shown to allow the calculation of optimum feeders with unprecedented accuracy. Discussion of this approach is detailed in Chapter 10 under Casting Rule 6.

7.1.3.2 Criteria functions

The development of computer software to predict the solidification of castings is not yet developed to predict the occurrence of porosity from first principles, i.e. calculating the pressure drop in the various parts of the casting, and thereby assessing the potential for nucleation and growth of cavities. This represents a Herculean task. As a useful shortcut, therefore, many workers have searched for parameters that can be relatively easily calculated and enable an assessment of the potential for pore formation.

Niyama et al. (1982) was perhaps the first to develop a useful criterion function. Dantzig and Rappaz (2009) give a rigorous and elegant account of his derivation. Based on a simple model assuming Darcy's law for the flow of residual liquid through the dendrite mesh, he proposed the parameter $G/R^{1/2}$ to assess the difficulty of providing feed liquid, where G is the temperature gradient at the solidus temperature and R the cooling rate. This is probably the most widely used criteria function. It has been found useful to predict the propensity for porosity in steels, often in the form assuming that porosity will occur when $G/R^{1/2}$ falls below some critical value in the region of 1 $K^{1/2}min^{1/2}cm^{-1}$. These awful units of the critical Niyama criterion (quoted shamelessly by Dantzig and Rappaz) translate with sufficient accuracy into the respectable SI equivalent 1 $K^{1/2}s^{1/2}mm^{-1}$ (for the purist 1.00 $K^{1/2}s^{1/2}mm^{-1}$ = 1.29 $K^{1/2}min^{1/2}cm^{-1}$).

In their study of the formation of porosity in steel plates of thickness 5–50 mm, with and without end chills, Minakawa et al. (1985) confirmed that usefulness of the Niyama criterion in assessing the conditions for the onset of porosity in their castings. They also looked at G the temperature gradient along the centreline of the casting at the solidification front, and the fraction solid along the centreline. Neither of these alone was satisfactory.

In another theoretical study, Hansen and Sahm (1988) support the usefulness of $G/V_S^{1/2}$ for steel castings. However, in addition they go on to argue the case for the use of a more complex function $G/V_S^{1/4}V_L^{1/2}$ where V_L is the velocity of flow of the residual liquid. They proposed this relation because they noticed that the velocity of flow in bars was 5 to 10 times the velocity in plates of the same thickness which, they suggest, contributes to the additional feeding difficulty of bars compared with plates. (A further contributor will be the comparatively high resistance to the plastic collapse of bars, compared with the efficiency of solid feeding in plates as will be discussed later.)

They found that $G/V_S^{1/4}V_L^{1/2}$ is less than a critical value, which for steel plates and bars is approximately 1 $Ks^{3/4}$ $mm^{-7/4}$. Their parameter is, of course, less easy to use than that of Niyama because it needs flow velocities. The Niyama approach only requires data obtainable from temperature measurement in the casting.

Carlson and Beckermann (2010) proposed a dimensionless form of the Niyama criterion (especially useful in view of the difficult units $K^{1/2}s^{1/2}mm^{-1}$) and find it to be useful for predicting shrinkage porosity in a steel, an Al alloy and a Mg alloy, demonstrating impressively wide applicability.

Unfortunately, however, there are many limitations of most of the other criteria functions that are widely overlooked. They include the following.

1. Strictly, they assess only the difficulty of interdendritic feeding.
2. They apply best to strong materials such as steels in relatively cold moulds. Here, interdendritic feeding can become impossibly difficult, generating high internal tension in the casting, a condition that the computer would interpret as leading to porosity. However, in conditions in which the solid is softer and can yield plastically, the mould can collapse slightly to give an internally sound casting. Such conditions apply, for instance, in steels cast into hot investment moulds and light alloys in cold moulds where significant solid feeding can occur, causing the criteria function to become inaccurate.
3. Criteria functions cannot predict conditions for porosity arising as a result of the many other mechanisms for the production of porosity in castings. These include the major shrinkage pores as a result of the isolation of major liquid regions, the creation of surface-initiated porosity and the mechanically entrained porosity originating from bubbles of air and mould gases introduced by poor filling systems. Experience shows that in general entrainment defects cause most of the porosity found in casting. Shrinkage porosity is actually quite rare because, as we have

noted previously, founders understand shrinkage and can avoid it. In fact, the ability to avoid shrinkage problems is continuously improving at this time because of the continuous development of prediction using computer models.

4. Sigworth et al. (1994) point out an obvious but often overlooked limitation of criteria functions that they cannot take account of the important effects of melt treatment, such as, in particular, its bifilm content.

7.1.4 FEEDING: THE FIVE MECHANISMS

During the solidification of a casting, the gradual spread and growth of the solid, often in the form of a tangled mass of dendrites, presents increasing difficulties for the passage of feeding liquid. In fact, as the freezing liquid contracts to form the solid, the pressure in the liquid falls, causing an increasing pressure difference between the inside and the outside of the casting. The internal pressure might actually fall far enough to become negative, as a hydrostatic tension.

The generation of reduced pressure, and even actual hydrostatic tension, is undesirable in castings. Such phenomena provide the driving force for the unfurling and inflation of bifilms, leading to reduced properties and the initiation and growth of volume defects such as porosity. Where internal defects do not open up, the reduced pressure can lead to surface sinks on castings.

There appear to be at least five mechanisms by which hydrostatic tension can be reduced in a solidifying material, although, of course, not all five processes are likely to operate in any single case. Adequate feeding by one or more of these feeding processes will relieve the stress in the solidifying liquid and thus reduce the possibility of the formation of defects.

I first identified and described the five feeding mechanisms as set out in Figure 7.27 in 1969. Since then, I see my drawing everywhere (I could draw better when I was young). In the original publication, solid-state diffusion was added as a sixth effect that would cause pore shape to change somewhat after solidification was complete. Shape changes in pores would occur because the forces of surface tension and mechanical stress are sufficient to cause material flow at temperatures near the melting point of the solid. Such changes to the pore shape and size are detectable under a microscope. However, these considerations are the reserve of the research scientist, and reflect the author's early interests, having been trained as a physicist. Nowadays, as a somewhat more practical foundryman trying to make good castings, the first five mechanisms are all that matter.

The mechanisms are dealt with in the order in which they might occur during freezing. The order coincides with a progressive but ill-defined transition from what might usefully be termed 'open' to 'closed' feeding systems.

7.1.4.1 Liquid feeding

Liquid feeding is the most 'open' feeding mechanism and generally precedes other forms of feeding (Figure 7.6). It should be noted that in skin-freezing materials it is normally the only method of feeding. The liquid has low viscosity, and for most of the freezing process the feed path is wide, so that the pressure difference required to cause the process to operate is negligibly small. Results of theoretical model of a small cylindrical casting 20 mm diameter (Figure 7.7) indicate that pressures of the order of only 1 Pa are generated in the early stages. By the time the 10 mm radius casting has a liquid core of radius 1 mm, corresponding to 99% solid, the pressure difference has increased only to 100 Pa which is approximately one-thousandth of an atmosphere and smaller than about one-tenth of the hydrostatic pressure due to depth. (It is worth emphasising that the theoretical model represented in Figure 7.7 and elsewhere in this book represents a worst case. This is because the temperature gradient in the solidified shell has been neglected. The lower temperature of the outer layers of the shell will cause the shell to contract, compressing the internal layers of the casting and thus reducing the internal hydrostatic tension. In some cases, the effect is so large that the internal pressure can become positive, as shown in the excellent treatment by Forgac et al., 1979.)

For all practical purposes, therefore, liquid feeding occurs at pressure gradients that are so low that these gentle stresses will never lead to problems.

The rules for adequate liquid feeding are the seven feeding rules listed in Section 7.1.3.

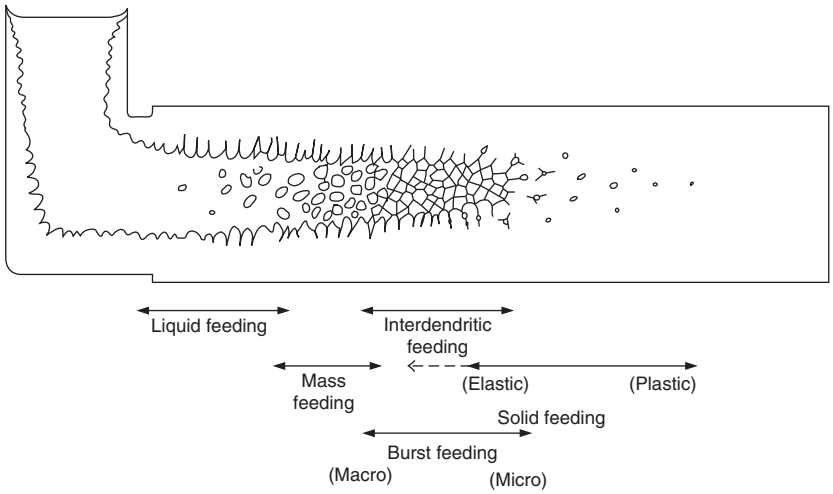

FIGURE 7.6

Schematic representation of the five feeding mechanisms in a solidifying casting (Campbell, 1969a,b).

Inadequate liquid feeding is often seen to occur when the feeder has inadequate volume. Thus liquid flow from the feeder terminates early, and subsequently only air is drawn into the casting. Depending on the mode of solidification of the casting, the resulting porosity can take two forms:

1. Skin-freezing alloys will have a smooth solidification front that will therefore result in a smooth shrinkage pipe extending from the feeder into the castings as a long funnel-shaped hole. In very short freezing range metals, the surface of the pipe can be as smooth and silvery as a mirror.
2. Long freezing range alloys will be filled with a mesh of dendrites in a sea of residual liquid. In this case liquid feeding effectively becomes interdendritic feeding, of course. In the case of an inadequate supply of liquid in the feeder, the liquid level falls, draining out to feed more distant regions of the casting, and sucking in air to replace it. The progressively falling level of liquid will define the spread of the porosity, decreasing as it advances because of the decreasing volume fraction of residual liquid as freezing proceeds. The resulting effect is that of a partially drained sponge, as shown in the tin bronze casting in Figure 7.8. Sponge porosity is a good name for this defect.

When sectioned, the porosity resembles a mass of separate pores in regions separated by dendrites. It is therefore often mistaken for isolated interdendritic porosity. However, it is, of course, only another form of a primary shrinkage pipe, practically every part of which is connected to the atmosphere through the feeder. It is a particularly injurious form of porosity in castings that are required to be leak-tight, especially because it can be extensive throughout the casting, as Figure 7.8 illustrates. Furthermore this type of porosity is commonly found. It is an indictment of our feeding practice.

The author recalls an investigation into the nature of the porosity in the centre of a balanced steel ingot. To ascertain whether the so-called secondary porosity was connected to the atmosphere via the shrinkage cavity in the top of the ingot, water was poured onto the top of the ingot. It created a never-forgotten drenching from the shower that issued from the so-called secondary pores. The lesson that the pores were perfectly well connected was not forgotten.

7.1.4.2 Mass feeding

Mass feeding is the term coined by Baker (1945) to denote the movement of a slurry of solidified metal and residual liquid. This movement is arrested when the volume fraction of solid reaches anywhere between 0 and 50%, depending on

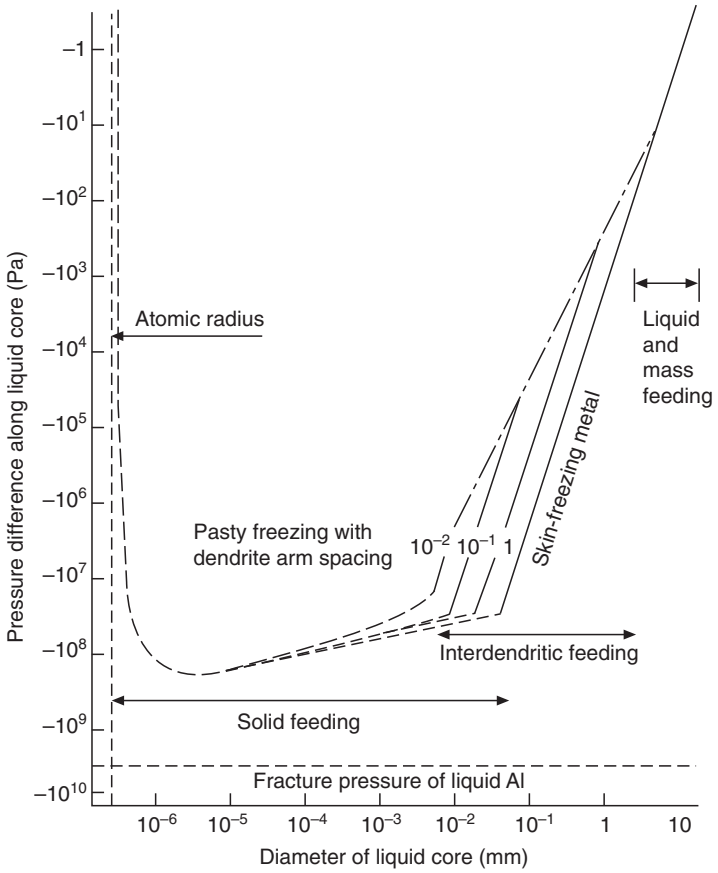

FIGURE 7.7

Hydrostatic tensions in the residual liquid calculated for the various feeding regimes during the freezing of a 20 mm diameter aluminium alloy cylinder (Campbell, 1969a,b).

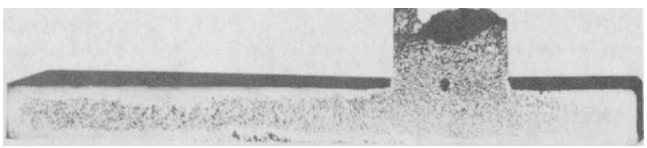

FIGURE 7.8

Porosity in the long freezing range alloy Cu-10Sn bronze, cast with an inadequate feeder, resulting in a spongy shrinkage pipe.

the pressure differential driving the flow, and depending on what percentage of dendrites are free from points of attachment to the wall of the casting. However, it seems that smaller amounts of movement can continue to occur up to about 68% solid which is the level at which the dendrites start to become a coherent network, like a plastic three-dimensional space frame (Campbell, 1969a,b).

In thin sections, where there may be only two or three grains across the wall section, mass feeding will not be able to occur. The grains are pinned in place by their contacts with the wall. However, as the number of grains across the section increases to between 5 and 10, the central grains are definitely free to move to some extent. In larger sections, or where grains have been refined, there may be 20 to 100 grains or more, so that the flow of the slurry can become an important mechanism to reduce pressure differential along the flow direction. Clearly, the important criterion to assess whether mass flow will occur is the ratio (casting section thickness)/(average grain diameter). This is probably one of the main reasons why grain refinement is useful in reducing porosity in castings (other important reasons being the greater dispersion of gases in solution, their reduced segregation, and the cleaning effect resulting from the sedimentation of bifilms if the grain refiner addition is correctly carried out in the ladle and allowed to settle).

(In passing, we may note that in some instances mass feeding may cause difficulties. There is some evidence that the flow of the liquid/solid mass into the entrance of a narrow section can lead to the premature blocking of the entrance with the solid phase. Thus the feed path to more distant regions of the casting may become choked.)

As mass feeding progresses, the point at which the grains finally impinge strongly and stop is the point at which feeding starts to become appreciably more difficult. This is the regime of the next feeding mechanism, interdendritic feeding.

7.1.4.3 Interdendritic feeding

Allen (1932) was one of the first to use the term 'interdendritic feeding' to describe the flow of residual liquid through the pasty zone. He also made the first serious attempt to provide a quantitative theory. However, we can obtain an improved estimate of the pressure gradient involved simply by use of the famous equation by Poisseuille that describes the pressure gradient dP/dx required to cause a fluid to flow along a capillary:

$$\frac{dP}{dx} = \frac{8v\eta}{\pi R^4} \tag{7.1}$$

where v is the volume flowing per second, η is the viscosity and R is the radius of the capillary. It is clear without going further that the resistance to flow is critically dependent on the size of the capillary. For a bunch of N capillaries which we can take as a rough model of the pasty zone, the pressure gradient is correspondingly reduced:

$$\frac{dP}{dx} = \frac{8v\eta}{\pi R^4 N} \tag{7.2}$$

For the sake of completeness, it is worth developing this relation to evaluate a more realistic channel that includes the effect of simultaneous solidification so as to close the channel by slow degrees. The treatment is based on that by Piwonka and Flemings (1966) (Figure 7.9). Given that the average velocity V is $v/\pi R^2$, and, by conservation of volume, equating the volume flow through element dx with the volume deficit as a result of solidification on the surface of the tube beyond element dx, we have, all in unit time:

$$\pi R^2 V = 2\pi R(L - x)\left(\frac{\alpha}{1 - \alpha}\right)\frac{dR}{dt} \tag{7.3}$$

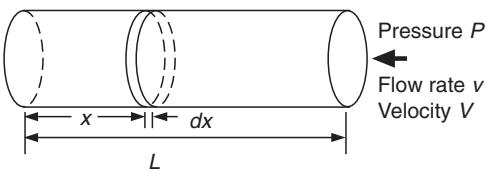

FIGURE 7.9

A tube of liquid, solidifying inwards, whilst being fed with extra liquid from the right.

By substituting and integrating, it follows directly that:

$$\Delta P = \frac{16\eta}{N}\left(\frac{\alpha}{1-\alpha}\right)\frac{dR}{dt}\cdot\frac{1}{R^3}\left(Lx - \frac{x^2}{2}\right) \tag{7.4}$$

We can find the maximum pressure drop ΔP at the far end of the pasty zone by substituting $x = 0$. At the same time, we can substitute the relation for freezing rate used by Piwonka and Flemings, $dR/dt = -4\lambda^2/R$ approximately, where λ is their heat-flow constant. Also using the relation $Nd^2 = D^2$ where d is the dendrite arm spacing and D^2 is the area of the pasty zone of interest, we obtain at last:

$$\Delta P = 32\eta\left(\frac{\alpha}{1-\alpha}\right)\frac{\lambda^2 L^2 d^2}{R^4 D^2} \tag{7.5}$$

This final solution reveals that the pressure drop by viscous flow through the pasty zone is controlled by several important factors such as viscosity, solidification shrinkage, the rate of freezing, the dendrite arm spacing and the length of the pasty zone. However, in confirmation of our original conclusion, the pressure drop is most sensitive to the size of the flow channels.

Additional refinements to this equation, such as the inclusion of a tortuosity factor to allow for the non-straightness of the flow do not affect the result significantly. However, more recent improvements have resulted in an allowance for the different resistance to flow depending on whether the flow direction is aligned with or across the main dendrite stems (Poirier, 1987).

The overriding effect of the radius of the flow channel leads to ΔP becoming extremely high as R diminishes. In fact, in the absence of nuclei that would allow pore formation to release the stress, the high hydrostatic stress near the end of freezing will be limited by the inward collapse of the solidified outer parts of the casting, as indicated in Figure 7.7. This plastic flow of the solid denotes the onset of 'solid feeding', the last of the feeding mechanisms. The natural progression of interdendritic feeding followed by solid feeding is confirmed by more recent models (Ohsasa et al., 1988a,b).

Effect of eutectic presence

The rapid increase of stress as R becomes very small explains the profound effect of a small percentage of eutectic in reducing the stress by orders of magnitude (Campbell, 1969a,b). This is because the eutectic freezes at a specific temperature, and the progress of this specific isothermal plane through the mesh corresponds to a specific planar freezing front for the eutectic. The front occurs ahead of the roots of the dendrites, so that the interdendritic flow paths no longer continue to taper to zero, but finish, abruptly truncated as shown in Figure 7.10. Thus the part of the dendrite mesh most difficult to feed is eliminated.

Larger amounts of eutectic liquid in the alloy reduce ΔP even further, because of the increased size of channel at the point of final solidification. As the percentage eutectic increases towards 100%, the alloy feeds only by liquid feeding, of course, which makes such materials easy to feed to complete soundness.

Because most long freezing range alloys exhibit poor pressure tightness, the use of the extremely long freezing range alloy 85Cu-5Sn-5Zn-5Pb for valves and pipe fittings seems inexplicable. However, the 5% lead is practically insoluble in the remainder of the alloy, and thus freezes as practically pure lead at 326°C, considerably easing feeding by acting analogously to a eutectic, as discussed previously.

The appearance of non-equilibrium eutectic in pure Fe-C alloys is predicted to be rather close to the equilibrium condition of 2%C (Clyne and Kurz, 1981) because carbon is an interstitial atom in iron, and therefore diffuses rapidly, reducing the effect of segregation during freezing. However, in the presence of carbide-stabilising alloys such as manganese, the segregation of carbon is enhanced to some extent, causing eutectic to appear not at the equilibrium 2%C but probably only somewhere near 1.0%C as seen in Figure 5.41. A similar result for 1%C1.5%Cr steels is shown in Figure 5.42.

In Al-Mg alloys, layer porosity is observed in increasing amounts as magnesium is increased, illustrating the growing problem of interdendritic feeding as the freezing range increases. However, at a critical composition close to 10.5%Mg, the eutectic beta-phase is first seen in the microstructure and the porosity suddenly disappears (Jay and Cibula, 1956).

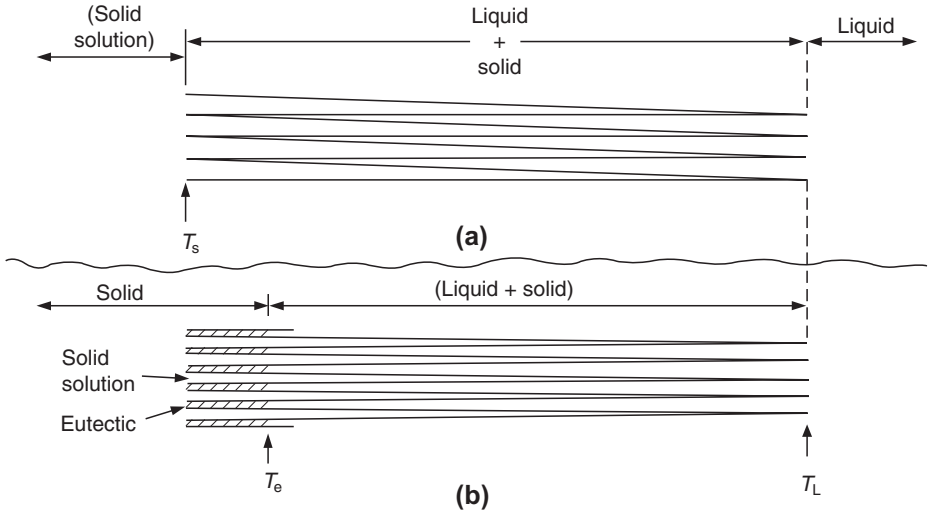

FIGURE 7.10

A diagrammatic illustration of (a) how the tapering interdendritic path increases the difficulty of the final stage of interdendritic feeding and (b) how a small percentage of eutectic will eliminate this final and narrowest portion of the path, thereby greatly easing the last stages of feeding.

The arrival of eutectic at 10.5%Mg confirms the non-equilibrium conditions and compares with the prediction of 17.5%Mg for equilibrium conditions. Lagowski and Meier (1964) found a similar critical transition in Mg-Zn alloys as zinc is progressively increased. Their results are presented in Figure 9.6.

However, one of the most spectacular displays of segregation of a solute element in a common alloy system is that of copper in aluminium. In the equilibrium condition, eutectic would not appear unless the copper content exceeded 5.7%. However, in experimental castings of increasing copper content, eutectic has been found to occur at concentrations in the 0.25–0.5%Cu range. This concentration corresponds to a peak in porosity, and the predicted peak in hydrostatic tension in the pasty zone (Figure 7.11).

Many property–composition curves are of the cuspoid, sharp peaked type (note that they are not merely a rounded, hump-like maximum). Examples are to be found throughout the foundry research literature (although the results are most often interpreted as mere humps!). For instance, in a series of bronzes of increasing tin contents, Pell-Walpole (1946) was probably the first to conclude that the peak in porosity at 5%Sn, not 14% as expected from the equilibrium phase diagram, was the result of the maximum in the effective freezing range. Spittle and Cushway (1983) find a sharp maximum in the hot-tearing behaviour of Al-Cu alloys at approximately 0.5–0.8%Cu (Figure 8.9). The analogous results by Warrington and McCartney (1989) can be extrapolated to show that their peak is nearer 0.5%Cu (Figure 8.6), close to the peak in porosity, as described previously.

7.1.4.4 Burst feeding

Where hydrostatic tension is increasing in a poorly fed region of the casting, it seems reasonable to expect that any barrier might suddenly yield, like the bursting of a dam. Feed metal would then suddenly flood into the poorly fed region. This feed mechanism was proposed by the author simply as a logical possibility (Campbell, 1969a,b). As solidification proceeds, both the stress and the strength of the barrier will be increasing together, but at different rates. Failure will be expected if the stress grows to exceed the strength of the barrier. The barrier may be only a partial barrier, i.e. a restriction to flow, and failure may or may not be sudden.

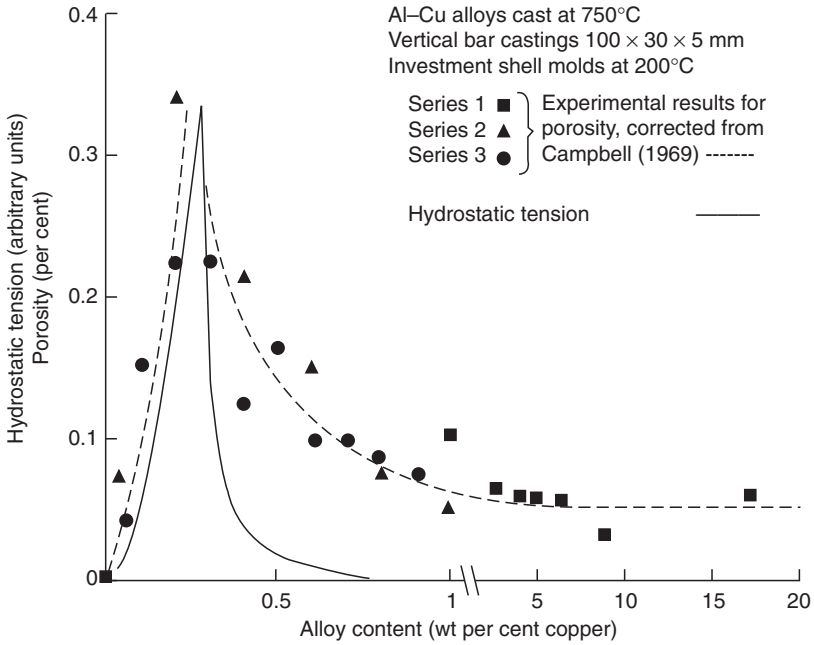

FIGURE 7.11

Predicted peak in hydrostatic tension in the pasty zone, and the measured porosity in test bars, as a function of composition in Al-Cu alloys (Campbell, 1969a,b).

In terms of Figure 7.12, the nucleation threshold diagram (explained later in Section 7.1.5.3; see Figure 7.21), the build-up of stress in the casting might be rapid, leading to the creation of a pore at P. However, if the casting is hotter, or is a weaker alloy, the development of stress will be somewhat slower, and might result in a burst of feed liquid by the collapse of a barrier to flow at point A. The internal stress will then be relieved, but after some additional build-up of gas in solution, the subsequent fall of pressure to B will result in a second burst event, once again relieving the internal stress, and returning the internal pressure to 1 atm. The effect of these bursts is to prevent conditions reaching the nucleation threshold, so that porosity is avoided.

If the feeding barrier is substantial, it may never burst, causing the resulting stress to increase and eventually exceed the nucleation threshold at P. This time, the release of stress, returning the internal pressure to 1 atm, corresponds to the creation and growth of a pore. There can be no further feeding of any kind in that region of the casting after a pore creation event; the driving force for feeding is suddenly eliminated.

Previously, the author has quoted the following observation as a possible instance of a kind of microscopic type of burst feeding. During observation of the late stages of solidification of the feeder heads of many aluminium alloy castings, it is clearly seen that the level of the last portion of interdendritic liquid sinks into the dendrite mesh not smoothly, but in a series of abrupt, discontinuous jumps. It was thought that the jumps may be bursts of feeding into interdendritic regions. However, it now seems more likely that the jumps are the result of the repeated, sudden failure of the surface oxide film, caught and stretched between supporting dendrites at the surface. The liquid draining down into the dendrite mesh will attempt to drag down its surface film, that will repeatedly burst and repair, resisting failure again for a time. The phenomenon is an illustration of the strength of the film, its capacity for stretching to some extent elastically and the capacity of the solidified metal in the feeder head at its freezing point to exhibit a certain amount of elastic recoil behaviour.

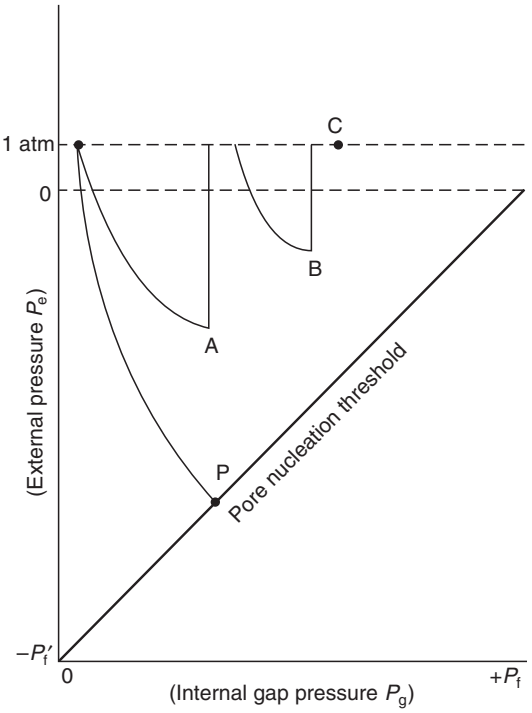

FIGURE 7.12

Gas-shrinkage map showing the path of development to early pore nucleation at P. In a contrasting case, slow mechanical collapse of the casting delays the build-up of internal tension, culminating in complete plastic collapse in the form of burst feeding processes at A and B. Such delay can be successful in avoiding pore nucleation because conditions never reach the pore threshold if, for instance, freezing is complete at C.

A macroscopic type of barrier can be envisaged for those parts of castings where mass flow has occurred, causing equiaxed crystals to block the entrance to a section of casting.

Macroscopic blockages have been observed directly in waxes, where the flow of liquid wax along a glass tube was seen to be halted by the formation of a solidified plug, only to be restarted as the plug was burst. This behaviour was repeated several times along the length of the channel (Scott and Smith, 1985).

In iron castings, such behaviour was intentionally encouraged in the early twentieth century. Nearly all large castings were subjected to 'rodding'—one or two men would stand on the mould and ram an iron rod up and down through the feeder top. Extra feed metal might be called for and topped up from time to time. This procedure would last for many hours until the casting had solidified. Nowadays, it is more common to provide a feeder of adequate size so that feeding occurs automatically without such strenuous human intervention!

On a microscale, a type of burst feeding is the rupture of the casting skin, allowing an inrush of air or mould gases (Figure 7.19). However, this is, of course, a gaseous burst that corresponds to the growth of a cavity, not a feeding process. Pellini (1953) drew attention to this possibility in bronze castings. It is expected that such surface-initiated porosity will be relatively common in castings of many long freezing range alloys.

In conclusion, it has to be admitted that whilst burst feeding might be an important feeding mechanism, it is not easy to quantify its effects by modelling. Despite some interest in using the concept of burst feeding as an explanation of some casting experiments, the explanations remain speculative. The existence of burst feeding has never been unambiguously

demonstrated. It therefore seems difficult to understand it and difficult to control it. At this stage, we probably have to content ourselves with the conclusion that logic suggests that it does exist.

7.1.4.5 Solid feeding

At a late stage in freezing, it is possible that sections of the casting may become isolated from feed liquid by premature solidification of an intervening region.

In this condition, the solidification of the isolated region will be accompanied by the development of high hydrostatic stress in the trapped liquid—sometimes high enough to cause the surrounding solidified shell to deform, sucking it inwards by plastic or creep flow. This inward flow of the solid relieves the internal tension, like any other feeding mechanism. In analogy with 'liquid feeding', the author called it 'solid feeding'. An equally good name would have been 'self-feeding'.

When solid feeding starts to operate, the stress in the liquid becomes limited by the plastic yielding of the solid and so is a function of the yield stress Y and the geometrical shape of the solid. (The yield stress Y is, of course, a function of the strain rate at these temperatures when assuming an elastic/plastic model.) The procedure is practically equivalent to the assumption of a creep stress model, and results in similar order-of-magnitude predictions for stress (Campbell, 1968a,b). For instance, for a sphere of radius R_0, with internal liquid radius R (Figure 7.3), the onset of complete plasticity is defined by:

$$P = 2Y \ln(R_o/R)$$

Mechanical engineers will recognise this relation as the classical formula for the failure of a thick-shell pressure vessel stressed by internal pressure to the point at which it is in a completely plastic state. This equation is expected to give maximum estimates of the hydrostatic tensions in castings because: (1) the shape is the most difficult to collapse inwardly and (2) the equation neglects the opposing contribution of the thermal contraction of the solidified shell which will tend to reduce internal tension (Forgac et al., 1979). Nevertheless, it is still interesting to set an upper bound to the hydrostatic tensions that might arise in castings.

This early model (Campbell, 1967) used the concept that the liquid radius R had to be expanded to some intermediate radius R', and the solid had to be shrunk inwards from its original internal radius $R + dR$ to the new common radius R'. At this new radius, the stress in the liquid equals the stress applied at the inner surface of the solid.

The working out of this simple model indicated that for a solidifying iron sphere of diameter 20 mm, the elastic limit at the inner surface of the shell was reached at an internal tensile stress of about 4 MPa (−40 atm); and by the time the residual volume of liquid was only 0.5 mm in diameter a plastic zone had spread out from the centre to encompass the whole shell. At this point, the internal pressure was in the range of approximately 20–40 MPa (−200 to −400 atm) and the casting was 99.998% solid. Solidification of the remaining drop of liquid increased the pressure in the liquid to approximately 100 MPa (−1000 atm). Later estimates using a creep model and cylindrical geometry confirmed similar figures for iron, nickel, copper and aluminium (Campbell, 1968a,b).

A minute theoretical point of interest to those of a scientific disposition is the effect of the solid–liquid interfacial tension. Although this is small, it starts to become important when the liquid region is only a few hundred atoms in diameter. The interfacial tension causes an inward pressure $2\gamma_{LS}/R$ that starts to compress the residual liquid. This is the explanation for the theoretical curves to take an upward turn in Figure 7.7 as freezing nears completion, creating a limit to the maximum internal tension.

We have to bear in mind that these estimates of the internal tension are upper bounds, likely to be reduced by thermal contraction of the shell, and reduced by geometries that are easier to collapse, such as a cylinder or a plate. Also the predictions are in any case lower for smaller trapped volumes of liquid, as might occur, for instance, in interdendritic spaces. Figure 7.13 shows schematically the effect of plastic zones spreading from isolated unfed regions of the casting.

For an infinite, flat plate-shaped casting in a skin-freezing metal, the internal stress developed is zero, which is an obvious solution because there can be no restraint to the inward movement of infinite flat plates separated by a solidifying liquid; the plates simply move closer together to follow the reduction in volume. For real plates, their surfaces are held apart to some extent by the rigidity of the edges of the casting, so the development of internal stress would be expected to be intermediate between the two extreme cases. The ease of collapse of the central regions of flat plates emphasises the importance of geometry.

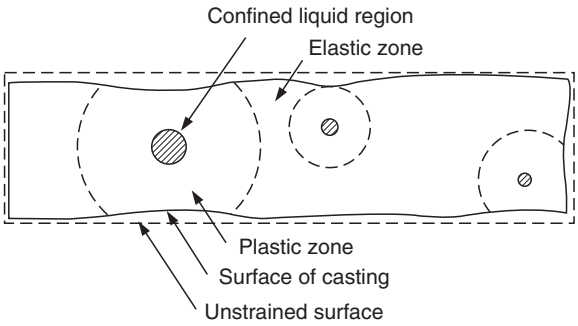

FIGURE 7.13

Plastic zones spreading from isolated volumes of residual liquid in a casting, showing localised solid feeding in action (Campbell, 1969a,b).

Figures 7.14 and 7.15 show results of some of my early experiments concerning porosity in small plates of an investment-cast nickel-based alloy. It happens to be an excellent example of solid feeding in action. At low mould temperatures, the solid gains strength rapidly during freezing and therefore retains the rectangular outer shape of the casting, and the steep temperature gradient concentrates the porosity in the centre of the casting. As mould temperature is

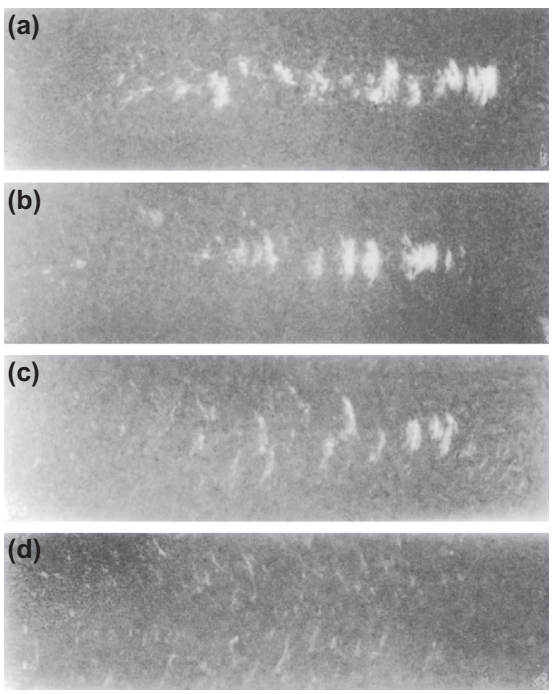

FIGURE 7.14

(a) Radiographs of bar castings 100 × 30 × 5 mm in nickel-based alloy cast at 1620°C in vacuum 15 μmHg into moulds at: (a) 250°C; (b) 500°C; (c) 800°C; and (d) 1000°C (Campbell, 1969a,b). Centre-line macroporosity is seen to blend into layer porosity and finally into dispersed microporosity.

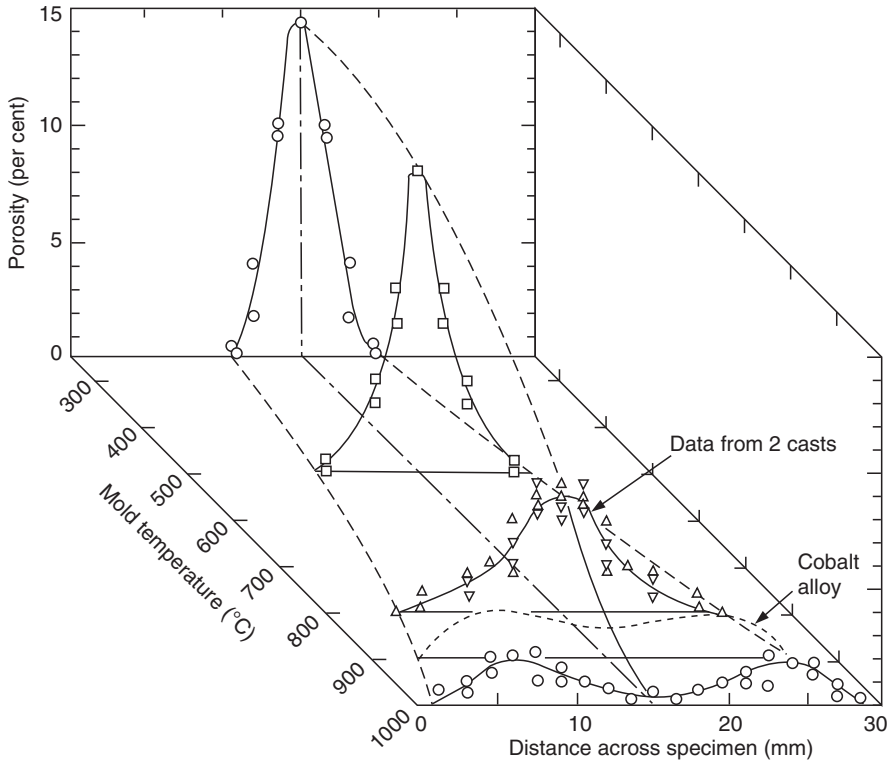

FIGURE 7.15

Porosity across an average transverse section of vacuum-cast nickel-based alloy as a function of mould temperature, quantifying the effect shown in this figure. The effect of solid feeding by the plastic collapse of the section is clear from the shape of the porosity distribution at high mould temperatures.

increased, the falling yield stress of the solidified metal allows progressively more collapse of the centre, solid feeding acting to reduce the total level of porosity. However, some residual porosity remains noticeable nearer the side walls, where geometrical constraint prevents full collapse. Note that these results were obtained in vacuum, with zero contribution from exterior positive atmospheric pressure. It follows, therefore, that all of the solid feeding in this case is the result of internal negative pressure. In fact, surface sinks are commonly seen in vacuum casting. Sinks are therefore not solely the consequence of the action of atmospheric pressure, as generally supposed.

Figure 7.16 shows solid-feeding behaviour in spherical wax castings. The example is interesting because it is evident that sound castings can, in principle, be produced without any feeding in the classical sense. In this case, it is clear that feeding can be successfully accomplished by skilful choice of mould temperature to facilitate uniform solid feeding.

Figure 7.17 shows a similar effect in unfed Al-12Si alloy as a function of increasing casting temperature. The full 6–7% of internal shrinkage porosity at low casting temperature is gradually reduced by external collapse of the casting as casting temperature increases (Harinath et al., 1979).

If solid feeding is controlled so that it spreads itself uniformly in this way, then the accompanying movement of the outer surface of the casting becomes negligible for most purposes. For instance, the high volume shrinkage of about 6% suffered by Al-Si alloys corresponds to a linear shrinkage of only 2% in each of the three perpendicular directions. For a

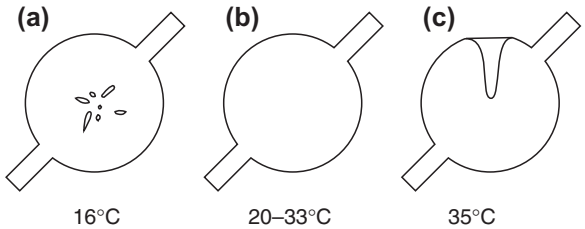

FIGURE 7.16

Cross-section of 25 mm diameter wax castings injected into an aluminium die at various temperatures. (a) a cold, strong solidified skin, creating internal shrinkage pores; (b) optimum conditions; and (c) a warm, soft solidified skin allowing an exterior collapse to form an externally connected shrinkage pipe.

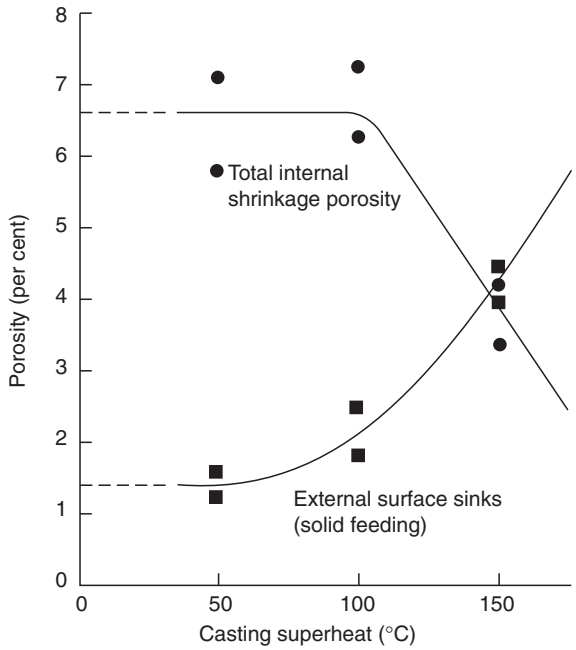

FIGURE 7.17

Al-12Si alloy cast into unfed shell moulds showing the full 6.6% internal shrinkage porosity at low casting temperature, giving way to solid feeding at higher casting temperature.

Data from Harinath et al. (1979).

datum in the centre of the casting, this means an inward wall movement of only 1% from each of the opposite surfaces. Thus a 25 mm diameter boss would be 250 μm small on radius if it were entirely unfed by liquid.

In practice, of the 6% volume contraction in aluminium alloy castings, usually about 5% is relatively easily fed by liquid and interdendritic modes, leaving only about 1% as a feeding problem, and thus available to be provided by solid feeding. This corresponds to an inward movement of a surface of only 0.16%, which is only about 40 μm for our 25 mm diameter casting. Thus dimensional errors resulting from solid feeding reduce to the point at which they become not measurable.

In contrast to the 0.25 mm worst case reduction in radius for the 25 mm diameter feature, if all the shrinkage were concentrated at the centre of the casting, the internal pore would have a diameter of 10 mm. This point has been made before, but is worth repeating. The difference between the extreme seriousness of internal porosity, compared with its harmless dispersion over the exterior surfaces of the casting is a key factor to encourage the development of casting processes that would automatically yield such benefits. The elimination of internal defects in the liquid that could nucleate a cavity is a major beneficial feature of a good casting process.

It is also worth emphasising that solid feeding will occur at a late stage of freezing even if the liquid is not entirely isolated. The case has been discussed in the section on interdendritic feeding, and is part of the meaning of Figure 7.7. It is also clear in Figure 7.15. The effect is the result of the gradual build-up of tension along the length of the pasty zone because of viscous resistance to flow. At the point at which the tension reaches a level where it starts to cause the collapse of the casting the region is effectively isolated from the feeder. Although liquid channels still connect this region to the feeder, they are by this time so small they become ineffective in delivering feed liquid.

An experimental result by Jackson (1956) illustrates an attempt to reduce solid feeding by increasing the internal pressure within the casting by raising the height of the feeder. Jackson was casting vertical cylinders 100 mm in diameter and 150 mm high in Cu 85-5-5-5 alloy in greensand. He employed a plaster-lined feeder of only 50 mm in diameter (incidentally, failing Feeding Rules 2 and 3, which explains why he observed such high porosity in his castings). Nevertheless, the beneficial effect of increasing the feeder height is clear in Figure 7.18. His data indicate that, despite the unfavourable geometry, if he had raised his feeder height to 250 mm, all exterior shrinkage would have been eliminated. The interior porosity would have fallen to about 2.0%, almost certainly being the residual effects from the combination of gas porosity, and the residual shrinkage from his poorly sized feeder.

In a study of two small shaped castings in three different Al-Si alloys, of short, medium and long freezing ranges, Li et al. (1998) measured the internal porosity of the castings by density, and the external porosity (the total surface sink effect) by measuring the volume of the casting in water. We found that the internal porosity in the castings in all three alloys was about the same at approximately 1 volume%. However, the external sinks grew from an average of 3.1, to 6.4 to 7.5 volume% for the short-, medium- and long freezing range alloys. This significant increase in solid feeding for the long freezing range material probably reflects the easier collapsibility of the thinner solidified shell and its internal mesh

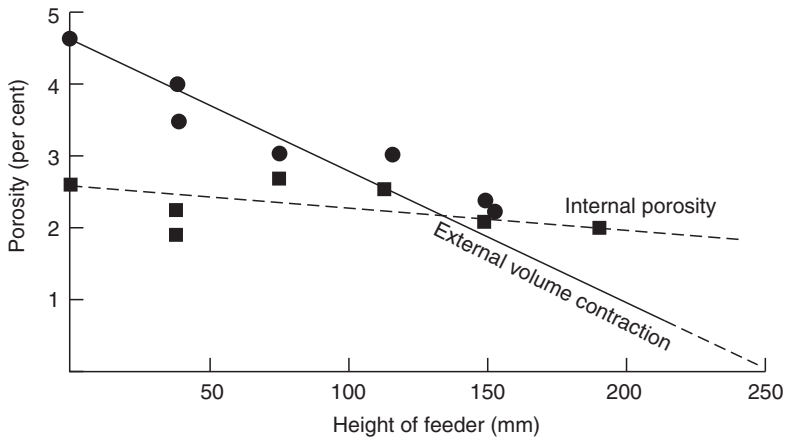

FIGURE 7.18

Gunmetal casting showing the reduction in solid feeding as liquid feeding is enhanced by extra height and volume of feed metal.

Data from Jackson (1956).

of dendrites. The more severe internal stress because of the greater difficulty in interdendritic feeding may also be a significant contributor. Conversely, of course, the absence of any corresponding increase in internal porosity confirms that feeding of the castings in the shorter freezing range alloys occurred by the simpler and easier more open liquid feeding mechanisms.

Amid the significant value of useful solid feeding, we need to keep in mind the possible dangers accompanying this feeding mechanism; hence, the brief summary that follows. Clearly, for the condition that the liquid is free from bifilms, the casting will not contain internally initiated pores. However it may generate:

1. Surface-initiated pores or even
2. Surface sinks.

In the presence of one or more easily opened bifilms, the situation changes significantly. The casting will now exhibit:

3. A large interior shrinkage pore in the presence of a bifilm in the stressed region, if the hydrostatic stress becomes sufficiently high and if the stressed volume is large.
4. A population of internal microscopic cracks. This is the subtle danger arising from the usual presence of a population of bifilms in the stressed liquid. In this situation, the compact bifilms are subjected to a tensile stress in the liquid, providing a driving force to unfurl. The mechanical properties, especially the ductility and ultimate tensile strength (UTS), of the casting are thereby impaired in this region, even though there may be no visible indication if the bifilms are not opened sufficiently to reveal their presence. In a nearby region of the casting that had enjoyed better feeding, bifilms would have remained fairly furled, so the ductility and UTS would have been higher.

A final personal remark concerning solid feeding that is a source of mystery to the author is the widespread inability of many to comprehend that it is a fact. This lack of comprehension is difficult to understand in view of the obvious evidence for all to see as surface sinks (even in castings solidified in vacuum) and that isolated bosses can be cast sound provided that the metal quality is good (i.e. few nuclei to initiate internal pores). Foundries that convert poor filling systems to well-designed filling systems suddenly find that internal porosity and hot tears vanish, but the castings now require extra feeding to counter surface sinks (Tiryakioglu, 2001). The increased solid feeding at higher mould temperatures is widely seen in investment castings. The easy collapse of flat plates, especially of alloys weak at their freezing points like Al alloys, explain their long and difficult-to-define feeding distances. The better-defined feeding distances of steels are the consequence of their better-defined resistance to collapse; their greater strength resisting solid feeding. Additionally, of course, hot isostatic pressing (hipping) is a good analogy of an enforced plastic collapse of the casting, as is also direct squeeze casting.

Who needs good imagination in the presence of all these facts?

7.1.5 INITIATION OF SHRINKAGE POROSITY

In the absence of gas, and if feeding is adequate, then no porosity will be found in the casting.

Unfortunately, however, in the real world, many castings are sufficiently complex that one or more regions of the casting are not well fed, with the result that the internal hydrostatic tension will increase, reaching a level at which an internal pore may ‘pop’ into existence in several ways. Conversely, if the internal tension is kept sufficiently low by effective solid feeding, the mechanisms for internal pore formation are not triggered; the solidification shrinkage then appears on the outside of the casting. All this is discussed in more detail later.

7.1.5.1 Internal porosity by surface initiation

If liquid from the feeder becomes cut off, the pressure inside the casting falls. Liquid that is still connected to the outside surface may then be drawn from the surface, causing the growth of porosity connected to the surface (Figure 7.19). The sucking of liquid from the surface in this way naturally draws in air, following interdendritic channels, spreading along these routes into the interior of the casting. The phenomenon is a kind of feeding by a fluid, where the fluid in this case is air. However, of course, this is hardly a feeding process but a pore growth process. This porosity in the interior of the casting is usually hard to distinguish from microporosity caused in other ways: on a polished section it appears to be a

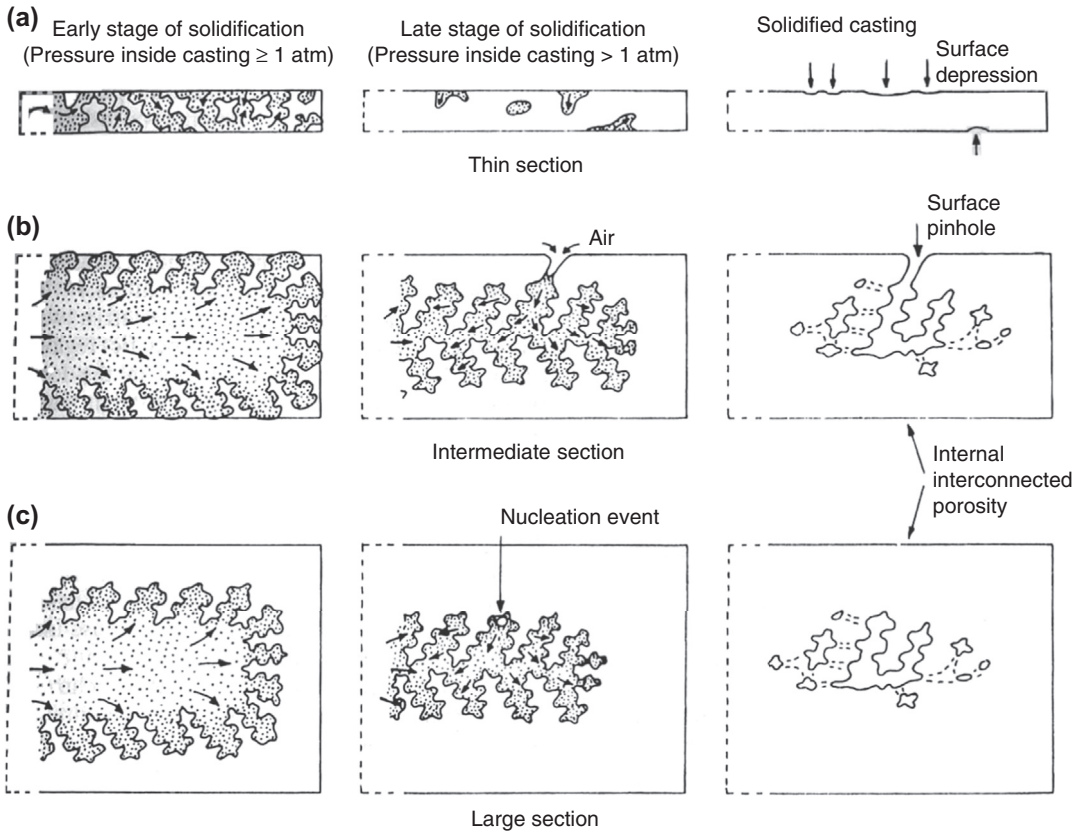

FIGURE 7.19

(a) Thin sections require little or no feeding because they can contain zero shrinkage porosity; (b) intermediate sections can develop surface connected porosity; (c) thick sections contain nucleated internal porosity (Campbell, 1969a,b).

series of separate interdendritic pores, whereas in reality it is a single highly complex shaped interconnected pore, linked to the surface. It is sometimes possible to identify its origins as surface-initiated porosity by its oxidised internal surface near to the surface of the casting. Deeper into the casting, away from the surface, the oxygen is totally consumed, so the surface film changes from an oxide to a nitride.

Figure 7.19 illustrates how the withdrawal of surface liquid is negligible in thin-section castings, explaining why thin sections require little feeding, or even no apparent feeding, but automatically exhibit good soundness. The effect is easily seen in gravity die castings because of their shiny surface when lifted directly from the die. In a section of intermediate thickness, the experienced caster will often notice a local frosting of the surface. This dull patch is a warning that interdendritic liquid is being drained away from the surface indicating an internal feeding problem that requires attention.

Pericleous and Bounds et al. (1997) was the first to predict this form of surface-initiated porosity using a computer model of the freezing of a long freezing range alloy. His result is shown in Figure 7.20.

This pore formation mechanism from the surface seems to be much more common than is generally recognised. It is especially likely to occur in long freezing range alloys at a late stage in freezing, when the development of the dendrite

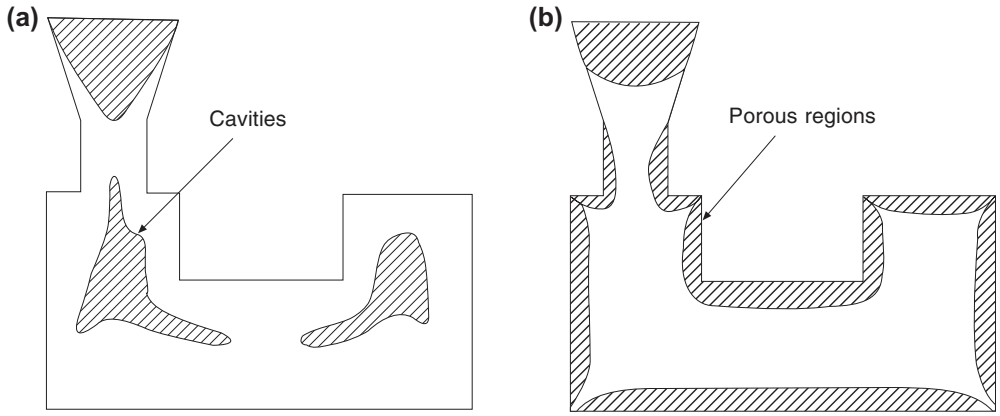

FIGURE 7.20

Regions of computer-simulated shrinkage porosity, (a) internally in a short freezing range alloy, and (b) externally (surface-initiated) in a long freezing range alloy. The latter was the first prediction of surface-initiated porosity by computer simulation.

After Pericleous and Bounds et al. (1998).

mesh means that drawing liquid from the nearby surface becomes easier than drawing liquid from the more distant feeder. The point at which liquid may be drawn from the surface may be anywhere (or practically everywhere) for an alloy of sufficiently wide freezing range.

However, in an alloy of intermediate freezing range, the initiation site is often a hot spot such as an internal corner or re-entrant angle. As has been mentioned before, the gravity die caster pouring an Al-Si alloy looks for such defects on each casting as it is taken from the die. If such a 'draw' or cavity or frost appearance is noticed in a re-entrant angle, he immediately doses the melt with sodium. The straightening of the solidification front (Figure 6.12(b)) strengthens the alloy at the corner so that it can better resist local collapse. The outcome is a pore hidden inside the casting if the melt quality is poor so that nucleation is easy. Alternatively, if the melt quality is good, no internal pore can easily form, so that the rise in internal tension will cause more general collapse of the casting. Solid feeding will have been encouraged.

The connection of two opposite surfaces of the casting by pores that are extensively connected internally is one of the major reasons why long freezing range alloys cannot easily be used for pressure-tight applications such as hydraulic valves or automobile cylinder heads. In such complex castings, it is often difficult to meet the essential requirement that the interior of the casting has a positive pressure at all locations so as to prevent surface-connected internal porosity.

7.1.5.2 External porosity (surface sinks)

If internal porosity is not formed (either by surface-linked initiation or nucleation events) then the lowering of the internal pressure will lead to an inward movement of the external surface of the casting (Figure 7.13). If the movement is severe and localised, then it constitutes a defect known as a '*sink*' or a '*draw*'. The feeding of the internal shrinkage by the inward flow of solid is, of course, '*solid feeding*' or '*self-feeding*'.

Adequate internal pressure within the casting will reduce or eliminate solid feeding, so maintaining the shape of the casting and keeping it sound. In such favourable feeding conditions, neither internal nor external porosity will occur.

If the remedy of the application of internal pressure is carried out too enthusiastically, the natural inward movement of solid feeding will be reversed, causing the casting to swell. Such growth is common in grey iron castings and castings

that have a high head of metal. Swelling of cast metal is also commonly seen in pressure die casting if the casting is removed from the die before it is fully solid. This is because the gas bubbles entrained by the extreme turbulence are under extremely high pressure. The technique is useful for identifying hot spots in the casting (i.e. regions last to freeze and which therefore require additional local cooling in the die to raise productivity). Gas entrained in hot spots can cause the casting to locally explode if released very early from the constraint of the die.

Returning to conventional gravity castings, in real situations it sometimes happens that a certain amount of external collapse of the casting will occur before the internal pressure falls to the level required to nucleate an internal pore. Once the pore is formed, the internal stress will be eliminated so that further solid feeding is arrested. The action of the remaining solidification shrinkage is simply to grow the pore. The final effect of solidification shrinkage on the casting is usually found to be partly external and partly internal as illustrated in Figure 7.4. The balance between external and internal porosity can be widely seen in foundries. Examples are seen in Al-12Si (Figure 7.18) and in aluminium-based metal/matrix composites (Emamy and Campbell, 1997).

7.1.5.3 Nucleation of internal porosity

Although the problem of the nucleation of cavities and bubbles is in principle similar to that of the nucleation of condensed phases such as the metal matrix and non-metallic inclusions, there are differences that make it worthwhile to look at non-condensed phases such as vacuums, vapours and gases separately in some detail. In particular, we shall find that there are special difficulties with the nucleation of gas and void phases, forcing us to adopt new concepts. We shall deal first with shrinkage cavities, then gas pores, not forgetting that both can cooperate in both the formation and growth of such volume defects.

Short-freezing-range alloys, such as aluminium bronze and Al-Si eutectic, do not normally exhibit surface-connected porosity. They form a sound, solid skin at an early stage of freezing, and liquid feeding continues unhindered through widely open channels. Any final lowering of the internal pressure from poor feeding towards the end of freezing may then create a pore by nucleation in the interior liquid. In this case, there is clearly no connection to the outside surface of the casting, as illustrated in the larger section shown in Figure 7.19(c). After nucleation, further solidification shrinkage will provide the driving force for growth of the pore, which, on sectioning or radiography, may be more or less indistinguishable from the surface-initiated type.

In alloys of short freezing range, therefore, porosity is probably normally nucleated, and is concentrated near the centre of the casting, usually well clear of the casting surface. In castings of large length to thickness ratio, this is widely referred to as centreline porosity. Thus unless subsequent machining operations cut into the porosity, castings in such alloys are normally leak-tight. (The leak paths commonly provided by folded oxide films or bubble trails generated during a turbulent fill are a separate problem requiring solution by other means such as improved filling, and/or the use of filters.)

Tiwara et al. (1985) has suggested a way of initiating internal porosity in specific regions of castings by the addition of nuclei in the form of fragments of refractory. These foreign particles contain much porosity, so that the growth of pores from such sites proceeds without difficulty. The result is a large internal pore, which, to some extent, can be sited in a chosen location in the casting. Additional feeders or chills are therefore not required, and internal porosity in an unwanted location is avoided. External porosity is also successfully avoided because internal pressure is prevented from falling to negative values. However, as inventive as this technique is, for the majority of castings that are required to be sound throughout, and are required to be free of pieces of refractory, it is, unfortunately, only of academic interest.

Homogeneous nucleation

Following the beautifully elegant approach by Fisher (1948), we can quantify the conditions required for the formation of porosity in liquid metals. A quantity of work is associated with the reversible formation of a bubble in a liquid. If the local pressure in the liquid is P_e, we need to carry out an amount of work P_eV to push back the liquid far enough to create a bubble of volume V.

The formation and stretching out of the new liquid–gas interface of area A requires additional work γA, where γ is the interfacial energy per unit area.

The work required to fill the bubble with vapour or gas at pressure P_i is negative and equal to $-P_iV$. (The negative sign arises because the pressure inside the bubble clearly helps the formation of the bubble, as opposed to the other work requirements, which tend to oppose bubble formation.) Thus the total work is:

$$\begin{aligned}\Delta G &= \gamma A + P_e V - P_i V \\ &= 4\gamma\pi r^2 + (4/3)\pi r^3(P_e - P_i)\end{aligned}$$

where clearly $(P_e - P_i)$ is the pressure difference between the exterior and the interior of the bubble which we may write as ΔP for convenience. Similarly to dense phase nucleation, a plot of ΔG versus bubble radius r shows a maximum that constitutes an energy barrier to nucleation, as in Figure 5.27. The critical radius r^* in this case is:

$$r^* = 2\gamma/\Delta P^* \tag{7.6}$$

Because bubbles growing from the bulk liquid will grow an atom at a time as the result of statistical thermal fluctuations, it is evident that small bubbles with radii less than r^* will tend to disappear. Only exceptionally will a long chain of favourable energy fluctuations produce a bubble exceeding the critical radius r^*. When this rare event does happen, the embryonic bubble will then have the potential to grow to an observable size.

Fisher goes on to apply some delightfully elegant rate theory to derive values for the critical pressure difference ΔP^* at which nucleation will occur. The reader is strongly recommended to consult Fisher's original paper. However, for our purposes, we can obtain a sufficiently good estimate very easily and quickly using Eqn (7.6). Using experimentally determined values of atomic sizes and surface energy γ for liquid metals, if we assume that the critical radius is perhaps in the region of a couple of atomic diameters (in the first edition of *Complete Casting Handbook,* the critical radius was erroneously assumed to be only one atomic diameter), we obtain Table 7.2.

The reasonable agreement between the calculated critical pressures is corroboration that the critical embryo is actually about four atoms across and therefore occupies the volume of approximately 50 vacancies. However, whether or not these figures really are accurate is a detail that need not concern us here. The important message is that the pressures that are required for nucleation are *extremely* high and reflect the real difficulty of homogeneous nucleation of pores in liquid metals. It is clear that the strengths of liquid metals are almost as high as those of solid metals (for liquid iron the fracture strength corresponds to nearly 8 GPa). As noted previously, this is hardly surprising because the atomic structure is similar, liquid metals being close packed random structures, compared with solid metals being close packed regular structures. In either case, the atoms are about the same distance apart, and it is similarly difficult to separate them; they are resistant to be forced apart to create a void.

The problem of nucleation is reduced by the presence of surface-active impurities in the liquid. The non-metals oxygen, sulphur and phosphorus are particularly active in iron melts: the presence of only 0.2 wt% of oxygen reduces the surface tension of liquid iron from 1.9 to approximately 1.0 Nm^{-1}. This approximately halves the estimates of the pressure required for nucleation as shown by Eqn (7.6). Similar reductions in surface tension (and therefore in fracture pressures) are to be found in liquid copper when contaminated with high levels of the non-metals O, S and P.

Such high concentrations of oxygen (and the other non-metals) are probably often found on solidification because of the concentration of solutes ahead of the freezing front. Once again, for the case of liquid iron, the partition coefficient for oxygen is approximately 0.05, giving a factor of 20 increase in concentration at the advancing front. Thus an average of only 0.01 wt% oxygen in the bulk melt can produce 0.2 wt% at the front.

If the levels of oxygen rise sufficiently to precipitate FeO as a liquid inclusion at the front, then the nucleation problem is reduced yet further because FeO has a surface tension of between 0.6 and 0.5 Nm^{-1}, depending on its oxygen content (Popel and Esin, 1956). Thus a gas pore will preferentially nucleate in such a liquid inclusion, where the critical pressure is easily shown to be reduced to around 1.7 GPa. Effectively, this is still homogeneous nucleation in a pure liquid where, in this case, the pure liquid in the liquid Fe is in the form of regions, possibly minute droplets, of FeO.

Even this pressure is still so high as to be probably unattainable. What other possibilities are there?

It is possible that nucleation might occur on a solid impurity particle. A solid foreign substrate, if a poorly wetted surface, might make a location for nucleation. This is known as heterogeneous nucleation. If this poorly wetted solid surface happened to be inside the liquid FeO inclusion, we shall see how we can reduce the critical fracture pressure 1.7 GPa yet further in the following section.

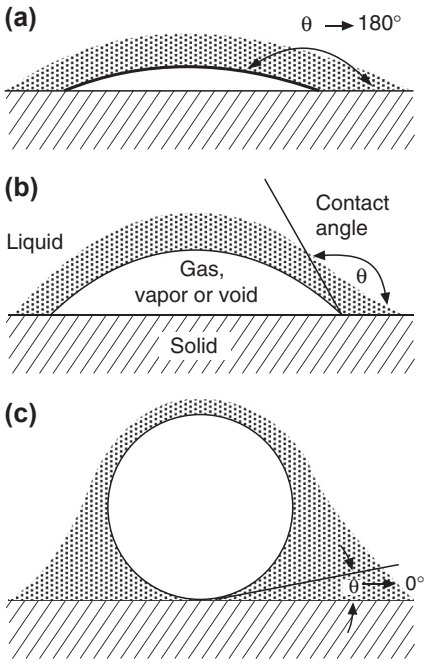

FIGURE 7.21

Geometry of a bubble in contact with a solid substrate showing (a) poor wetting and easy decohesion of liquid from the solid; (b) medium wetting; and (c) good wetting in which liquid cohesion to the solid is high, and the bubble is displaced out of contact with the solid.

Heterogeneous nucleation

Fisher considers the case of the nucleation of a bubble against the surface of a solid substrate. The liquid is considered to make an angle θ with the solid. This contact angle defines the extent of wetting; $\theta = 0°$ means complete wetting, whereas $\theta = 180°$ is complete non-wetting. The geometry is shown in Figure 7.21. Fisher shows that nucleation is easier by a factor:

$$P^*_{het}/P^*_{hom} = 1.12\left\{(2 - \text{Cos}\theta)(1 + \text{Cos}\theta)^2/4\right\}^{1/2} \tag{7.7}$$

The factor 1.12 arises because of the fewer sites for nucleation on a plane surface of atoms, compared with the greatly increased number of possibilities in the bulk liquid. This factor alone makes the nucleation of pores on wetted surfaces unfavourable. In fact, nucleation on solid surfaces does not become favourable until the contact angle exceeds 60–70°, as shown in Figure 7.22. For this reason the nucleation of pores against the growing solid such as a dendrite is *not* favoured (because a melt wets the solid formed from itself).

This factor is contrary to those other factors that favour the nucleation of a pore close to a front. The favourable factors include the high gas contents and low surface tension usually present in the highly segregated liquid. Additionally, there are likely to be inclusions present, pushed and concentrated by the advancing front into the residual liquid. Again, the inclusions that are pushed by the front are likely to be the non-wetted variety, and so will constitute good nuclei for pores. Contrary, therefore, to many published opinions elsewhere, the interface is theoretically *not* a favoured site. Yet, paradoxically, in practice, pores will nucleate there because of all the other favourable conditions that prevail adjacent to an advancing solidification interface. The received wisdom turns out to be correct for the wrong reasons!

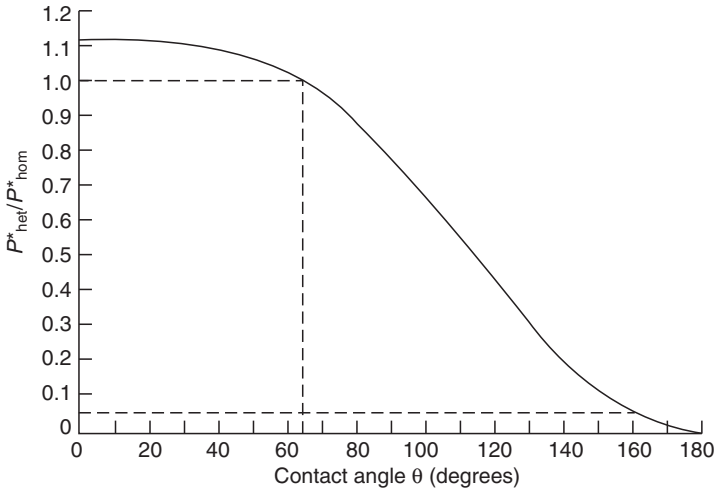

FIGURE 7.22

Relative difficulty of nucleating a pore as the contact angle with the solid changes from wetting to non-wetting. Only when the angle exceeds about 65° does heterogeneous nucleation on the solid become favourable.

It is also important to note that not all inclusions are good nucleation sites for porosity. Those that are well wetted will not be favoured. These include the rather more metallic inclusions such as borides, carbides and nitrides. (However, being well wetted, they are mostly good nuclei for the solid phase, and so can assist with grain refinement, as we have seen at several points in Section 5.)

The wetting requirements for the nucleation of pores are completely opposite: good nuclei must be not wetted. Such substrates include the non-metals such as oxides. However, the situation is especially bad for *entrained* oxides as will be described later in this chapter.

The reader should be aware that there is widespread misunderstanding of the important fact outlined previously: that the nuclei required for the formation of a solid (i.e. for grain refinement) are quite different to the nuclei required for the formation of pores and voids.

A nice experiment was carried out by Gernez in 1867 in which he demonstrated that crystalline solids which had been grown in the liquid and had never been allowed to come into contact with air were incapable of inducing effervescence in a liquid supersaturated with gas. Otherwise identical solids that had surfaces which had been allowed to dry always caused effervescence.

Oelsen describes a related experiment that he carried out in 1936 in which he isolated a sample of liquid iron on all sides by a liquid slag. Because the iron contained 2% carbon and 0.035% oxygen, it was supersaturated considerably in excess of equilibrium. In fact, Oelsen estimated that the internal pressure of carbon monoxide would be approximately 40 atm. When an iron rod was immersed in the melt to destroy the perfection of the containment, a violent eruption of gas immediately occurred, which ceased once again when the rod was withdrawn.

Figure 7.22 indicates that as the contact angle increases to 180° any difficulty of heterogeneous nucleation should fall to zero. In fact, there are good reasons to believe that such perfect non-wetting is probably not possible, and that the maximum contact angle attainable in practice is perhaps close to 160°. Certainly, no contact angle greater than this appears ever to have been observed (see, for instance, the work by Livingston and Swingley (1971)). Assuming this to be true, then from Figure 7.22, we see that heterogeneous nucleation on the most non-wetted solid known, having a contact angle of 160°, requires only about one-twentieth of the pressure required for nucleation in the bulk liquid.

Returning to our liquid FeO inclusion in solidifying iron: if a highly non-wetting inclusion were present inside the liquid FeO inclusion, then the lowest pressure for nucleation of a pore in this complex inclusion would be approximately 1.7 GPa/20 = 85 MPa. Although this pressure is still high, it might now (just) be attainable in iron and steel castings. In Al and Mg alloys, such a nucleation condition from an equivalent complex inclusion seems unlikely to be attained because these weaker materials would collapse plastically under the internal tension.

Similar reasoning can almost certainly be applied to other alloy systems: complex inclusions are likely to be present in all alloys. In fact, it seems likely that most if not all inclusions are complex. The apparent simplicity of many inclusions may be an illusion; microscopic regions of impurities, perhaps only an atom or so thick, may be distributed in patches. It would be difficult to find such patches, and, conversely, difficult to prove that they did not exist.

Perhaps therefore the large fracture pressures predicted by the classical nucleation theory are to be expected to be always reduced by the presence of low surface energy liquid inclusions that in turn contain very poorly wetted solid particles. If this is the case, then assuming that all the values are reduced from their homogeneous nucleation values by the same total factor approximately 83 found for pure iron, the final column in Table 7.2 is estimated.

There is a natural concern that although these stresses are greatly reduced from those required for nucleation in the pure liquid, they are still probably too high to be attainable. Thus, in a nutshell, even fairly dirty liquid metals do not meet a reasonable criterion for fracture considering the classical nucleation theory.

Thus, although the formation of pores by random, thermal atomic fluctuations within the liquid and against plane solid surfaces, has been a problem in classical physics that has fascinated many scientists since the first attempt by Fisher in 1948, all of the solutions that have been found so far (see, for instance, the short review by Campbell (1968)) have shown that pores are difficult, and actually, probably impossible, to nucleate, despite invoking the most active of heterogeneous substrates.

If liquid metals do not fracture, the internal initiation of porosity in castings is impossible. Nevertheless, the fact is that pores in castings are the norm rather than the exception. Clearly, there is a major mismatch between theory and fact. The failure of classical nucleation theory to account for porosity is not widely appreciated. In this work, the fundamental inability of the classical theory has driven the search for other pore initiation processes as outlined later.

This conclusion is so important and so surprising that it is worth emphasising by stating it another way. The student will usually have been persuaded that because classical homogeneous nucleation of pores in liquid metals is difficult, classical heterogeneous nucleation on a solid particle must therefore occur. The key conclusion from our previously discussion is that this is almost certainly untrue. Classical nucleation of a cap-shaped bubble cannot occur even on the most non-wetted solid. This alarming fact forces a re-evaluation of initiation processes for porosity in castings.

Other potential processes are examined later in Section 7.1.5.4. However, it will become clear that the most likely candidate mechanism for pore initiation are entrainment defects, as will be described later in the Section 7.1.5.4.

Nucleation conditions for shrinkage pores

The problem of the nucleation of shrinkage cavities has been widely overlooked. Somehow it has been assumed that they are fundamentally different to gas pores, and that they 'just arrive'. After all, it is argued, they *must* occur in an unfed isolated volume of liquid because the concept of shrinkage means that there is a volume deficit. It is assumed that this volume deficit *must* result in a cavity.

However, as we have seen previously, there really is a difficulty in the initiation of a cavity in a liquid. The various analogous systems described in Section 7.1.2.1 demonstrate that the liquid can withstand hydrostatic tension, and may never fail. If we accept this, then it follows that the liquid is stretched elastically, and the surrounding solid drawn inwards, first elastically, then plastically as the stress in the liquid increases (Campbell, 1967). These predictions explain many common observations in the foundry, as will be referred to repeatedly in this work. Only if the stress in the liquid reaches the critical fracture pressure P_f will a pore appear, growing in milliseconds to a size which will dispel the stress. This is the instant at which the pore grows explosively, releasing the tension in the liquid.

Thus, in case of any doubt, all the conclusions reached previously for nucleation of pores in liquids, estimated by Fisher's formula, apply to the nucleation of shrinkage cavities. These are briefly summarised later.

Fracture strengths are, of course, reduced by the presence of weakly bonded surfaces in the liquid. Thus the previous discussion on heterogeneous nucleation also applies. Shrinkage cavities are therefore expected to nucleate only on non-wetted interfaces.

Good nuclei for shrinkage cavities include oxides. Complex inclusions that consist of low-surface-tension liquid phases containing non-wetted solids might be especially efficient nuclei, as have also been discussed.

Unfavourable nuclei on which the initiation of a shrinkage cavity will *not* occur include wetted surfaces such as carbides, nitrides and borides, and other metal surfaces such as the surfaces of dendrites that constitute the solidification front. (Readers need to beware that many authors assume, incorrectly, that dendrites are good nuclei for pores although, perhaps somewhat perversely, pores often do nucleate at a dendritic front for other reasons as listed in Section 7.1.5.3). All these substrates are unfavourable for decohesion simply because the bonding between the atoms across the interface is so strong. This is reflected in the good wetting (i.e. small contact angle) of the liquid on these solids.

Interestingly, although oxides are included previously as good potential nuclei for pores, this is only true of their non-wetted surfaces. Those surfaces that have grown off the melt, and thereby in perfect atomic contact with the melt, are not expected to be good nuclei. This illustrates the important distinction between wetting defined by contact angle, and wetting defined as being in perfect atomic contact with the liquid. Ultimately, it is the atom-to-atom contact, and the strong interatomic bonding that is important.

Nucleation conditions for combined gas and shrinkage pores

Following Fisher's analysis through once again, considering now that there is gas at pressure Pg on the inside of the pore effectively pushing and a negative pressure Ps in the bulk liquid effectively pulling the embryonic pore into existence, the final result for the critical fracture pressure Pf is:

$$Pf = Pg + Ps \tag{7.8}$$

This equation illustrates how gas and shrinkage cooperate to exceed the critical pressure for nucleation. The significance of this equation can perhaps be better appreciated by deriving an analogous relation as follows.

If we write the condition for simple mechanical equilibrium of a bubble of radius r in a liquid of surface tension γ, in which the bubble has internal pressure Pi and external pressure in the liquid Pe, we have:

$$2\gamma/r = Pi - Pe \tag{7.9}$$

When the pore is of critical size, radius r^*, and when the internal pressure is the pressure of gas Pg in equilibrium with the liquid, and the external pressure Pe is the (negative) pressure because of shrinkage $-P_S$, then Eqn (7.8) becomes the analogue of Fisher's equation:

$$2\gamma/r^* = Pg + Ps \tag{7.10}$$

The fracture pressures of various liquid metals can then be estimated from this relation assuming that r is approximately one or two atomic diameters, giving the values presented in Table 7.2.

The cooperative action of gas and shrinkage quantified previously in Eqns (7.8) and (7.10) was predicted by Whittenberger and Rhines (1952). Their ground-breaking concept was enshrined by them in a nucleation diagram as shown in Figure 7.23. We shall devote some space here to a consideration of this insightful map and show how it can be developed to a fascinating degree of sophistication, greatly assisting the description of pore-forming conditions within a casting.

Turning now to a detailed consideration of Figure 7.23: for a well-fed casting, $Ps = 0$, and as freezing proceeds the gas is progressively concentrated in the residual liquid, progressively raising the equilibrium gas pressure. Thus conditions in the casting progress along the line ADCE. At point E, the conditions for heterogeneous nucleation of a gas pore on nucleus one are met, so that a gas pore will pop into existence at that instant. The initial rapid growth of the gas bubble will deplete its surroundings of excess gas in solution, so that conditions in the locality of the bubble will reverse off the nucleation threshold, back towards D. Thus a second pore will be unable to nucleate in the immediate neighbourhood of the first pore. Other gas pores may nucleate elsewhere, beyond the diffusion catchment area of pore number 1.

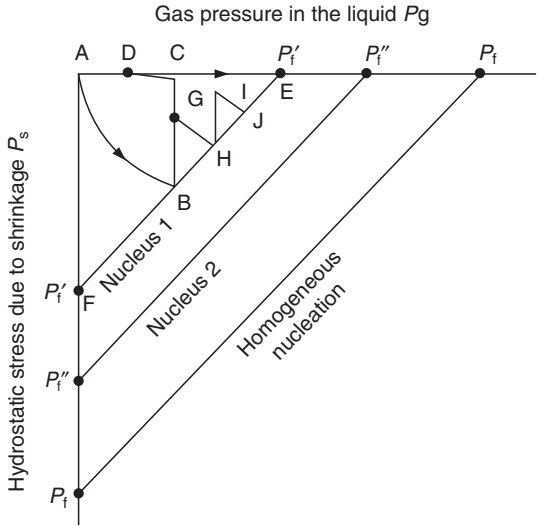

FIGURE 7.23

Gas-shrinkage map showing the path of conditions within the residual liquid in the casting in relation to the nucleation threshold for pore formation.

Notice also that other heterogeneous nuclei are also present, floating about in the liquid (threshold two in Figure 7.23) but, being less favourable, are not activated.

We turn now to the quite different situation where the casting is free from gas, but is poorly fed. The internal pressure Ps in the casting falls because of the action of shrinkage, progressing along the line AF. At F, the fracture pressure for nucleation on heterogeneous nucleus one is met, and a cavity forms. The hydrostatic tension is explosively released and conditions in the casting shoot back to point A.

In practice, both gas and shrinkage will be present to some degree in the average casting, and both will cooperate, causing the conditions to progress along a curve AB. In the absence of any foreign nuclei, it is unlikely that the condition *Pf* would be met before the casting had solidified completely. This is because the homogeneous nucleation threshold is so far away. (Figure 7.23 is not to scale. If it had been, then the heterogeneous threshold would have been a minute triangle only a millimetre or two in size up at the top left hand corner of the page, making all the action undecipherable!) Thus the casting would have been sound if no favourable inclusions had been present. However, in the presence of nuclei one and two, the combined gas and shrinkage pore will form at B on nucleus one. Nucleus two will never be needed.

On the formation of a mixed pore at B, the pressure in the liquid immediately reverts to point C. Subsequent slower diffusion of gas into the pore will deplete the immediate surroundings of the pore, causing the local environment to progress to D. Outside this diffusion distance, conditions elsewhere in the casting continue to be free of stress and may progress to point E, at which many more gas pores may nucleate. These will add to the original mixed pore that will in the meantime have continued to grow under the combined action of shrinkage and gas.

The area of influence of the release of the hydrostatic tension from shrinkage has been assumed in the previously discussion to apply to the whole casting. In practice, it is true that its influence is vastly greater than that of the depletion of gas. The distance over which shrinkage is depleted is probably a factor of 1000–10,000 times greater than that of gas. This is evident from the fact that diffusion distances of solutes in the liquid are usually measured in micrometres, whereas the distances between layers in typical layer porosity can be measured in millimetres or centimetres. As will be explained in Section 7.1.7.2, each layer in layer porosity represents a separate nucleation event, effectively isolated from its neighbouring layer, because the threads of liquid that connect the two have become so fine as to be practically impassable because of viscous restraint.

Thus in terms of our nucleation diagram, Figure 7.23, the nucleation event at B may cause the reduction in tension in its own locality to drop to nearly zero at point C. However, at a distant location elsewhere, it may drop to only to about one-quarter of the original tension at G (as is explained in the case of the formation of layer porosity to be discussed in Section 7.1.7.2). A second nucleation event may then occur at H, leading via I to a third pore formation event at J, and so on.

The nucleation diagram is useful for visualising the effect of such variables as casting under an applied pressure, so that the starting point A is raised, effectively making the nucleation threshold more distant. If it is sufficiently distant then there is a chance that it may not be reached before the casting has solidified.

The diagram also illustrates how it is of little benefit to the soundness of a casting to melt in vacuum and cast in vacuum (although it may be better for other reasons to cast in vacuum, to avoid any back pressure of gas that might resist the filling of very thin sections for instance. It may also be useful to avoid the entrainment of a protective gas such as argon, which cannot be subsequently diffused out, nor fully closed by hipping). This is because both the gas pressure and the pressure in the liquid are both shifted by 1 atm, in the same direction, meaning that the pore nucleation threshold remains the same distance away, cancelling any advantage. Conversely, melting under vacuum but solidifying under atmospheric pressure is seen to be a benefit, pushing the threshold away by 1 atm pressure.

7.1.5.4 Non-classical initiation of pores

High-energy radiation

The radioactive decay of naturally occurring isotopes, and, unfortunately, contaminating artificial radioactive elements, occurs around us all at every point of our lives. Naturally occurring radioactive materials are relatively common in metals and alloys, and general radioactive contamination is presently increasing annually, arising from industrial and medical sources and general fall-out since the first nuclear explosions in 1945. This is a sad outcome, but even if all future contamination of the environment were to be prevented, we will still have to come to terms with accepting the historical legacy of a radioactive environment as a fact of life.

Liquid metals are, in common with all other present-day materials, subjected to a constant barrage of high-energy particles from these internal radioactive decay processes. The passage of these high-energy particles through the liquid causes thermal or displacement spikes, the name given to regions of intense heating, or actual displacement of atoms, effectively raising the local temperature of the liquid to well above its boiling point. It is possible, therefore, that these transient heated regions might become vapour bubbles sufficiently large to satisfy Eqn (7.1), thus constituting effective nucleation sites for gas or shrinkage pores.

Johnson and Orlov, in their review (1986), describe defect regions in solid metals of up to 100 atoms in diameter. Energy can be channelled away from such events along crystallographic directions in ordered solids, reducing the local damage. However, the lack of any long range order in liquids means that no such safety valve is possible, so that energy deposition will be much more localised. It follows that the production of a bubble of 100 atoms diameter in liquid iron should be easy, giving an equivalent fracture pressure of approximately 1500 atm, much lower than that required for classical homogeneous nucleation. In liquid FeO, the fracture pressure would be 400 atm. If the event occurred close to a non-wetted surface, then the fracture pressure would be only 20 atm. Such pressures would be much more easily met in castings.

Analogous events are actually observed directly in the bubble chamber, a device full of a transparent liquid that can be vapourised by a high-energy particle, defining its path by a string of nucleated vapour bubbles. It is sobering to note that a bubble chamber can only be constructed using steel made before 1945, in Europe commonly sourced from the German battleships on the seabed at Scapa Flow in the north of Scotland. Later steel introduces too much spurious background radiation.

Claxton (1967) has carried out a detailed study of the nucleation of vapour bubbles in liquid sodium subjected to a wide variety of different high-energy particles, including photons, electrons, protons, neutrons, alpha-particles, xenon and strontium as fission fragments and alpha-recoils. His preliminary analysis suggests that the only interactions capable of initiating nucleation of bubbles are ‘knocked-on’ atoms of the liquid produced by fast neutrons. Claxton (1969) suggests that for heavy recoils arising from alpha-particle decay the rate of energy transfer in liquid aluminium would be about three times higher than that in sodium, and in liquid iron should be about 10 times, giving rise to the possibility of nucleation, depending on the isotope responsible.

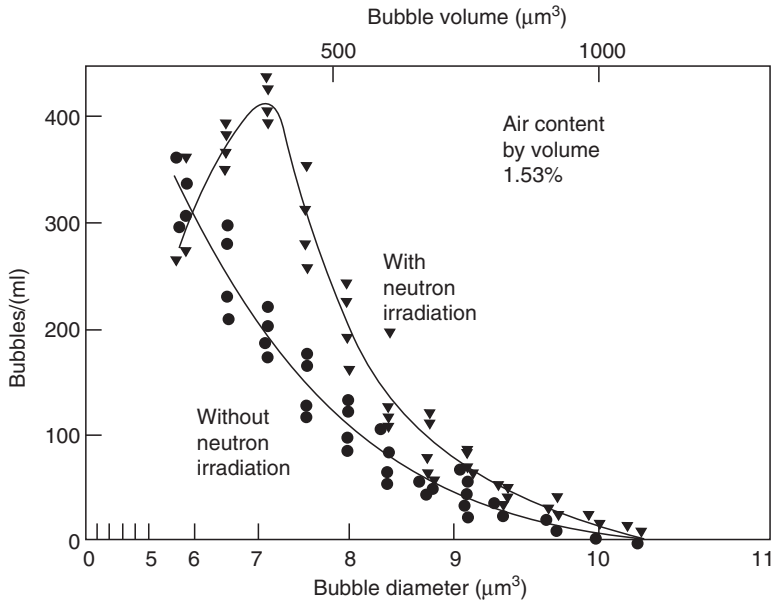

FIGURE 7.24

Micro-bubble spectrum in tap water with and without neutron irradiation (Hammitt, 1973).

Significantly, the micro-bubble spectrum in water is seen to be augmented when the water is irradiated with neutrons (Figure 7.24).

Additional factors that are likely to enhance any effects of the presence of radioactive isotopes in metals will be the concentration of such elements ahead of the freezing front. This is precisely where such events can be most effective. The region has high gas content, low surface tension and high density of assorted solid debris, some of which may be effective nuclei.

Furthermore, if a particularly troublesome radioactive isotope happened to be present in the melt, as an alloy in solution, it would be fundamentally different in character from suspensions of bubbles or inclusions in that it could not simply be eliminated by sedimentation or filtration. These uncertainties have never been investigated.

Differences in the levels of contamination by trace isotopes may be just one of many possible reasons for the occasional different behaviour from one batch of metal to the next that is often experienced in the foundry, and that often seems inexplicable. Kato (1999) is one of the first to record a check for the presence of alpha-emitters in his high-purity copper castings. It is a concern that one day such checks may have to become a routine.

Pre-existing suspension of bubbles

Several studies have indicated that there may be a micro-bubble spectrum in most liquids.

Studies on tap water have demonstrated that there seem to be approximately 300 bubbles of around 5 μm diameter in each millilitre (Figure 7.24). Hammitt (1973) has carried out work that implies similar distributions of bubbles in liquid sodium circulating as coolant in atomic reactors. Even higher densities of bubbles have been measured by Outlaw et al. (1981) in vacuum-cast pure aluminium (Figure 7.25). Although, of course, we have to be careful not to assume that this pore distribution in the solid reflects that originally present in the liquid, the result does underline that there are distributions of fine pores in circumstances in which we may not have any reason to suspect their presence.

Chen and Engler (1994) examine the very old proposal that pores exist in irregular crevices of solid inclusions. They propose that for a conical cavity a gas pocket would have an indefinite existence (they neglect the complications of

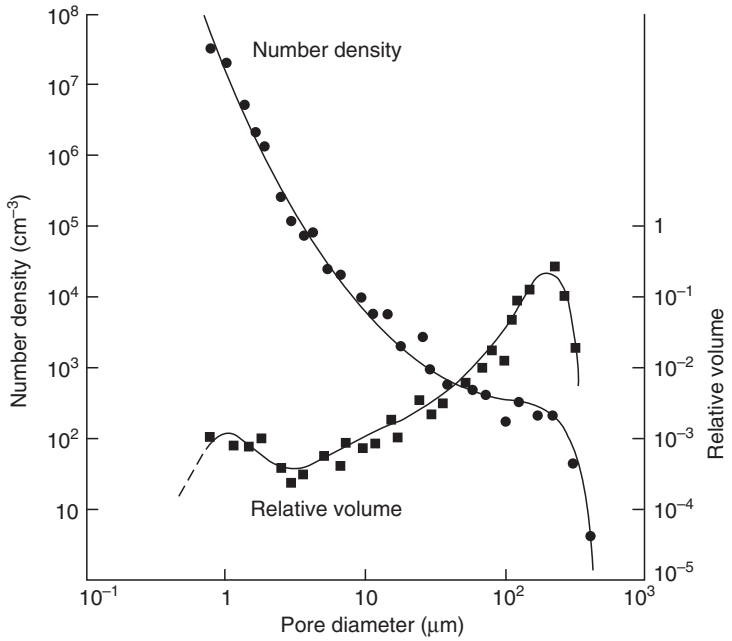

FIGURE 7.25

Hydrogen porosity in vacuum melted and cast 99.99Al. Total porosity is 0.71% (Outlaw et al., 1981).

chemical reactions and dissolution that we shall consider later). In the case of old oxides, from the surfaces of melting or holding furnaces, that have been relatively recently entrained, this model is probably accurate. Even so, it seems likely that in most current situations, this source of inclusions will be of less importance than new films from more recent entrainment events. Bifilms are expected to exist in many liquid metals and alloys. They are not envisaged as a distribution of spherical pores, but as a wide spectrum of sizes and shapes of films of air trapped between folded entrained surface films (the crack-like pores illustrated by Chen and Engler are good examples of bifilms in the early stages of opening). The films will usually be oxides, but may be several other non-metallic phases such as graphite or nitrides etc. The bifilms are, of course, a kind of crevice, so that, to some extent, the theory elaborated by Chen and Engler remains appropriate. Even so, we shall see how the bifilm model as a somewhat flexible folded film, exhibiting some rigidity and enclosing films and bubbles of entrained gas, in general, fits the facts more closely than that of a model of a solid particle with a gas-filled crevice.

For an entrained oxide film, the oxygen in the air entrapped in the folded film will be quickly consumed by reaction with the metal to form more oxide. The nitrogen may subsequently be consumed more slowly to form nitrides. Ultimately, however, there will be a tiny residue of only about 1% of the original volume of entrapped air, consisting mainly of argon. The inert gases are practically insoluble in liquid metals (Boom et al., 2000). Thus a spectrum of very fine volumes of inert gas, trapped within oxide fragments, will be expected to be rather stable over long periods of time.

Figure 7.26 shows the order of magnitude relation showing the size and number of bubbles equivalent to that volume percentage of porosity. For instance, 1% porosity can correspond to either a mere 10 pores per millilitre when the pores are 1 mm in diameter, or 10 million pores per millilitre when the pores are only 10 μm in diameter. (In Figure 7.26, the scale of gas content of the melt, assuming the melt to be aluminium, is of course only accurate at larger bubble sizes.

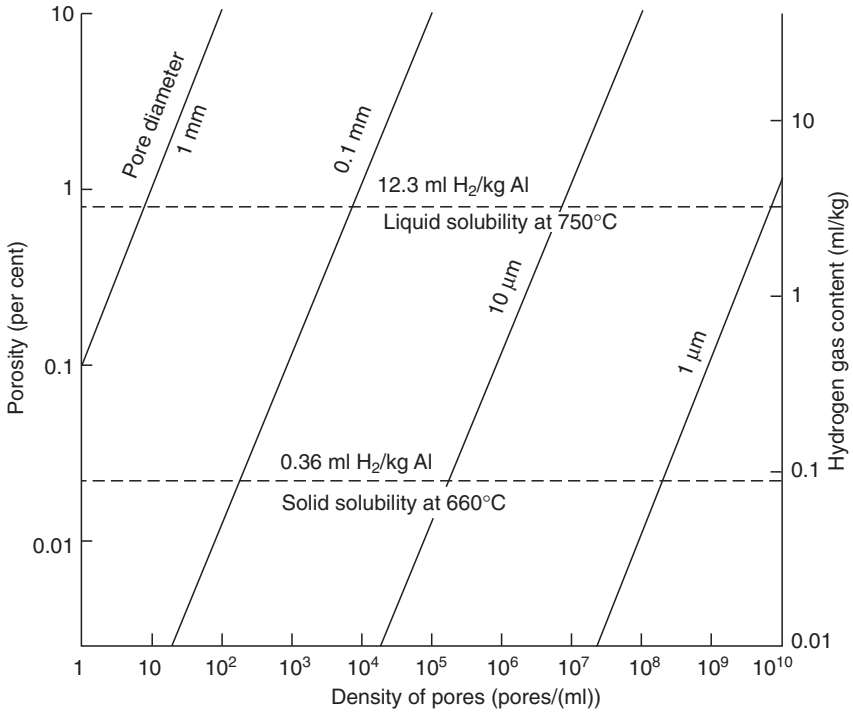

FIGURE 7.26

General relation between volume % porosity and number and size of pores. The solubility of hydrogen in aluminium is superimposed.

It becomes increasingly inaccurate as sizes fall below 0.1 mm in diameter because the internal gas becomes increasingly compressed by the action of surface tension.)

In other more reactive metals, such as liquid titanium, both oxygen and nitrogen have high solubility, leaving only the inert gases that may be insoluble. A micro-bubble distribution introduced on the surface oxide (if any) may be less stable in this material after the oxide has dissolved because the bubbles would be more free to float out. Similarly, in other high-temperature liquids such as irons and steels the greater speed of reactions, the higher density of the melt and its higher surface tension will all tend to limit the lifetime and spread of sizes of any micro-bubble population introduced from this source. Nevertheless, enough of the population may still survive for long enough to cause problems in the short time needed to achieve solidification.

Pore initiation on bifilms

In contrast with all other pore initiation mechanisms, apart from the pre-existing population of pores with which this section has much in common, the bifilm is seen to possess the potential to initiate pores with negligible difficulty. It simply opens by the separation of its unbonded halves. Surface tension is not involved (as is usually assumed when nucleating a pore in a liquid). This is simply a mechanical action between parallel films of (effectively) vanishingly thin oxide separated by a vanishingly thin layer of gas. The acid test of any theory of pore initiation is its capability to explain the experimental data that has previously appeared to be inexplicable. Such data are described later.

The definitive research on the growth of porosity in aluminium alloy castings was that carried out at Alcan Kingston Laboratories by a team led by Fred Major (Tynelius et al., 1993). In this exemplary work, small tapered plates and end-chilled plates of Al-7Si-0.4Mg alloy were cast under varying conditions to separate the effects of gas content, alloy composition, freezing time, and solidus velocity on the growth of porosity in the castings. The reader is recommended to consult this impressively logical piece of work; the first of its kind, and not since repeated at the time of writing.

Normally of course, the effects of solidification time, temperature gradient, and solidification rate are all so closely linked that they are effectively inseparable in most practical casting experiments. However, the experiment was cleverly designed so that the effect of casting geometry was separated out, revealing that the most appropriate thermal parameters to predict porosity were the solidification time and solidus velocity. These gave better results than any of the various temperature gradient terms. They also quantified the dominant effect of hydrogen and the important contribution of strontium.

The outstanding mystery from this work was the parameter 'areal pore density' (i.e. the number of pores per unit area). The results are shown in Figure 7.27. It was found that at short solidification times the pore density *increased* with increasing hydrogen content. However, at long solidification times, the pore density *decreased* as hydrogen content increased. The authors correctly surmised that this curious and baffling result must depend somehow on the nucleation processes at work. However, the finding has remained unexplained ever since. We shall see how the action of bifilms explains this enigma in a natural way.

We assume that conditions at the lower left corner of Figure 7.27 will be characterised by convoluted bifilms of which only the longest and outermost fold is inflated with sufficient gas to be seen as a pore on a polished section. With time (going vertically up the figure), or with additional concentration of gas (travelling along the bottom towards the right side of the figure), the bifilm will partly inflate additional sections, thus creating what would appear to be a cluster of small pores. Eventually, as the remaining sides of Figure 7.27(a) are traversed in progress towards the top right corner, the separate micro-inflated bifilm sections will become sufficiently inflated that the whole bifilm will unfurl, blowing up like a single spherical balloon.

The interpretation of Figure 7.27(a) is outlined in Figure 7.27(b). In the lower left hand corner, gas content is so low and time available so short that any bifilms will be mostly still be closed, having been ravelled up by the action of bulk turbulence. If anything, only the longest section of the bifilm at the outside of the compacted inclusion will be observable as a pore on a polished section because this part of the bifilm will open first, having the largest area to gain gas from solution, and being unshielded from the arrival of supplies of diffusing gas. (Internal folds within the convoluted film will be shielded from outside supply of gas until the defect unfolds.)

As we move from the lower left hand corner up to the top left hand corner, the increased solidification time will have allowed additional gas to diffuse to the bifilm and will begin to open many of the folds. We can call this the micro-inflated stage. A polished section through the bifilm will give the appearance of about 10 times the number of pores, in agreement with observations (Figure 7.27(a)). On the other hand, a move from the lower left corner directly to the lower right corner will similarly micro-inflate the bifilm. Although the time is still short, the amount of gas available is now sufficient to achieve this.

Finally, moving to the top right gives sufficient time and sufficient gas to power the complete inflation of the film. This is expected to occur by successive unfolding actions, as fold after fold opens out. Finally, the bifilm is fully inflated like a balloon. Thus on a polished section only one pore is seen. The main features of Figure 7.27(a) are thereby explained.

Keen readers can check the observed pore densities from the original publication, allowing a rough calculation of the number of bifilms in the original cast metal and the size distribution of the final pores. A further check is the total fraction of porosity. Such checks confirm the consistency of the whole scenario.

The assumption that bifilms are present allows a description of porosity in terms of initiation and growth characterised by considerable sophistication and complexity; the important experimental work by Fred Major would probably otherwise remain unexplained and inexplicable.

As an additional related exercise, we can gain some idea of the rate of unfurling of bifilms from a simple mechanical model as illustrated in Figure 7.28. We shall assume that the unfolding of the bifilm is resisted by a force F of the same type as that resisting the motion of a sphere in a viscous liquid (as in the derivation of Stoke's law). Thus the force would be $3\pi\eta RV$ if it were evenly distributed over the square face of area $R \times R$. Because the velocity V is that at the tip of the

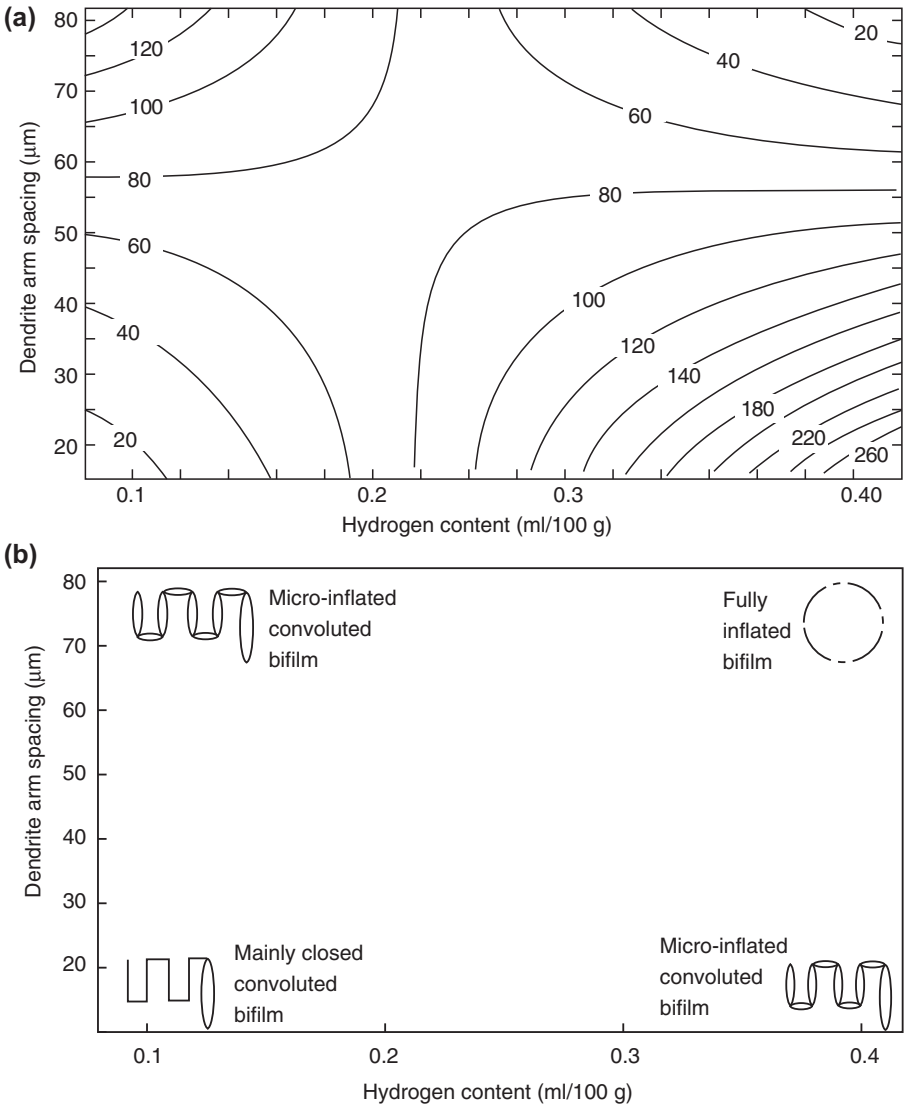

FIGURE 7.27

(a) Experimental results by Tynelius et al., (1993) showing that pore density per cm^2 (the numbers in the figure) increases at fast freezing rates (small dendrite arm spacing, DAS) but decreases at slow freezing rates (large DAS); (b) interpretation by a bifilm model.

bifilm and the pivot of the bifilm is fixed, on average, the resisting force is $3\pi\eta RV/2$. The opening force is that due to the pressure P in the gas phase of the bifilm, acting over the area hR. Equating moments we have:

$$2PRh \cdot (h/2) = 3\pi\eta RV \cdot (R/2)$$

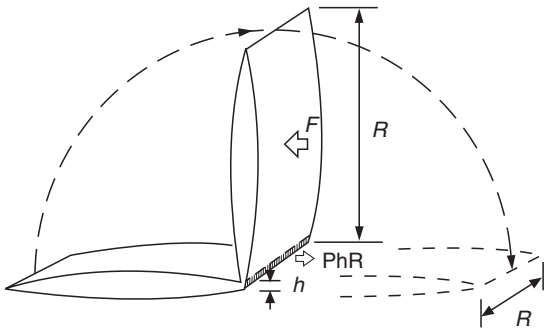

FIGURE 7.28

Model of the unfolding of a bifilm.

so that we can find the opening time t from the speed V and the distance travelled πR:

$$\begin{aligned} t &= \left(3\pi^2/2\right)(\eta/P)(R/h)^2 \\ &= 15(\eta/P)(R/h)^2 \end{aligned} \tag{7.11}$$

For viscosity $\eta = 1.4 \times 10^{-3}$ Nsm^{-2}, and reasonable figures for P of about 0.2 atm (0.2×10^5 Pa) above ambient, and for $R = 5$ mm and $h = 5$ μm, t is only approximately 1 s. Whereas if $R = 10$ mm and $h = 1$ μm, t is approximately 2 min. Thus the rate of opening is seen to be highly dependent on the geometry of the bifilm, as might be expected. Nevertheless, the rates are of the correct order of magnitude to explain the rate of loss of properties in most ordinary castings as the freezing time increases. This wide scatter in the performance of bifilms supports the interpretation of variable nucleation conditions surmised as a result of the sub-surface porosity described in Section 7.2.

7.1.6 GROWTH OF SHRINKAGE PORES

For internal shrinkage pores that are nucleated within a stressed liquid, the initial growth is extremely fast; in fact, it is explosive! The elastic stress in the liquid and the surrounding solid can be dissipated at the speed of sound. The tensile failure of a liquid is like the tensile failure of a strong solid; it goes with a bang.

On a more gentle scale, the audible clicks that are heard as pores nucleate within the melted Tyndall volumes in ice are an exact analogy, and a reminder of the smaller but not negligible tensile stress that is supported in the liquid water before a cavity is nucleated (see Section 7.2.2.1).

In the direct observation of the freezing of Pb-Sn alloys under a glass cover, Davies (1963) recorded the solidification of isolated regions of alloy on cine film at 16 frames per second. It was observed that as these regions shrank, a pore would suddenly appear in between frames. Thus the growth time for this initial growth phase had to be shorter than approximately 60 ms. Almost certainly it was very much faster than this. If in fact the rate of expansion is close to the speed of sound, close to 6 kms^{-1} in liquid aluminium, a pore 1 mm in diameter will form 1000 times faster, in 0.1 μs.

After this explosive growth phase, the subsequent growth of the pore observed by Davies was more leisurely, occurring at a rate controlled by the rate of solidification. Thus this second phase of growth is controlled by the rate of heat extraction by the mould.

For pores that are surface-initiated, the initial stress is probably lower, and the puncture of the surface will occur relatively slowly as the surface collapses plastically into the forming hole. Thus the initial rapid growth phase will be less dramatic.

For shrinkage porosity that grows like a pipe from the free surface of the melt, there is no initial fast growth phase at all. The cavity grows at all stages simply in response to the solidification shrinkage, the rate being dictated by the rate of extraction of heat from the casting.

7.1.7 SHRINKAGE PORE STRUCTURE

7.1.7.1 Shrinkage cavity or pipe

During liquid feeding, the gradual progress of the solidification front towards the centre of the casting is accompanied by the steady fall in liquid level in the feeder. These linked advances of the solid and liquid fronts generate a smooth conical funnel as shown in Figure 7.29. This is a shrinkage pipe.

It is sometimes called a primary shrinkage pipe to distinguish it from so-called secondary shrinkage seen on sections cut through the casting. Secondary shrinkage appears to take the form of a scattering of disconnected pores below the primary pipe. Generally, however, it is easy to demonstrate that water, or a dye, poured in the top of the primary pipe will find its way into most, if not all, of the so-called secondary cavities. Thus in reality the secondary shrinkage cavities are merely the extension of the primary pipe. Thus the primary shrinkage cavity penetrates further into the casting than might be apparent at first sight, as Figure 7.29 makes clear.

In the situation where the shrinkage problem is in an isolated central region of the casting, a narrow freezing range material will give a smooth single cavity. This is occasionally called a macropore to distinguish it from microporosity. There has been much written to emphasise the differences between these two forms of porosity. However, as will be clear from evidence presented in the next section, there seems to be no fundamental difference between them; one gradually changes into the other as conditions change from micro-volumes to macro-volumes of unfed regions, and from skin freezing to pasty freezing. Figure 7.8 illustrates a macropore in a bronze casting of very long freezing range, resulting in a single tapering cavity that has numerous branches, and appearing on a cut section to be thousands of separate cavities constituting a spongy structure.

In the case of the single isolated area of macroporosity, it is important to note that its final location will not be in the thermal centre of the isolated region, as might at first be supposed. This is because the shrinkage pore could be nucleated anywhere within the volume of isolated, stressed liquid. However, immediately after it is formed, it will float to the top of the isolated liquid region. Conversely of course, the situation can be viewed from the point of view of the liquid. This phase, being heavier, will sink, finding its own level in the bottom of the isolated region. The final position of the shrinkage cavity in this case will be as shown in Figure 7.30. Also, of course, the shape and the position of the porosity can be altered by changing the angle of the casting, because the pore floats (or the residual liquid finds its lowest level). An analogy is a stoppered bottle, partly filled with liquid, which is turned through different angles. The bottle corresponds to the outline of the isolated liquid volume in Figure 7.30.

Note once more that the long parallel walls of the casting give a corresponding long tapering extension of the shrinkage cavity. On a cut section, any slight out-of-straightness of this tubular cavity can once again be easily misinterpreted as dispersed porosity, so-called ‘secondary pipe’, as it weaves its way in and out of the plane of sectioning Figure 7.30 (stage 4). In a casting of more complicated shape the shape of the shrinkage pore will take on a corresponding complexity.

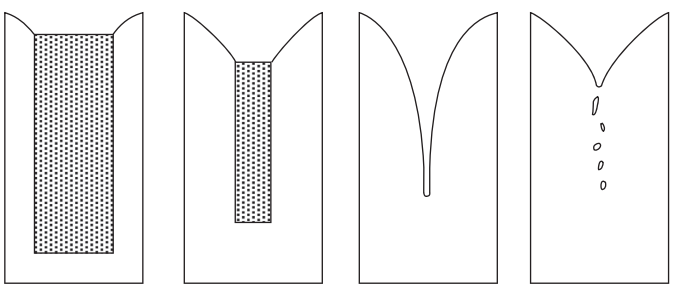

FIGURE 7.29

Stages in the development of a primary shrinkage pipe. Stage 4 is the appearance of stage 3 on a planar cut section if the central pipe is not exactly straight (i.e. it is not a series of separate pores).

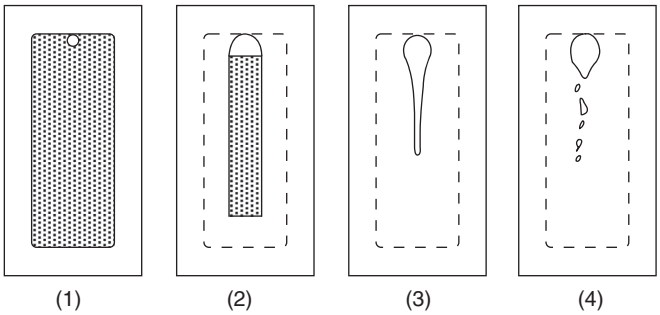

FIGURE 7.30

Stages in the development of an internal shrinkage cavity. Stage 4 is again the equivalent cut section to stage 3. Note that the porosity is not concentrated in the thermal centre, but is offset from the centre of the trapped liquid region, outlined by the broken line, by gravity.

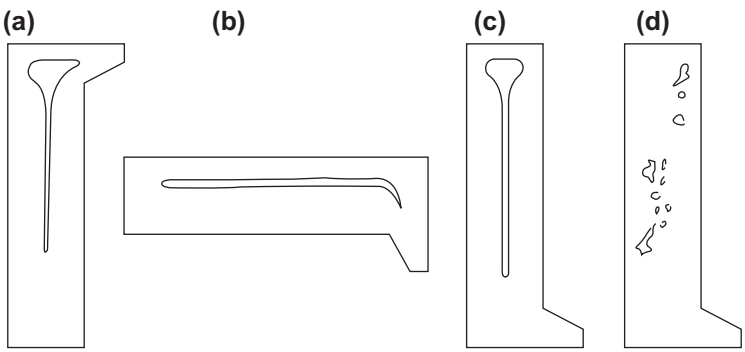

FIGURE 7.31

((a)–(c)) Shrinkage cavity in a short freezing range alloy as a function or orientation. Porosity shown in (d) illustrates some other source of porosity (it cannot be a shrinkage type because of its random form, not linked to the casting geometry).

The effect of gravity on the final form and distribution of porosity is illustrated in Figure 7.31. Clearly, the porosity can be moved from one end of the casting to the other simply by making the casting in a different orientations, a, b and c. (Figure 7.31(d) is simply slipped in to emphasise that porosity having no relation to the casting geometry cannot be shrinkage porosity.)

7.1.7.2 Layer porosity

Alloys of long freezing range are particularly susceptible to a type of porosity that is observed to form in layers parallel to the supposed positions of the isotherms in the solidifying casting. It is known as layer porosity.

Conditions favourable to the formation of layer porosity appear to be a wide pasty zone arising from long freezing range and/or poor temperature gradients. Poor gradients are typical of alloys of high thermal conductivity (such as the light alloys and copper-based alloys) and of moulds having low rate of heat extraction either because of their high temperature (such as in investment casting) or low thermal conductivity (as in sand or plaster castings).

Given these favourable conditions for layer porosity, this variety of porosity has been observed in practically all types of casting alloys, including those based on magnesium (Lagowski and Meier, 1964), aluminium (Pollard, 1964), copper (Ruddle, 1960), steels and high-temperature alloys based on nickel and cobalt (Campbell, 1969a,b). An example in steel is shown in Figure 7.32 and in a nickel-based vacuum cast alloy in Figure 7.14.

It has been argued (Liddiard and Baker, 1945; Cibula, 1955) that layer porosity is the result of thermal contraction, in a manner analogous to hot tearing. Briefly, the theory goes that after the establishment of a coherent dendrite network by the impingement of the dendrite tips, subsequent cooling causes the structure to shrink, imposing tensile stresses on the network, causing the network to tear perpendicularly to the stress, i.e. parallel to the isotherms. If the tears are not filled by the inflow of residual liquid, then layers of porosity are frozen into the structure. Baker (1945) attempted to test whether the porosity was the result of thermal contraction on cooling by casting test pieces in a mould designed to accentuate hot tearing. However, no significant increase in layer porosity was found.

The negative result of Baker's critical experiment is substantiated by numerous observations, particularly the observations by Lagowski and Meier (1964) on Mg-Zn alloys covering the range of zinc contents up to 30% zinc. These clearly reveal that hot tearing peaks at 1%Zn, corresponding to the maximum of the thermal contraction, and well separated from layer porosity that peaks at 6%Zn (Figures 8.8 and 9.11).

Finally, the thermal contraction model is seen in any case to be fundamentally flawed; it is not easy to envisage how such differential cooling could arise to pull apart the centre, when the whole casting is solidifying in the absence of significant temperature differences. In any case, close inspection of the pore structure reveals that it is not the dendrite mesh that is pulled apart; the mesh remains in place, and only the residual interdendritic liquid is missing.

FIGURE 7.32

Radiograph of interdendritic porosity in a carbon steel (Campbell, 1969a,b).

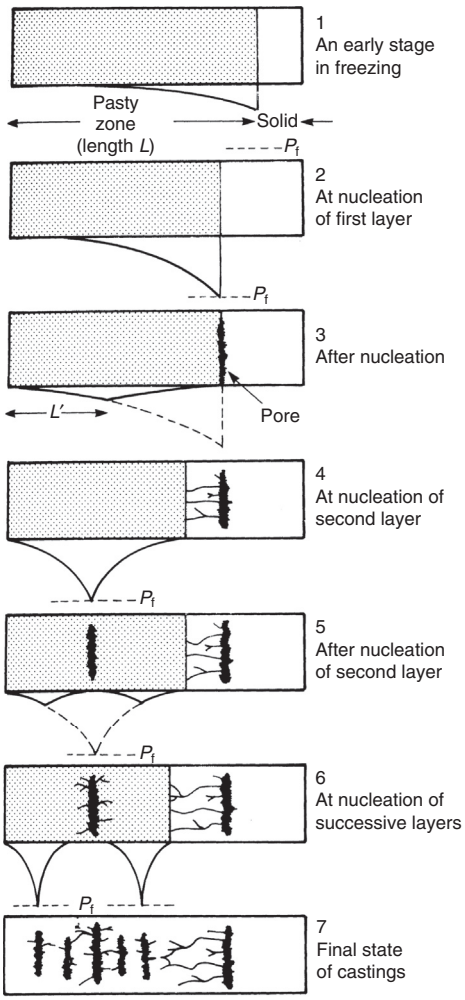

FIGURE 7.33

Schematic representation of the formation of layer porosity (Campbell, 1968a,b).

I therefore felt it necessary to forward a new explanation of layer porosity (JC, 1968c). The new approach avoided the difficulties mentioned previously because it was based not on thermal contraction in the solid as a driving force, but on the contraction of the liquid on solidification; the problem was interpreted as a feeding problem.

The sequence of events in the solidifying casting is shown in Figure 7.33. The stress in the liquid is assumed to be zero near to the feeder on the extreme left. From Eqn (7.5), it is clear that the hydrostatic tension increases parabolically with distance x through the pasty zone of length L, as shown in stage 1, Figure 7.33. The stresses continue to increase with advancing solidification (as the radius R of interdendritic channels continues to decrease) until the local stress at some point along the parabola exceeds the threshold at which a pore will form (by either internal nucleation on an inclusion or by surface puncture). This threshold is labelled the fracture pressure P_f in stage 2.

As soon as a pore is created by some mechanism, it will immediately spread along the isobaric surface (this surface of constant pressure also probably coincides with an isothermal surface and an isosolid surface), forming a layer and

instantly dissipating the local hydrostatic tension. The elastic energy that is available for the initial explosive growth stage is proportional to the difference in areas under the pressure-distance curves before and after this growth. The energy is clearly proportional to the area $L \times Pf$ under the curve. As discussed in the previous section, this first stage of growth would last probably only microseconds, or at the most, milliseconds.

As solidification proceeds further, the solidification contraction in the centre of the remaining liquid region is now fed both from the feeder and by fluid (whether residual liquid, gas or vapour) from the newly created pore. This is a slower growth phase for the new pore, extending via channels towards the region requiring feed metal. The new layer-shaped pore effectively provides a free liquid surface, adjacent to which no large stresses can occur in the liquid.

The maximum stress in the liquid has at this stage fallen by approximately a factor of 4 because the effective length L has now approximately halved. However, because of the progressive decrease in radius R of the interdendritic channels, stress once again gradually increases with time until another pore formation event occurs as at stage 4.

Further nucleation and growth events produce successive layers until the whole casting is solidified. The final state consists of layers of porosity that have considerable interlinking.

Although these arguments have been presented for the case of porosity being formed only by the action of solidification shrinkage, the reader is reminded that the action of gas and shrinkage in combination also fits the facts well as discussed in Section 7.1.5.3 and illustrated in Figure 7.23.

It is important to observe that layer porosity is quite different to a hot tear. A hot tear is formed by the linear contraction of the casting pulling the grains and/or dendrites apart. When they are sufficiently separated, there is insufficient residual liquid to fill the increasing volume, so that a true crack opens up. The crack, of course, supports no load, and represents a serious defect.

In contrast, layer porosity is formed by the nucleation of a pore in the residual liquid. The liquid is in a state of hydrostatic tension, so that the pore spreads along the surface of maximum hydrostatic tension, through the liquid phase. The dendrites stay fixed in place. The final defect is a layer-like pore threaded through with dendrites. It is akin to a crack spot-welded at closely spaced points, and so has considerable tensile strength. On a polished microsection therefore, a hot tear is clear, whereas porosity as part of a layer may or may not be easily identified. It only becomes really clear on a radiograph when the radiation is aligned with the plane of the layers. The layer porosity illustrated in this book (Figures 7.14 and 7.32) are taken from radiographs.

Figures 7.14 and 7.15 show layer porosity in an investment casting as a function of conditions that vary progressively from skin freezing to pasty freezing. It reveals that macroscopic centreline porosity, layer porosity and microscopic dispersed porosity transform imperceptibly from one to the other as mould temperature alone is increased, effectively reducing the temperature gradient during solidification. It is clear, therefore, contrary to many widely held views, that there are no fundamental differences between the various types of macroporosity and microporosity. They are simply different growth forms of shrinkage porosity under different solidification conditions.

Similarly, Jay and Cibula (1956) carried out interesting work on Al-Mg alloys, in which they showed that as the gas content of the alloy was increased, the porosity changed gradually from layer porosity to dispersed pinhole porosity (Figure 7.34). Thus these two extreme categories of shrinkage and gas microporosity were demonstrated to be capable of being mixed, allowing a complete spectrum of possibilities from pure shrinkage layer type to pure dispersed gas type.

This merging and overlap of all the different types of porosity makes diagnosis of the cause of porosity sometimes difficult in any particular case. However, it is better to know of this difficulty, and thus be better able to guard against falling into the trap of being dogmatic. Section 7.3 gives some guidance on the diagnosis of the various types of porosity.

The previous classical description of the formation of layer porosity was conceived before the discovery of bifilms. Thus the theory, based on the nucleation of pores by the accumulated build up tension because of the difficulty of interdendritic flow, and their subsequent growth along isobaric surfaces, seems to me probably still essentially correct. However, now that the presence of bifilms has been realised, it is necessary to take account of the effect they may have in such situations where interdendritic feeding is difficult. It seems likely that bifilms would interfere with the flow of residual liquid through the dendrite mesh. The close spacing of dendrites, providing support for the films, would ensure

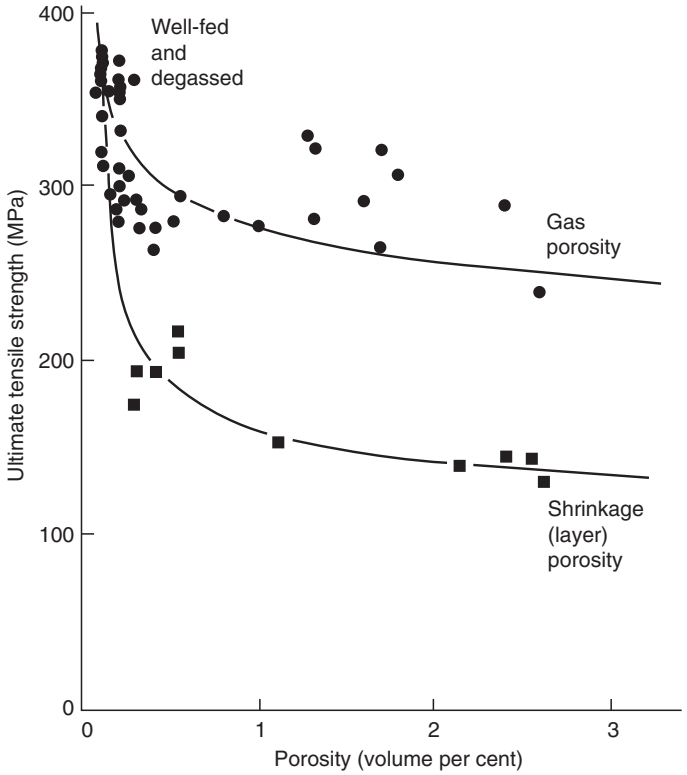

FIGURE 7.34

Reduction in UTS of an Al-11.5Mg alloy by dispersed porosity and by layer porosity.

Data from Jay and Cibula (1956).

that they would be capable of resisting large pressure differences across their surface. Thus bifilms transverse to the flow would halt the upstream flow, but be sucked open by the downstream demand, creating a series of shrinkage cavities arranged generally transverse to the flow direction. Such a scenario is not greatly different from that of the classical theory presented previously and might be difficult to separate experimentally because the nucleation events in both explanations would be assumed to be bifilms. Ultimately, cleaning the melt will be a certain technique to eliminate layer porosity irrespective of its formation mechanism.

7.2 GAS POROSITY

Sub-surface porosity in casting is a common fault, if not more common than any other type of gas porosity from gases in solution in the metal. Sometimes, the sub-surface pores are broken into by the loss of surface scale during heat treatment, as is common for steel castings, or are broken into during shot blasting to clean the castings. However, sometimes the problem is not seen until the first machining cut. Pores can originate by completely different processes (1) from entrained air bubbles during turbulent pouring; (2) from core blows or condensation on chills; and (3) by the precipitation of gas from solution in the melt. The processes are considered in order later.

7.2.1 ENTRAINED PORES (AIR BUBBLES)

Sub-surface pores can form as a result of the flotation of air bubbles that have been entrained during the pouring of a casting. These bubbles are about 5 mm in diameter or smaller because larger bubbles will in general escape, but at 5 mm and below they do not have sufficient buoyancy to break through the double oxide (their own oxide skin and the oxide skin on the surface of the casting) when they reach the surface of the casting, and so remain trapped. They sit immediately under the surface of the casting, only two oxide thicknesses deep, and so extremely near to the surface and extremely easily broken into. These bubbles are always clustered in specific sites, having floated into position, often above ingates, and have a spread of sizes, typically 1–5 mm in diameter.

This 5 mm limit on size is the result of a mechanical limitation and is a certain identification of these pores as being air bubbles entrained during the pouring of the casting. This size of bubble is too large to be generated by a diffusion reaction, as described later, thus they are definitely not, for instance, hydrogen pores nucleated and grown in situ during the freezing of the casting. It is a waste of time therefore to attempt to remove them by degassing the melt!

There is a large amount of research literature claiming that such bubbles in cast irons, associated with oxide slags, are the result of a reaction between the carbon in the iron and the oxygen in the slag, to create a CO bubble. This is clearly a mistake for a variety of reasons.

1. The bubbles are nearly always too large to be produced by a diffusion reaction.
2. The size range of bubbles corresponds to bubbles entrained by turbulent filling systems.
3. The filling systems are always turbulent.
4. The slag is nearly always generated in the filling system by the turbulent mixing of the melt and air, and so naturally occurs in association with the entrained air (although it is recognised that after swimming through the melt, the bubble will have acquired a contribution of CO, and probably H_2).

It is important to recognise the sub-surface bubbles generated by a turbulent filling system. They are quite different to those bubbles formed in situ during solidification which are characterised by their uniform size (i.e. typically 0.5 mm in diameter or smaller for castings up to a few hundred kilograms or so, hence normally smaller than one tenth of the size of entrained air bubbles) and uniform distribution over much of the outer surface of the casting (in contrast with the clustering of entrained air bubbles). Sometimes in situ formed bubbles are uniformly distributed only the upper parts of the casting because the pressure at greater depth suppresses the formation of bubbles.

A widely accepted theory of the origin of the in situ grown sub-surface porosity has been summarised by Turkdogan (1986). He describes how sub-surface porosity occurring in cast irons and steels poured into greensand moulds is a consequence of metal-mould interaction. Gas bubbles form in crevices of the mould in contact with the metal, and bubble into the metal, where they become trapped during the early stages of solidification. The action of alloying elements on the process is discussed in terms of their effect on the surface tension of the liquid metal; a lower surface tension allows bubbles to enter the metal more easily, thereby increasing the sub-surface porosity.

The theory is similar to the micro-blow theory outlined later in Chapter 10, Rule 5. However, micro-blows are probably effectively suppressed by the presence of a strong surface film, such as is normally found on many Al alloys, irons and steels. Thus there are several difficulties with the theory as put forward by Turkdogan.

1. The metal does not in general enter the crevices of the mould. The high surface tension (plus the effect of a strong, fairly rigid surface film) causes the liquid to bridge between high spots, leaving the crevices empty. Mould washes that promote the wetting of the mould by the metal, such as those that are based on sodium silicate, actually reduce sub-surface porosity.
2. The pressure required to force small bubbles (radius of 1 mm or less) into the liquid metal against the resistance of surface tension is high. Conversely, it is known that the pressures attainable at the surface of a mould, from which gas can easily migrate away through the mould to the atmosphere, are very low. Thus it seems

unlikely that small bubbles could be forced into the metal in this way. (Large bubbles, with radii measured in centimetres, and therefore small pressure requirements, can be forced in to the metal from outgassing cores; Chapter 10, Rule 5.)

3. Tellurium additions to cast iron reduce surface tension and should, according to the penetration theory, increase porosity. In fact, tellurium additions are found to decrease porosity.
4. The theory is not capable of explaining the occurrence of sub-surface porosity in inert moulds such as investment moulds, which are free from gas-forming materials such as moisture and hydrocarbons.

Features 1 and 2 of the list may not always be relevant, because the micro-blow conditions may apply as described in Chapter 10, Rule 5. However, features 3 and 4 remain important damning evidence.

We shall therefore assume that in general the formation of sub-surface porosity does not occur by mechanical penetration of the liquid surface by bubbles from the mould.

7.2.2 BLOW HOLES

When sand cores are surrounded by liquid metal, the heating of the core will expand its content of air contained between sand grains and will start to degrade its binder causing gas to be generated. Normally, the core will be designed to permit gas to escape through the core prints and so be dissipated in the mould. In this way, high gas pressure inside the core can be avoided.

In some circumstances, however, the gas in the core may be generated at such a high rate, as in a thin core in a steel casting, faster than it can escape. Its internal pressure may then rise to a level higher than that in the liquid, forcing a bubble out into the melt. This forcing of gas into the liquid can be nearly explosive. The gas bubble is *blown* into existence. *Blow defect* is therefore a good name for this type of gas pore.

The reader needs to be aware that the name '*blow-hole*' is, unfortunately, widely misused to describe almost any kind of hole in a casting. In this work the name '*blow-hole*', '*blowhole*' or simply '*blow*', is strictly reserved solely for those defects which are forced (actually '*blown*') into the liquid metal via the forced mechanical penetration of the liquid surface. The term is therefore quite specific and accurately descriptive. (The term excludes pores nucleated internally by the precipitation of gas dissolved in the liquid, or diffusing in from the surface, and also excludes bubbles entrained by surface turbulence.) The reader is encouraged to use the name '*blowhole*' with accuracy.

The contribution of surface tension to increasing the pressure required is practically negligible in the case of *core blows* because of the large size of the bubbles that are formed in this process (Figure 7.35). Core blow bubbles are large, lazy, wobbling bubbles, containing gas at low pressure. They are quite unlike micro-blows, if these exist, to be discussed later. The effect of surface tension at such small radii causes these tiny bubbles to behave like hard spheres resembling mini ball bearings.

Core blow bubbles create trails as they rise through a melt. The trails are, of course, a similar form of bubble damage to that of turbulence-entrained bubbles discussed under Rule 4. However, they are sufficiently distinct that they benefit from separate consideration.

For instance, bubble damage arising from surface turbulence in the filling system takes quite a different form. The bubbles are generated by the high velocities in the front end of the system (in the basin, sprue or runner). The high shear stresses in the melt, especially in tall castings, ensure that the bubbles are chopped mainly into small sizes, in the range 1–10 mm diameter. Some of the smaller bubbles have been observed in video radiographic studies to coalesce in the gate. These coalesced bubbles float quickly, before any significant solidification has taken place, and so burst at the liquid surface and escape. A bubble smaller than about 5 mm in diameter has only a tenth of the buoyancy of a 10 mm bubble, and cannot force the splitting of the oxide films that bars its escape. Bubble 'A' in Figure 7.36(a) illustrates such a case. If such a bubble succeeds to reach the top of the casting it therefore remains trapped at a distance only a double oxide skin depth beneath the surface of the casting.

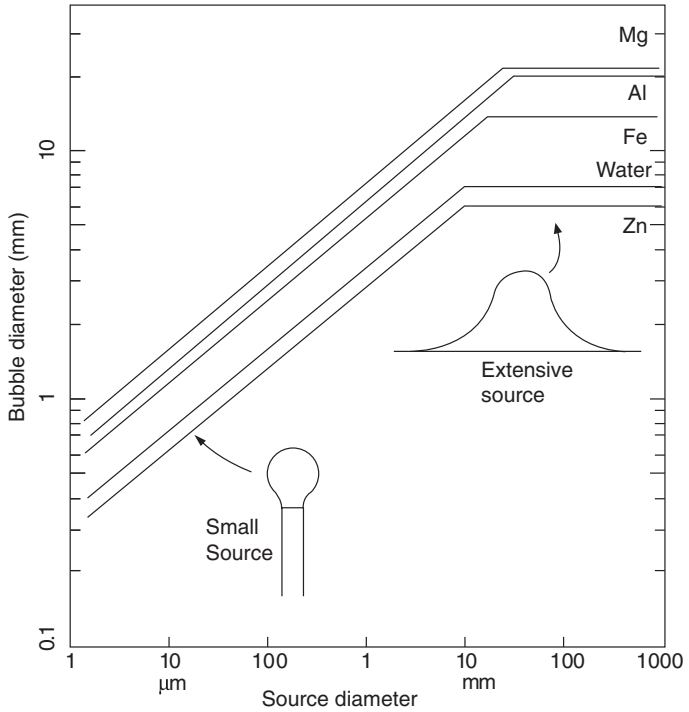

FIGURE 7.35

Size of bubbles detaching from a range of sizes of source in a variety of liquids.

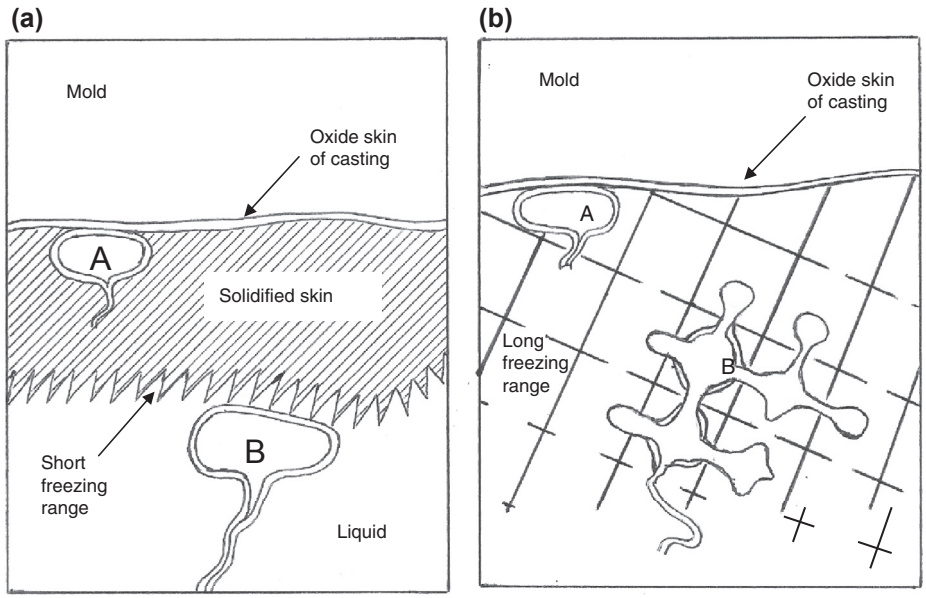

FIGURE 7.36

Bubbles arriving at the cope in (a) a skin-freezing alloy and (b) a long freezing range alloy. Bubbles 'A' arrive early, probably originating from entrainment during pouring. Bubbles 'B' arrive late; in the dendritically freezing alloy the bubble now grows interdendritically, but can, of course, be grown either by additional gas or by shrinkage.

The bubble given off by the outgassing of a core is quite different. These bubbles are large. In irons and steels, the single core blow bubble is about 13 mm in diameter. In light alloys, the effective bubble diameter is approximately 20 mm (Figure 7.36(b)). Although these large bubbles have high buoyancy, they are not produced immediately. The timing of their eruption into the melt determines the kind of defect that is formed in the casting.

If, in relatively thick sections, the bubble detaches before any freezing, the repeated arrival of bubbles at the surface of the casting can result in repeated build-up of bubble skins, forming multiple leaves of oxide, well-named as an *exfoliation defect* (Figure 7.37(a)). Exfoliated structures are those that have been expanded and delaminated, like puff pastry, or like the conversion of slate rock into vermiculite or like leaves from a book.

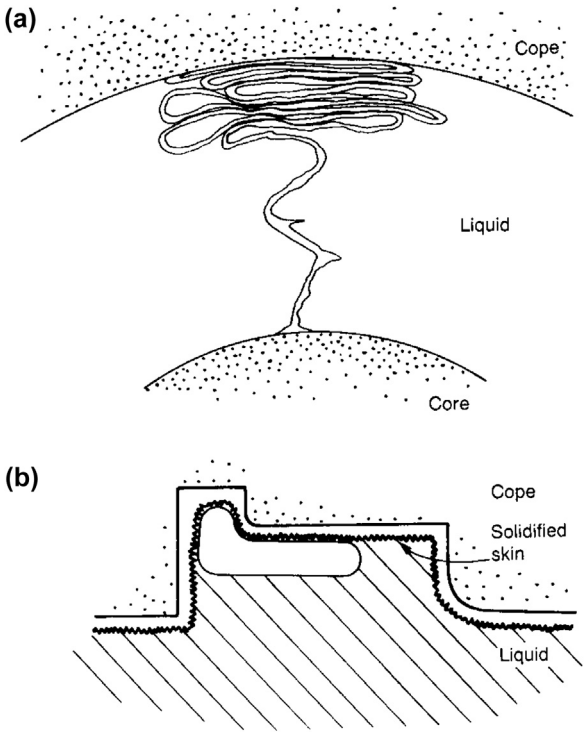

FIGURE 7.37

(a) An exfoliated dross defect produced by copious gas from a core blow before any solidification; (b) trapped gas from a core blow evolved sometime after solidification.

Exfoliated dross defects are recorded for steels containing 0.13C, 1Cr, 0.5Mo and 0.4A1 (Frawley et al., 1974), and for ductile iron (Loper and Saig, 1976). The content of film-forming elements in these alloys is of central significance. For ductile iron (containing magnesium) the defect is described as a wrinkled or pastry-like area, and when chipped out appears to be a mass of tangled flakes resembling mica that can be easily peeled away. Polished microsections of the defect confirmed its structure as composed of tangled films, and contrasted with the structure of the rest of the casting which was reported as excellent. Exfoliated defects are observed in irons and steels where the earlier outgassing of the core precedes any significant freezing of the skin of the casting (this contrasts of course with the light alloys where the leisurely development of pressure in the core usually allows time for some skin freezing of the casting, with the consequent development of a characteristic massive bubble under the solidified skin) (Figure 7.37(b)).

Once a core has blown its first bubble, additional bubbles are easily formed because the bubble trail seems usually to remain intact and keeps re-inflating to pass additional bubbles along its length. The bubbles contain a variety of gases, including water vapour, that are aggressively oxidising to metals such as aluminium and higher melting point metals. Bubble trails from core blows are usually particularly noteworthy for their characteristically thick and leathery double oxide skin, built up from the passage of many bubbles. This thick skin is part of the reason why core blows result in such efficient leak defects through the upper sections of castings. Bubble trails from core blows are particularly damaging because they are, of course, automatically connected from a cored volume of the casting, and often penetrate to the adjacent core (because little solidification will usually have occurred between cores to stop it). Alternatively, in thicker sections, they travel from the core to the very top of the casting.

After the emergence of the first blow into the melt, the passage of additional bubbles contributes to the huge growth of some blow defects. Often the whole of the top of a casting can be hollow. The size of the defect can sometimes be measured in fractions of metres. An accumulating bubble will spread under the dendrites, as, inversely, a large limp balloon would float down to sag on the tips of conifer trees.

These trapped bubbles are recognisable in castings by their size (often measured in centimetres or even decimetres!), their characteristic flattened shape and their position several millimetres under the uppermost surfaces of local regions of the casting (Figure 7.37(b)). In addition, of course, they will faithfully follow the contours of the upper surface of the casting. Like the bubble trail mentioned previously, the core blow defect is sometimes so impressively extensive as to be difficult to perceive on a radiograph.

As an example, the author remembers making a delightful compact aluminium alloy cylinder block for a small pump engine. At first sight, the first casting appeared excellent and unusually light. It seemed that the designer had done a good job. A close study of the radiograph revealed it to be clear of any defects. However, on standing back to take a more general view it was noticed that a curious line effect, as though from a wall thickness, could not be found on the designer's drawing. It took some time to realise the casting was completely hollow; the smooth and extensive form of the core blow faithfully followed the contours of the casting. The prolific outgassing of the water jacket core around the bores of the block was found to be the source. The water jacket core was stood upright on its core prints (the only vents) that located in the drag. The problem arose because of the very slow filling velocity that had been chosen. Vapours were driven ahead of the slowly rising metal, concentrating in the tip of the water jacket core (unfortunately unvented at its top). Thus, by the time the melt arrived at the top, it was unable to cover the core because of the rate of gas evolution. One unhelpful suggestion was that the technique seemed an excellent method for making ultra-light-weight hollow castings. The problem was solved by simply increasing the fill rate, covering the core by the melt before outgassing started. Core gasses were then effectively sealed into the core, and were vented in the normal way via the prints at the base of the core.

A lesson is clearly drawn from this experience: it is far better if possible to vent cores from their top. A somewhat slow filling rate is then not such a danger.

In the case of core blows completely through thin walls, the bubble has no chance to grow to a large size before it has penetrated the wall. Thus the 'bubble trail' becomes merely a hole in the wall of a thin wall casting. Figure 7.38(a) shows a fracture surface made through a core blow defect in a grey iron casting that provided a leak path through the wall thickness (the left and right hand edges of the wall can be seen in the figure). The other images in this figure illustrate progressively closer views of this defect, revealing its astonishing detailed structure. The bubble trails are formed from an oxide in the form of a glassy iron silicate. Figure 7.38(b–d) shows the unusual form of these trails; they appear to reveal clusters of paths made by individual bubbles. Cast iron appears unique in that its bubble trails appear to detach from the matrix. (Similar behaviour has been noted for the lustrous carbon film that forms on the liquid iron meniscus, but becomes trapped against the mould during mould filling, and finally detaches from the casting and adheres to the mould surface after the casting is shaken out; see Section 6.5.)

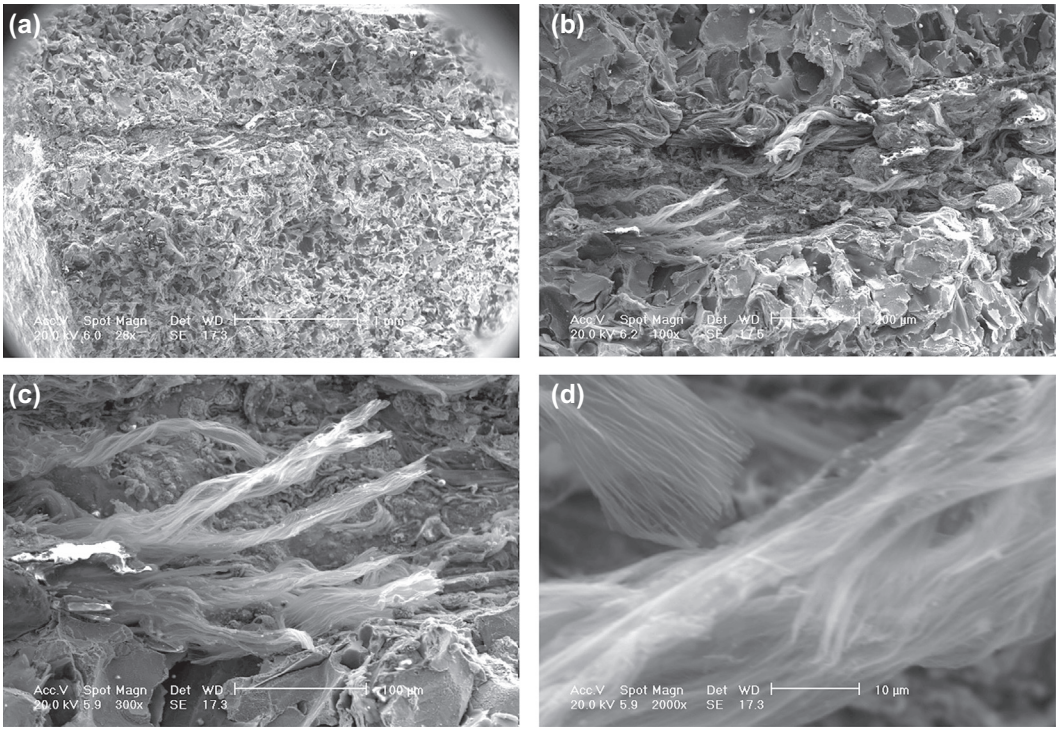

FIGURE 7.38

A leakage defect from a core blow through a 4 mm wall in grey iron. (a) Secondary electron image of a fracture through the defect, showing the leakage channel only about 300 μm diameter; (b) an irregular group of glassy silicate bubble trails near the centre of the leak path; (c) closer view of the twisted form of some silicate trails; (d) close-up of translucent glassy fluted trails (foreground trail is necessarily out of focus).

At other times, the bubbles trails are formed from a lustrous carbon film (Figure 7.39). The carbon film appears to be somewhat more rigid than most oxide films, as suggested by its characteristic smooth surface shown in Figure 7.39(b) and (c), resisting the complete collapse of the trail, and retaining a more open centre. In effect, the bubbles punch holes through the cope surfaces of the casting, so that their more open trails, as irregular tubes, form highly efficient leak paths.

The core blow seen in Figure 7.39(a) has caused a severe leak through the wall of an iron casting. The detail is revealing: the region A is a carbon based bubble trail; C is a portion of matrix iron, whereas B is an irregular mass of iron silicates that was probably the original series of bubble trails when the emerging gases from the core blow were mainly expanding air and water vapour, both highly oxidising, and thus creating glassy silicate trails at that early stage. While the water vapour is evaporating from the core, the temperature of the core is held down at close to 100°C. When the core is finally dry, its temperature now increases sufficiently to drive off carbonaceous volatiles. These would now react on contact with the matrix to create carbonaceous bubble trails. However, in the meantime, the original glassy silicates would partially melt and be churned by the continuing and possibly accelerating maelstrom of gases into irregular masses of slag (the iron silicates). The finding of slag in castings, especially in bubble trails, is usually the result of the local

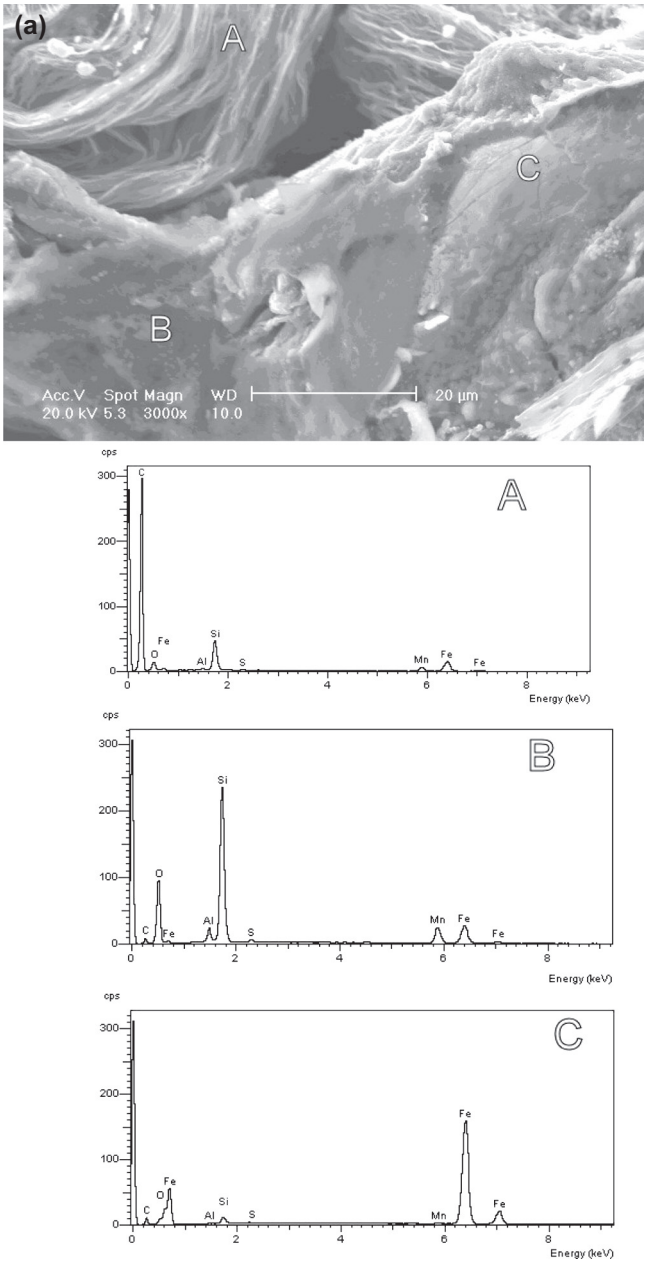

FIGURE 7.39

Bubble trail that had caused a leak, probably formed later by core blow in grey iron. (a) General view inside trail showing 'A' carbon films, 'B' oxides (silicates) and 'C' matrix alloy; (b) other areas of carbon film; (c) close-up of plate-like carbon film.

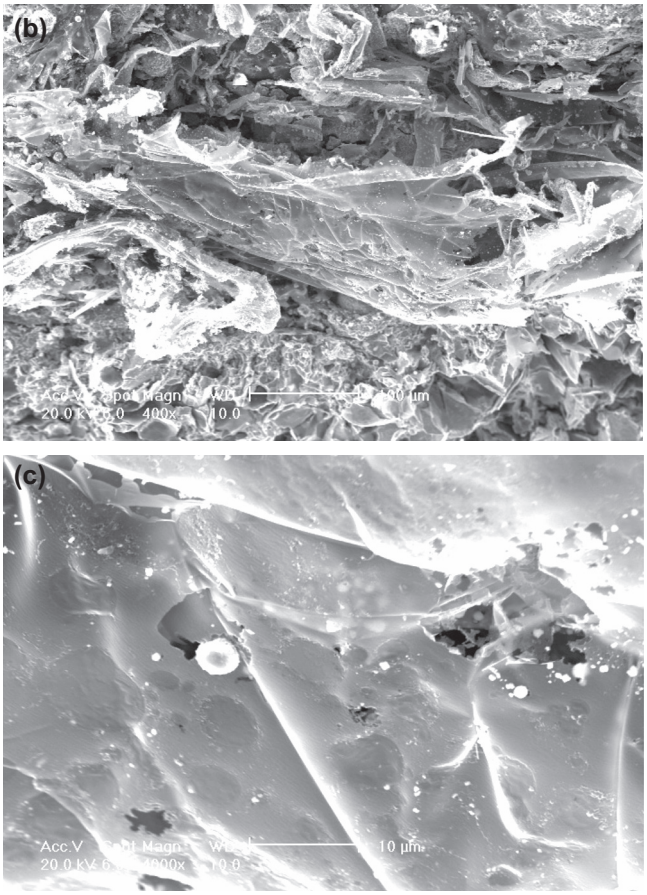

FIGURE 7.39 Cont'd

generation of slag by local oxidation of the melt; in my experience, especially when using a good offset step basin, the appearance of slag is rarely the result of the ingress of slag from the poured metal; it is the result of in situ creation of oxides by entrained air or core gases.

Blows can sometimes form from moulds. Whereas founders are familiar with the problem of blows from cores, blows from moulds are rarely considered. In fact, this is a relatively common problem (even though this section remains entitled 'Core Blows' as a result of common usage). The huge volumes of gas that are generated inside the mould have to be considered. They need room to expand and escape. Any visitor to an iron or steel foundry will be impressed with the jets of burning gasses issuing from the joints of moulding boxes. Effectively the gases and volatiles will be fighting to get out. It is prudent therefore to provide them with escape routes because the alternative escape route via the liquid metal in the mould cavity can spell disaster for the casting.

Mould or core blows usually emerge from the highest point of the core, especially if this is a sharply upward-pointed shape, like a steeple of a church (Figure 7.40). The bubbles will collect and detach preferentially upward from an upward-pointing shape. (The detaching bubble is the upside-down equivalent of the drop of water falling preferentially from the

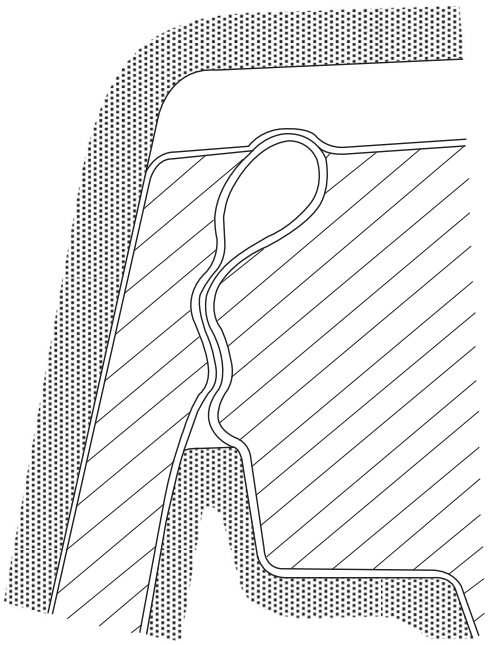

FIGURE 7.40

Detachment of a bubble from the top of a core, bequeathing a bubble trail as a permanent legacy of its journey. This bubble, unusually, may be early enough to escape at the free surface of the rising metal.

tip of a downward-pointing stalactite.) Such shapes are therefore best avoided or the whole mould assembly turned upside down for casting. Core bubbles will, of course, detach from flat surfaces but with much greater reluctance.

Theory indicates (Campbell, 1971) that the size of a detaching bubble is linked to the size of the source. The results of calculated bubble diameters are shown in Figure 7.35 and reveal that even though a bubble might detach from a horizontal surface, and so be of maximum size, its size is limited to 10–15 mm or so, depending on the liquid. However, final sizes of core blow defects vary in size typically from 10 to 100 mm in diameter, showing that they are usually the accumulation of many bubbles, or possibly even the result of a constant stream of gas funnelled along a single bubble trail, arriving and coalescing under the solidifying skins of castings.

Blows from cores surrounded by light alloys are relatively gentle; leading to the generation of one or usually a succession of large bubbles. The minimum diameter of bubble that can form on a core is perhaps 10–20 mm (Figure 7.35). If the core contains gas at sufficient pressure to overcome the hydrostatic pressure and cause a blow defect, then it will usually have enough volume to continue to blow for some time. In this way, strings of bubbles from the core can accumulate to create a massive single gas cavity near the top of the casting. The diameter of this cavity can easily reach 100 mm. The whole top half of a casting can be made hollow by this process. (It suggests an interesting manufacturing technique for hollow ware!)

For cores surrounded by liquid cast iron, or even more especially, steel, the effects are explosive. The very much higher temperature ensures that the core outgassing occurs with much greater energy and much earlier, before much if any freezing of the metal has taken place. Instead of bubbles issuing from the pressurised source, gas can escape as high velocity jets. Metal can therefore be violently ejected from the open tops of moulds and the resulting casting is usually found to contain a mass of confusing defects; the quality of the casting can be effectively destroyed. There are usually no remains of the single large void or heavily oxidised bubble trail as is found for the gentler reactions in the light alloys.

In the light alloys, the core will usually take time to absorb heat, and build up its pressure before blowing; during this time, the top of the casting will usually have become partly frozen. Thus because of its late arrival, a core blow in these metals is often some distance beneath the top surface, with its upper surface faithfully following the contours of the top of the casting. (Note that this behaviour contrasts sharply with (1) 'real' gas porosity that starts only 1 or 2 mm sub-surface and contrasts with (2) turbulence-entrained gases that arrive early, together with entry of the liquid metal into the mould, and which are prevented from escape only by the thickness of the surface oxide film.)

In the event of large cavities in the top of the casting, an unvented core should always be viewed with suspicion. All cores benefit from being internally vented to reduce the build-up of pressure that might lead to blows. It is also important to be aware of blows from sources other than cores and moulds. The practical and quantitative aspects of this subject are addressed in Section 10.5.

Micro-blows

It is conceivable that small pockets of volatiles on the surface of moulds might cause a small localised explosive release of vapour that would cause gas to be forced through the (oxidised) liquid surface of the casting to form an internal bubble. Poorly mixed sand containing pockets of pure resin binder might perform this. Alternatively, sand particles with small cavities filled with a volatile binder material might act as cannons to blast pockets of vapour into the metal. On arrival of the hot metal, the small pocket of binder would be expected to heat to a temperature probably well above its boiling point. Thus after a few seconds the superheated binder would explosively vapourise, like a cannon, firing its vapour jet into the casting. There seems strong evidence that the synthetic spherical particle aggregates made from powdered refractories are in this category. Close examination of these under the scanning electron microscope might reveal evidence of a neck connecting to the external atmosphere.

Other evidence for micro-blows comes from the strip casting of steel between twin rolls (Ha et al., 2008). 'Dent' defects are observed that are 0.3–1.5 mm in diameter and up to 0.5 mm deep. Sometimes taking the form of a simple depression, but sometimes a characteristic form of a blow defect, connected to the surface with a narrow neck linked to an internally spherical shape. These miniature gas pockets were found to be the result of the roughness of the roll surface, so that gases entrapped in microscopic depressions in the roll surface expanded on arrival of the melt, causing a gas bubble to be driven into the liquid.

Figure 7.35 indicates that for the blowing of bubbles of less than 1 mm diameter in some common liquid metals, the source of the high-pressure gas needs to be only a few micrometres in diameter. The pressures inside such minute bubbles are easily shown to be high, of the order of 1 MPa (10 atm).

For sand castings, there is no direct evidence for this mechanical mechanism of sub-surface pore formation. The mechanism for the creation of sub-surface porosity remains obscure. It awaits creative and discriminating experiments to separate the problem from classical processes such as diffusion, in which the gases travel from the mould, across the mould/metal interface into the casting as separate atoms, albeit in swarms, the interface being mechanically undisturbed by this inward flow of elements. Such diffusive transfer is assumed in most of the remainder of this book. However, the reader should be aware of the possibility of mechanical transfer of gases, possibly as eruptive events, disrupting the casting interface as minute explosions.

An observation of a surface interaction that is worth reporting, but whose cause is not yet known, is described below. It may therefore have been allocated to the wrong section of the book. It is hoped that future research will provide an answer.

In the study of interactions between chemically bonded sand moulds and liquid metals, a novel and simple test was devised in the author's laboratory (Mazed and Campbell, 1992). It was prosaically named the 'wait and see' test. It consisted simply of a flat horizontal surface of a bonded aggregate onto which a small quantity of metal was poured to give a puddle of 50–100 mm in diameter. The investigator then waited to see what happened. If anything was going to happen it was not necessary to wait long.

When Al-7Si alloy was poured on to the flat surface of either a phenolic-urethane (PF) or furane/sulphonic acid (FS) bonded silica sand the puddle of liquid alloy maintained its mirror smooth upper surface. The same was true when Al-7Si-0.4Mg alloy was poured on PF-bonded sand. When the puddles of liquid metal had finally solidified, they had retained their top mirror-like surfaces and after sectioning were found to be sound.

However, when Al-7Si-0.4Mg alloy was poured on the FS-bonded sand, the effect was startlingly different. After several seconds, a few bubbles not exceeding 1 mm in diameter were observed to arrive at the surface, underneath the surface oxide film, raising up minute bumps on the mirror surface. After a few more seconds, the number increased, finally becoming a storm of arriving and bursting bubbles, destroying the mirror. The final sessile drop was found to be quite porous throughout its depth, corroborating the expectation that the bubbles had entered the drop at its base because of a reaction with the sand binder.

That this reaction was only observed with certain binders and with certain alloys originally suggested to the author a chemical mechanism. At the time of the work, this was thought unlikely because the diffusive transfer of gas into the melt would result in gas in solution. Having an equilibrium pressure of only about 1 atm (because the pressure at the mould surface was originally thought to be limited to this level), it would have been difficult to nucleate small bubbles. However, it has been more recently realised that the presence of bifilms in the alloy practically eliminates the nucleation problem, and so might make the process feasible. This will be especially true because some melts will, partly by accident and partly as a result of alloy susceptibility, have different quantities and different qualities of bifilms. The 0.4Mg-containing alloy would have been expected to contain a different concentration and a different type of bifilm compared to the Mg-free Al-Si alloy.

Even so, a mechanical process cannot be ruled out at this stage. For instance the presence of Mg in the Al-7Si alloy may cause MgO formation at the metal/mould interface leading to a convoluted and microscopically fractured surface oxide film that may be more easily penetrated by high-pressure gas. High local pressures might arise particularly if the FS binder was not as well mixed as the PF binder, leaving minute pockets of pure binder in the sand mixture of the plate core. Thus the quality of mixing may be important.

Clearly, there is no shortage of important factors to be researched. Probably it will always be so. In the meantime, the best we can do is be aware of the possible effects and possible dangers, and have patience to live with uncertainty until the truth is finally uncovered.

7.2.3 GAS POROSITY INITIATED IN SITU

General

I hesitate to call this ‘true gas porosity’, but that would convey the correct sense. It is porosity that arises as a result of gas, in solution in the liquid metal, which precipitates out during solidification.

It is necessary to re-emphasise that the formation of pores is not necessarily easy. The presumption that pores form immediately on solidification or because the solubility limit has been reached is, unfortunately, a widespread delusion. The gas in solution in the liquid, rejected ahead of the advancing solidification front, can reach high levels of supersaturation without the formation of a single pore if no convenient nucleation sites are present. The gas would simply remain in supersaturated solution. For aluminium alloys, the presence of supersaturated hydrogen in the solid does not appear to be harmful. For hydrogen in ferritic steels, however, the hydrogen may lead to the serious problem of hydrogen embrittlement. (Although even this does not seem to be certain. Even hydrogen embrittlement in steels may be a bifilm problem. If it is, this would explain why it has proven so difficult to understand over the many years that the phenomenon has been the subject of intensive research.)

In this section, we shall assume that there are plenty of nuclei on which gases can precipitate during freezing. The only viable nuclei will normally be bifilms because they offer such an easy precipitation site and minimal (if somewhat variable) resistance to unfurling.

In metals that solidify dendritically, the precipitated gas appears in the interdendritic spaces, and so is a well-dispersed, fine precipitate. This is its usual form. For castings of a few kilograms in weight the pores are usually in the range of 0.01–0.5 mm in diameter, and uniformly distributed throughout the whole casting. They can be up to a millimetre or so in diameter for larger castings. In general, however, these pores are so small that they are often invisible on a machined surface of an Al alloy because a cutting tool with a carbide tip will smear the metal over, concealing such microscopic defects. On the other hand, a diamond-tipped tool will cut cleanly, and thus render the defect visible, perhaps with the aid of a magnifying glass.

Al alloy automotive pistons in the United Kingdom used to be machined with carbide-tipped tools. On the introduction of polycrystalline diamond–tipped tools in the 1970s, the piston foundries were brought to an alarming stop. They were suddenly confronted with the appearance of porosity in their castings as a result of the cleaner cut of the sharper diamond tools. In reality, of course, the pistons were unchanged. However, no customer was prepared to buy pistons that were clearly peppered with holes. The industry was forced to make a traumatic leap in the quality of its liquid metal, and lived to fight another day.

It has to be kept in mind that the source of gas in solution can be that in the metal from the melting conditions. For a sand casting, additional gas in solution will have been acquired during its journey through the runner, and from continuing reaction with the mould during and after mould filling. All of these sources cooperate, and may raise the gas content of the metal over the threshold at which pores will initiate and grow.

We shall see how it is to be expected that gas pores will form as the consequence of normal segregation ahead of the solidification front, and the normal processes of nucleation and growth of pores from gases in solution in the metal. A supply of gas diffusing from the mould or core into the casting surface will enhance the effect. Also, assuming the presence of bifilms completes a convincing model as we shall see.

We have seen in Section 5.3.1 how the early growth of the freezing front from the mould wall is planar because of the high temperature gradient. Thus the 'snow plough' build-up of solute occurs, starting from the original solute content C_0, and increasing over the first millimetre or so of travel of the front, until the solute reaches a level at which a pore may nucleate (Figure 5.39). Thus the gas content concentrated in this way is too low in the first 1 mm or so to create significant porosity, whereas across all the central parts of the casting pores are possible. A typical form of this porosity is shown in Figure 7.41. It should perhaps be better named surface-layer-free porosity because, if the gas content of the melt is sufficiently high, the porosity in such cases is rarely simply sub-surface, but is distributed everywhere *except* in the 1 mm surface layer as Figure 7.41 illustrates. (The 1 mm beneath the surface contrasts with entrained air bubbles which are only a couple of oxide film thicknesses away from the surface.)

This microsegregation process is common in many alloy systems where the solute has a low partition coefficient k, resulting in a high concentration of solute ahead of the advancing front. (Recall from Section 5.3.1 that the maximum concentration of solute is C_0/k.) For these systems, sub-surface porosity is the standard form of gas porosity. It may or may not be the result of the release of gas from a metal-mould reaction that can subsequently diffuse into the casting. Such a source will certainly increase the gas available, and may in fact be the sole source of gas. However, it must not be forgotten that sub-surface porosity is the normal appearance of gas porosity whether metal-mould reactions contribute or not.

For instance, Klemp (1989) describes sub-surface porosity in a low-alloy steel cast into an investment mould. Such moulds are fired at high temperature (commonly about 1000°C) and can be safely assumed to be dry and free from outgassing materials. In this case, the sub-surface porosity is definitely *not* the result of surface reaction; the gases were already in solution in the cast metal at the moment of pouring.

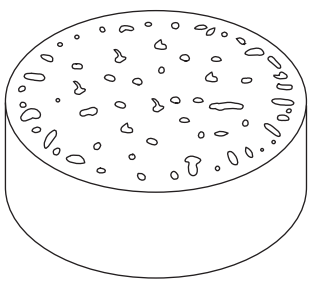

FIGURE 7.41

Sub-surface porosity revealed on a cut section of a bar casting.

In contrast, but not in conflict, Turkdogan (1986) reports subsurface porosity in cast irons cast in greensand, but had no reports of any such defects in irons cast into iron moulds. In this case, the porosity in the greensand moulds *is* the result of surface reaction; little gas was in solution in the cast metal.

We have discussed the action of bifilms to initiate porosity in liquid metals in Sections 7.1.5.3 and 7.1.5.4. The interesting feature of the mechanical model for the opening of bifilms in relation to the growth of pores is illustrated in Eqn (7.11). If the gas in solution in the liquid is assumed to be hydrogen, and assuming it to be approximately in equilibrium with the entrapped gas in the bifilm, the internal pressure will be proportional to $[H]^2$ (other diatomic gases will act similarly of course, although their approach to equilibrium may be slower because of their slower rates of diffusion to the bifilm). The rate of unfurling is therefore especially sensitive to the amount of gas in solution in the alloy.

In the case of iron and steel where an important contributor to the internal pressure will be expected to be carbon monoxide, CO, the internal pressure will approach that dictated by the product of the activities of carbon and oxygen in the melt, approximately [C].[O]. In addition, of course, nitrogen and hydrogen will also contribute to the total pressure.

In one of the most exciting pieces of research ever published in this field, Tiberg (1960) describes the growth of CO bubbles in liquid steel whilst actually observing the inside surface of the growing bubbles. He achieves this miracle by using high-speed cine-film to record the nucleation and growth of bubbles on the inside wall of a fused silica tube that contained the steel. (One day, in the 1970s, I was introduced in passing to a pleasant young Scandinavian. His name turned out to be Tiberg. I enquired whether it his work on observing bubble growth inside liquid steel because this was the most exciting research I had ever read. He affirmed it was him, agreeing that it was the most exciting research he had ever carried out. We shook hands in on such a warm and unexpected discovery of mutual interests. We had only time to bid each other farewell. We have never met since.)

The classical theories of pore growth assume that the geometry of the pore and its collection volume are spherical, and that growth is steady. This seems to be far from true in the experiment in which Tiberg tested these assumptions.

At high rates of growth, he found that the speed of expansion of the bubble surface dr/dt was indeed constant from the time the bubble was first observed at a size of 30 μm. However, after the addition of the deoxidisers, aluminium or silicon, the growth rate was slower and varied considerably from one bubble to another. In some bubbles growth suddenly halted and then continued at a slower rate. In fast-growing bubbles a small bright spot was observed.

The observation of the bright spot is interesting. It is most likely to have been an inclusion of alumina or silica (perhaps actually in the form of a bifilm) because this behaviour was only observed after the addition of the corresponding deoxidiser. The transparency or translucency (or even its hollowness if in the form of a partially opened bifilm) of the inclusion would have allowed the interior of the inclusion to be visible, giving an observer a view into the interior of the melt. This would appear as a bright enclosure, the classical 'black body cavity' of the physicist, radiating a full spectrum corresponding to the temperature of the interior of the steel, and therefore appearing as a bright spot. (The remainder of the bubble surface radiating its heat away to the outside world via the transparent silica vessel, and partially reflecting the cooler outside environment from its surface, would therefore appear cooler). We may speculate that the enhanced rate of transfer of gas into the bubble may have resulted from either (1) the short-circuiting of a surface layer that was hindering the transfer of gas into the bubble or (2) the attached inclusion having a large surface area and a high rate of diffusion for gas. Its surface area would then act as a collecting zone, funnelling the gas into the growing bubble through the small window of contact. A bifilm would have been expected to be especially effective in this way.

Tiberg's extraordinary observations link with work by the Japanese researcher, Kita (1979), who studied the insides of pores in steels by scanning electron microscope. He found that the inner surfaces of pores had curious markings, with radial 'petals', like flowers, suggesting that this may have been the site of gas leaking into the pores via some special route. The details of the markings were different for pores created by hydrogen, nitrogen and carbon monoxide. In addition, some markings were clearly oxide inclusions.

It seems therefore that the growth of pores in steels, and perhaps in most liquid metals, is complicated, and far removed from the ideal spherical model assumed in all the theoretical approaches to the problem. This subject would greatly benefit from a more thorough study with modern research equipment.

In the absence of more detailed information, we shall continue to assume that the growth of gas pores in liquid metals is controlled mainly by the rate of diffusion of gases through the liquid metal. There are many data in support of this,

especially in simple systems such as the Al-H system. In general metal systems, the rate of growth is probably dominated by the rate of arrival of the fastest diffusing gas. From Figure 1.4(c), it is clear that in liquid iron, hydrogen has a diffusion coefficient approximately 10 times higher than that of any other element in solution. Thus the average diffusion distance d is approximately $(Dt)^{1/2}$ so that in comparison with other diffusing species, the radius over which hydrogen can diffuse into the bubble is $(10/1)^{1/2} = 3$ times greater. Thus the spherical volume over which hydrogen can be collected by the bubble, in comparison with other diffusing species, is therefore $3^3 = 30$ times greater. Thus it is clear that hydrogen has a dominant influence over the *growth* of the bubble.

It should be remembered that hydrogen makes a comparatively small contribution to the *nucleation* of the bubble because it concentrates relatively little ahead of the advancing freezing front, in comparison with the combined effects of oxygen and carbon to form CO in liquid iron and steel. The situation is closely paralleled in liquid copper alloys, where oxygen controls the nucleation of pores because of the snow plough mechanism, whereas hydrogen contributes disproportionately to growth because of its greater rate of diffusion.

This clarification of the different roles of oxygen and hydrogen in copper and steel explains much early confusion in the literature concerning which of these two gases was responsible for subsurface pores. Zuithoff (1964, 1965) published the first evidence that confirmed the present hypothesis for steels. He succeeded in showing that aluminium deoxidation would control the appearance of pores. Clearly, if the oxygen was high, then pores could nucleate, but they would not necessarily grow unless sufficient hydrogen was present. Conversely, if hydrogen was high, pores might not form at all if no oxygen was present to facilitate nucleation. The hydrogen would therefore simply remain in solution in the casting. The same arguments apply, of course, to the roles of hydrogen and oxygen in copper-based alloys.

A useful simple test for steels that deserves wider use is proposed by Denisov and Manakin (1965): a sample test piece was developed 110 mm high, and 30 × 15 mm at the top, tapering down to 25 × 12 mm at the base. A metal pattern of the sample quickly creates the shaped cavity in the sand, into which the metal is poured. Immediately after casting, the sample is knocked out and quenched in water. It is then broken into three pieces in a special tup. The entire process takes 1–2 min. It was found that the tapered test piece gave an accurate prediction of the risk of subsurface porosity; if such problems were seen in the sample, they were seen in the castings and vice versa. The test therefore warned of danger, and avoiding action could be taken, such as the addition of extra deoxidiser to the ladle. This test for steel castings cast in greensand moulds should be applicable to other alloy and sand systems prone to this problem. Although the simplicity and apparent usefulness of this test is commendable, perhaps the 'wait and see' test by the author, described in Section 10.5.4 might be even simpler and quicker. Quick, reliable tests for use on the shop floor are very much needed. The reader is recommended to try these techniques.

In some alloy systems, the rate of growth of pores is not expected to be simply dependent on the rate of diffusion in the matrix. The rate can also be limited by a surface film.

Ultimately however, the maximum amount of gas porosity in a casting depends partly on simple mechanics, as illustrated by the well-known ***general gas law***. The use of this law assumes that the gas in the pore behaves as a perfect gas, which is an excellent approximation for our purposes. We shall also assume that all the gas precipitates (which is a less good approximation of course).

$$PV = nRT \tag{7.12}$$

where n is the amount of gas in gram-moles (in much use of this equation, n is somewhat misleadingly assumed to be unity), R is the gas constant 8.314 $JK^{-1}mol^{-1}$, and P is the applied pressure in $N/m^2 = Pa$.

The equation can be restated to give the volume V explicitly as:

$$V = nRT/P \tag{7.13}$$

It follows as a piece of rather obvious logic that the volume of the porosity is directly proportional to n, the amount of gas present in solution. This is graphically shown in Figure 7.42. The effect appears to have been well understood by Percy Riley, a well-known and irrepressible character in the early days of the development of the Al casting industry in the United Kingdom. He was an ex-Foseco employee working as a representative for Frankel Alloys Limited. He is said to have travelled around the country with a trunkload of potatoes in his car. All casting problems at that time were solved

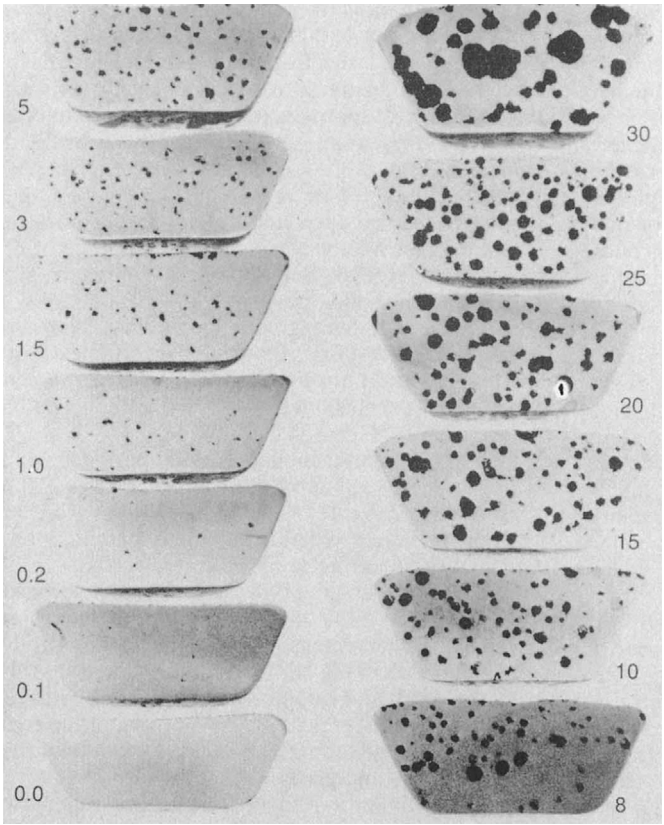

FIGURE 7.42

Gas porosity at various percentage levels in sectioned samples from the reduced pressure test.

Courtesy Stahl Speciality Co. (1990).

by adding potatoes to the melt. Clearly, the generous supply of hydrogen expanded bifilms giving copious hydrogen porosity, but shrinkage problems were solved. Percy's approach is not necessarily recommended at this time.

The relation of hydrogen porosity to hydrogen content is revealed in Figure 7.42. This test shows cut sections of a small sample of melt cast into a metal cup about the size of an egg cup and then solidified in vacuum. The test is sometimes known as the reduced pressure test (RPT) or the *Straube-Pfeiffer test*. The solidification under reduced pressure expands the pores, making the test more sensitive and easier to use than the old foundry trick of pouring a small pancake of liquid onto a metal plate, and watching closely for the evolution of tiny bubbles (you need good eyes for this).

The general gas equation also shows that the volume of a gas is inversely proportional to the pressure applied to it. For instance, in the RPT, to determine the amount of hydrogen in a liquid aluminium alloy, the percentage porosity is commonly expanded by a factor of 10 by freezing at 0.1 atm (76 mmHg) residual pressure rather than at normal atmospheric pressure (760 mmHg).

This sensitivity to pressure needs to be kept in mind when using the test. For instance, if the vacuum pump is overhauled and starts to apply not 76 mmHg (0.1 atm) but only 38 mmHg (0.05 atm) as a residual pressure, then the porosity in the test samples will be doubled, although, of course, the gas content of the liquid metal will be unchanged. Rooy and Fischer (1968) recommend that for the most sensitive tests the applied pressure should be reduced to

2–5 mmHg (approximately 0.003–0.006 atm). Clearly this will yield about a further 10-fold increase in porosity in the sample for any given gas content. However, care needs to be taken because these simple numerical factors are reduced by the additional loss of hydrogen from the surface of the test sample during the extra time taken to pump down to these especially low pressures, plus the losses of bubbles by bursting at the surface of the melt. In general, my experience is that a residual pressure of 76 mmHg (0.1 atm) is about right for all practical purposes, and most RPT kits operate at this value.

As has been mentioned before in the case of vacuum casting, the effect of pressure on pore growth is an excellent reason to melt and pour under vacuum, but to solidify under atmospheric pressure. It makes no sense to solidify under vacuum from the point of view of controlling porosity because pore expansion will act to negate the benefits of lower gas content (although solidification under vacuum may be important to prevent attack of the surface of the casting by nitrogen and oxygen if air is admitted to the vacuum chamber at an early stage). In terms of the general gas law, the pore volume V will be decreased by lower n, but increased correspondingly by low P. Whether the effects will exactly cancel will depend, among other things, on whether the melt has had time to equilibrate with the applied vacuum so as to reduce its gas content n. Taylor (1960) gives a further reason for not freezing under vacuum: For a nickel-based alloy containing 6% aluminium, the vapour pressure of aluminium at 1230°C is sufficient to form vapour bubbles at the working pressure of the vacuum chamber. He correctly concludes that the only remedy is to increase the pressure in the chamber immediately after casting. During the melting of TiAl intermetallic alloys at temperatures close to 1600°C, the evaporation of Al causes a loss of Al from the alloy, and a messy build-up of deposits in the vacuum chamber. Melting under an atmosphere of argon greatly reduces these problems. However, pouring under argon cannot be recommended if the pouring is turbulent, because of the danger of the entrainment of argon bubbles (another reason for the adoption of counter-gravity filling of moulds).

If the rate of diffusion of the gas in the casting is slow, the volume of the final pore will be less than that indicated by the general gas law and be controlled by the time available for gas to diffuse into the pore. In Figure 7.5, the benefits of increasing feeder size are seen to be enjoyed up to a critical size. After that, any further increase in the feeder merely delays solidification of the casting so that gas porosity increases.

Although these general laws for the volume of a gas-filled cavity are well known and nicely applied in various models of pore growth (see for instance the elegant work by Kubo and Pehlke (1985), Poirier (1987) and Atwood and Lee (2000)), some researches have shown that the detailed mechanism of the growth of pores can be very different in some cases.

A direct observation of pore growth has been carried out for air bubbles in ice. At a growth rate of 40 μms^{-1}, Carte (1960) found that the concentration of gas built up to form a concentrated layer approximately 0.1 mm thick. He deduced this from observing the impingement of freezing fronts. When the bubbles nucleated in this layer, their subsequent rapid growth so much depleted the solution in the vicinity of the front that growth stopped and clear ice followed. The concentration of gas built up again and the pattern was repeated, forming alternate layers of opaque and clear ice.

On examination of the front under the microscope, Carte saw that the bubbles seemed to originate behind the front; the first 0.1 mm deep layer of solid appeared to be in constant activity; threads of air approximately 10 μm in diameter spurted along what seemed to be water-filled channels, and were squeezed out of the ice. Sometimes bubbles arrived in quick succession, the first being pushed away and floating to the surface. Those bubbles that remained attached to the front would then expand, but finally be overtaken and frozen into the solid. It seems that pore growth might involve more turmoil than we first thought! Much of this activity arises, of course, from the expansion of the ice on freezing, and so forcing liquid back out of interdendritic channels. The opposite motion will occur in most metallic alloys as a result of the contraction on freezing. Also, it is to be expected that the movement in metals will be somewhat less frenetic. Nevertheless, no matter how the pore might grow in detail, we can reach some conclusions about the final limits to its growth.

Poirier (1987) uses the fact that the pore deep in a dendrite mesh will grow until it impinges on the surrounding dendrites. The radius of curvature of the pore is therefore defined by the remaining space between the dendrite arms. However, of course, although the smallest radius defining the internal pressure is now limited, the pore can continue to grow, forcing its way between the dendrite arms. Again, as has been mentioned before, an interdendritic morphology should not be taken as the definition of a shrinkage pore. Whether grown by gas or shrinkage, its morphology as spherical or interdendritic is merely an indication of the timing of its growth relative to the timing of the growth of the dendrites. Thus round pores have grown early. Interdendritic pores have grown late. Either can have been driven by gas or shrinkage, or both.

Fang and Granger (1989) found that hydrogen porosity in Al-7Si-0.3Mg alloy was reduced in size and volume percentage, and was more uniformly distributed, when the alloy was grain refined. In this case, the growth of bubbles will be limited by their impingement on grains. It may be that a certain amount of mass feeding may also occur, compressing the mass of grains and pores. In later work Poirier et al. (2001) confirm by a theoretical model that finer grains do reduce porosity to some degree. If grain refinement were made in the ladle, inadvertently cleaning the melt, the reduced bifilm content would probably have resulted in fewer but larger pores. This was not observed and so, with perhaps some surprise, can be concluded to be unimportant in this work.

Another limitation to growth occurs when the bubble can escape from the freezing front. This will normally happen when the front is relatively planar, and is typified by the example of the rimming steel ingot. In general, however, escape from a mesh of dendrites is likely to be rare.

A final limitation to growth is seen in those cases where the porosity reaches such levels that it cannot be contained by the casting. This occurs at around 20–30% porosity. During the freezing of the sample in the reduced pressure test, gas can be seen to escape by the bursting of bubbles at the surface of the sample. The effect is suggested in Figure 7.42. Also, Figure 7.43 shows that as gas in increased, measurements of porosity above 20% in such samples show a lower rate of increase of porosity than would be expected because of this loss from bubbles bursting at the surface, releasing their gas to the environment. (The theoretical curve in Figure 7.43 is based on 1% porosity in the solid being equal to 10 mL hydrogen in 1000 mL aluminium; this is equivalent to 10 mL hydrogen in 2.76 kg aluminium, or 0.362 mL hydrogen in 1 kg aluminium. Incidentally, Figure 7.43 also shows the enormous reduction in porosity as a result of increasing the difficulty of nucleation, because of the removal of nuclei by filtration. Clean metal makes better castings.)

It is worth drawing attention to the considerable volume of work over many years in which people have drilled into steel castings immersed in mercury or oil and have collected and analysed the gases in pores. In almost every case, the dominant gas was hydrogen. This led early workers to conclude that the bubbles were caused by hydrogen (see, for instance, the review of early work by Hultgren and Phragmen in 1939). This was despite calculations by Muller in 1879

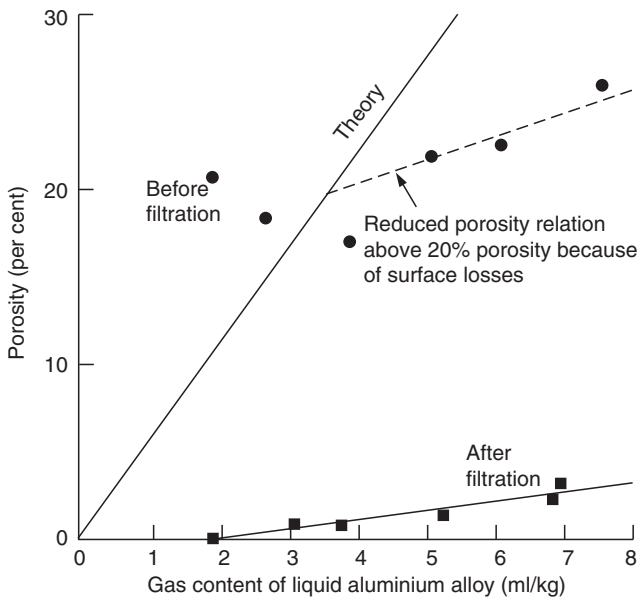

FIGURE 7.43

Porosity of RPT samples frozen at 0.005 atm as a function of gas content.

Data from Rooy and Fischer (1968).

that the CO pressure in pores in steel castings was up to 40 atm and the consequent correct deduction by Ledebur in 1882 that the hydrogen content of pores in steel castings at room temperature was the result of the continued accumulation of hydrogen after solidification was complete.

We can see that the high final hydrogen content of pores at room temperature is a natural consequence of the high rate of diffusion of hydrogen in both the liquid and solid states. Thus hydrogen is the dominant gas contributing to the growth of pores, and continuing to contribute additional gas during the cooling to room temperature.

Even after the casting reaches room temperature the growth of gas pores may still not be complete! Talbot and Granger (1962) showed that hydrogen in cast aluminium could continue to diffuse into pores in the solid state during a heat treatment at 550°C. Porosity was found to increase during this treatment, with pores becoming larger and fewer. With very long annealing in vacuum, the hydrogen could be removed from the sample and the porosity could be observed to fall or even disappear.

We have so far in this section discussed mainly porosity which can be uniformly distributed throughout the section of a casting, even though subsurface porosity, or perhaps more accurately, if more clumsily termed, 'subsurface porosity-free zone', is a product of the accumulation of segregated gas ahead of an advancing planar solidification front. It is a condition partway between the completely uniform distribution of gas pores as discussed earlier, and the highly directional form that is to be discussed later.

In metals that solidify on a planar front the gas pores may grow, keeping pace with the growth of the front, causing long, tunnel-like defects that are sometimes called wormholes (Figure 7.44). They are often observed in ice cubes because tap water generally freezes on a fairly planar front. The pores may be up to 1 mm or so in diameter and of various lengths of up to 100 mm or more. An example of pores nearly 20 mm long is seen in Figure 7.45. This radiograph of an aluminium-bronze plate cast in a sand mould using non-degassed metal contrasts with a similar radiograph of a plate (not shown) cast from properly degassed melt, in which no defects at all could be seen.

Beech (1974) was perhaps the first to point out that the environment of a long bubble is not necessarily homogeneous. In other words, what may be happening at one end of the bubble may be quite different from what is happening at the other. This is almost certainly the case with the kind of subsurface porosity that continues to grow into an array of wormholes. The metal-mould reaction will continue to feed the base of the bubble, which of course remains within the diffusion distance of the surface. If the gas content of the melt is high the front of the bubble may also be gaining gas from the melt. However, if the melt has a low gas content, the front part of the bubble may lose gas. The bubble effectively acts as a diffusion short-circuit for the transfer of gas from the surface reaction to the centre of the casting. The effect is shown diagrammatically in Figure 7.44.

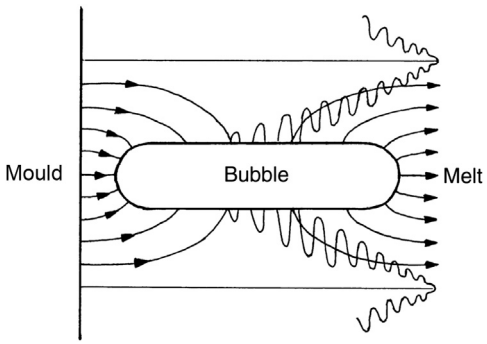

FIGURE 7.44

Subsurface pore growing in competition with dendrites, into a melt of low gas content. The pore gains gas by diffusion form the surface reaction, and loses it from its growing front.

After Beech (1974).

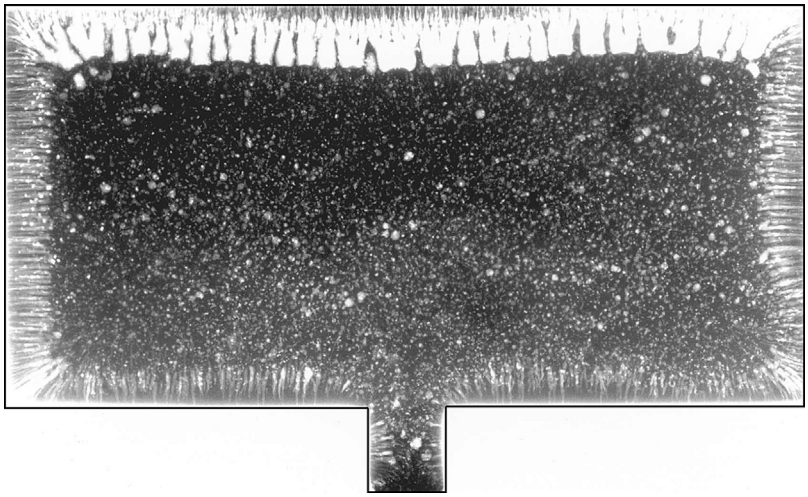

FIGURE 7.45

Radiograph of a Cu-10Al casting 200 × 100 × 10 mm with a high hydrogen content poured at 1285°C with gate velocity 0.85 ms^{-1} into a sand mould (Helvaee and Campbell, 1997).

Depending on the relative rates of gain and loss, the pore may grow or even give off bubbles from the growing front. Alternatively, it may stop growing and thus be overtaken by the dendrites and frozen into the thickening solid shell. The swellings and narrowings of these long bubbles probably reflect the variation in growth conditions, such as sudden variations in gap between the casting and the mould, or variations from time to time of convection currents within the casting.

The long CO bubbles in rimming steel ingots, cast into cast iron moulds, were a clear case where the growing bubble was fed with gas from the growing front, and not from the mould surface.

Conversely, in aluminium bronze castings made in greensand moulds Matsubara et al. (1972) provides an elegant and clear demonstration of the feeding of the pore with gas from the mould, together with the combined effect of residual gas in the metal. Radiographs show wormhole porosity approximately 100 mm long. The amount of porosity was shown to increase as the gas content of the metal was increased, and as the water content of the moulds was increased from 0 to 8%. Halvaee and Campbell (1997) illustrates a similar structure for aluminium bronze cast into a sand mould bonded with a phenolic urethane resin (Figure 7.45). A proper melting procedure to give a low gas content in the melt before casting eliminated the porosity completely.

In this section on gas porosity, we have so far discussed gases in general. In many cases, it is not easy to make a clear separation in this account of the various gases because all cooperate in some alloy systems and many systems are analogous. However, a rough division particular to each gas will now be attempted, the reader being requested to bear in mind the necessarily ragged edges between sections.

Hydrogen porosity

It is important to remember that both water and hydrocarbons (that are available in abundance from the sand binders employed in most sand castings) can decompose at the metal surface, both releasing hydrogen. The surface of the melt and the casting will therefore have no shortage of hydrogen; in fact, from Section 4.4, it is seen that in general the mould atmosphere often contains up to 50% hydrogen, and may be practically 100% hydrogen in many cases.

What happens to this hydrogen?

Although much is clearly lost by convection to the general atmosphere in the mould, some will diffuse into the metal if not prevented by some kind of barrier (see later). If the hydrogen does manage to penetrate the surface of the casting, how far will it diffuse?

We can quickly estimate an average diffusion distance d from the useful approximate relation Eqn (1.5), $d = (Dt)^{1/2}$. Some researchers increase the right hand side of this relation by a factor of two in a token attempt to achieve a little more accuracy. We shall neglect such niceties, and treat this equation merely as an order of magnitude estimate. Taking the diffusion rate D of hydrogen as approximately 10^{-7} m^2s^{-1} for all three liquid metals, aluminium, copper and iron (see Figures 1.4 (a), (b) and (c)) then for a time of 10 s d works out to be approximately 1 mm. For a time of 10 min, d grows to approximately 10 mm.

Clearly, hydrogen from a surface reaction can diffuse sufficiently far in the time available during the solidification of an average casting to contribute to the formation and growth of subsurface porosity in most of our engineering metals.

The distance that the front has to travel before the solute peak reaches its maximum is actually identical to the figures we have just derived, as explained in Section 5.3.1. Thus conditions are exactly optimum for the creation of the maximum gas pressure in the melt at a point a millimetre or so under the surface of the casting. The high peak will favour conditions for the nucleation of pores whilst the closeness to the surface will favour the transport of additional gas, if present, from a surface reaction. Naturally, if there is enough gas already present in the melt, then contributions from any surface reaction will only add to the already existing porosity.

In an investigation of a wide variety of different binders for the moulding sand, Fischer (1988) finds that subsurface porosity in copper based castings is highly sensitive to the type of binder, although degassing and deoxidising of the metal did help to reduce the problem. These observations are all in line with our expectations of contributing agencies.

In aluminium alloys where hydrogen gas in solution in the melt segregates strongly on freezing, the partition coefficient is approximately 0.05, corresponding to a concentrating effect of 20 times. Figure 7.46 shows subsurface porosity in an Al-7Si-0.4Mg alloy solidified against a sand core bonded with a phenolic urethane resin. The general gas content of the casting is low, so that pores are only seen close to the surface, within reach by diffusion of the hydrogen from the breakdown of the resin binder. Some of the pores in Figure 7.46(a) are clearly crack-like, and seem likely therefore to have formed on bifilms.

Close-up views of another casting showing sub-surface porosity in the same alloy and same bonded sand (Figure 7.47(a)) confirms that the pores are of widely different form, some being perfectly round (Figure 7.47(b)), some dendritic (Figure 7.47(c)) and some of intermediate form (Figure 7.47(d)). It seems reasonable to assume that all the pores experienced the same environment, consisting of a uniform field of hydrogen diffusing into the melt from the degeneration of the core binder. Their growth conditions would therefore have been expected to be identical. Their very different forms cannot therefore be the result of growth effects (i.e. some are not shrinkage and others gas pores). The differences therefore must be a result of differences in ease of nucleation. The simple explanation is that the round pores nucleated early because of easy nucleation, and thus grew freely in the liquid. The dendrite-lined pores are assumed to have nucleated late, as a result of a greater difficulty to nucleate, so that they expanded when the matrix dendrites were already well advanced. The differences in ease of nucleation can be easily understood in terms of the randomly different conditions in which the nuclei, bifilms, are created. Some bifilms will come apart easily, whereas others will be ravelled tightly, or may be partially bonded as a result of being older or being contaminated with traces of liquid salts from the surface of the melt.

The case of some subsurface pores initiating their growth very late, when freezing must have been 80% or more complete, raises an interesting extrapolation. If the bifilms had been even more difficult to open, or if not even present at all, then *no* pores would have nucleated. This situation may explain the well-known industrial experience, in which subsurface porosity comes and goes, is present one day, but not the next, and is more typical of some foundries than others. It is a metal quality problem.

Note that both round and dendritic pores can be both gas pores. They could also both be shrinkage pores, or both generated by combined gas + shrinkage contributions. Whether grown by gas or shrinkage, or both, the shape difference merely happens because of the timing of the pore growth in relation to the dendrite growth. Although it common for gas pores to form early and so be rounded, and shrinkage pores to form late and so take on an interdendritic morphology, it is not necessary. It is very important not to fall into the standard trap of assuming that round pores result from gas and dendritic forms result from shrinkage.

The work by Anson and Gruzleski (1999) describes particularly careful work in an attempt to distinguish between gas and shrinkage pores. Their study concentrated on the appearance and spacing or pores. They pointed out that, on a

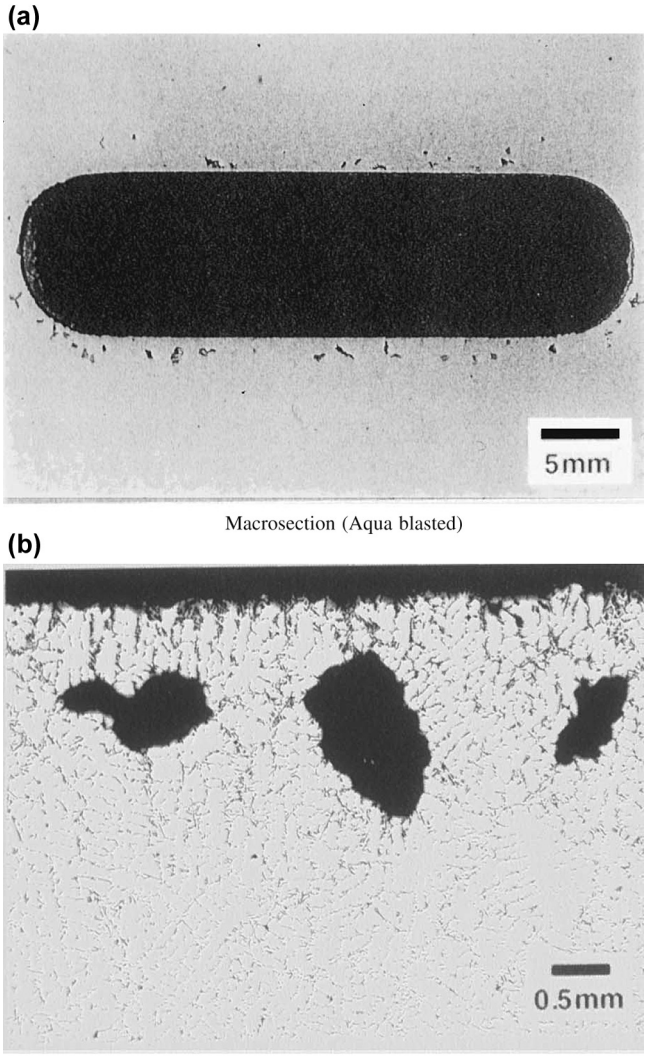

FIGURE 7.46

(a) Polished section, lightly blasted with fine grit, showing subsurface porosity around a sand core in an Al-7Si-0.4Mg alloy casting of low overall gas content; and (b) an enlarged view of some pores on a polished section.

polished section, groups of apparently separate, small interdendritic pores were almost certainly a single pore of irregular shape (Figure 7.48). Despite apparently clear differences in shape and spacing, it is finally evident in their case that all pores were gas pores because they all grow at the same rate as hydrogen is increased. In this case the pores that were assumed to be shrinkage pores were almost certainly partially opened and/or late opened bifilms. Their irregular cuspoid outlines probably derived partly from the irregular, crumpled form of the bifilms, together with their late opening in the

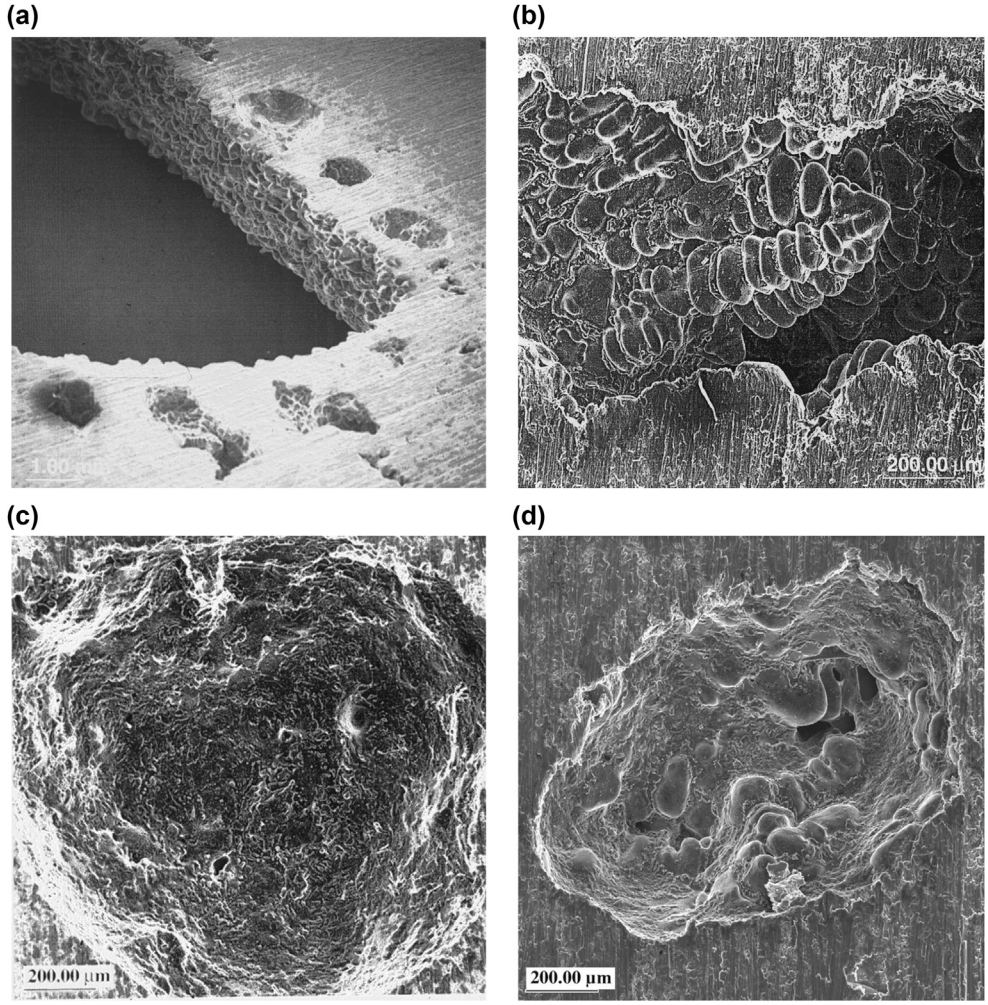

FIGURE 7.47

Thin slice of an Al-7Si-0.4Mg alloy casting taken from around a phenolic urethane bonded sand core. (a) A general view, showing the sand-cast surface made by the core and several subsurface pores; and close-ups of (b) a dendritic pore; (c) a spherical pore; and (d) a mixed pore.

interdendritic spaces. Such mis-identification of pore shapes is easily understood, and is common. We need to be on our guard against such mistakes.

Carbon, oxygen and nitrogen

For the case of the casting of aluminium alloys, we have only to concern ourselves about hydrogen, the only known gas in solution.

For the case of copper-based alloys, several additional gases complicate this simple picture. The rate of diffusion of oxygen in the liquid is not known, but is probably not less than 10^{-8} m^2s^{-1}. In the case of liquid iron-based alloys,

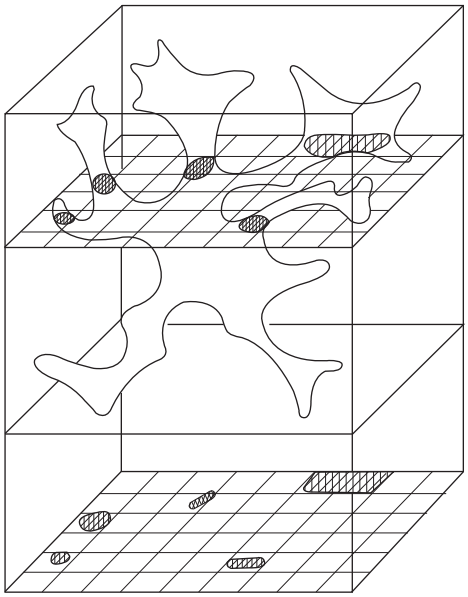

FIGURE 7.48

Complex interdendritic pore, appearing as a group of pores on a polished section.

After Anson and Gruzleski (1999).

oxygen and nitrogen, diffuse at similar rates (Figure 1.4). Thus for all of these liquids the average diffusion distance d is 1–2.5 mm for the time span of 1–10 min. It seems therefore that all these gases can enter and travel sufficiently far into castings of all of these alloy systems to contribute to the formation of porosity.

In copper-based alloys, the effect is widely seen and attributed to the so-called 'steam reaction' (Eqn 6.3). It seems certain, however, that SO_2 and CO will also contribute to the total pressure available for nucleation in copper alloys that contain the impurities sulphur and carbon. Carbon is an important impurity in Cu-Ni alloys such as the monels. Zinc vapour is also an important contributing gas in the many varieties of brasses and gunmetals.

From the point of view of nucleation, the action of oxygen is likely to be central. This is because it is probably the most strongly segregating of all these solutes (with the possible exception of sulphur). Thus deoxidation practice for copper-based alloys is critical.

When gunmetal has been deoxidised with phosphorus, Townsend (1984) reports that an optimum addition is required, as illustrated in Figure 7.49. Too little phosphorus allows too much oxygen to remain in solution in the melt to be concentrated to a level at which precipitation of water vapour will occur as freezing progresses. Too much phosphorus will reduce the internal oxygen to negligible levels, suppressing this source of porosity. However, the melt will then have enhanced reactivity with its environment, the excess phosphorus picking up oxygen and hydrogen from a reaction at the metal surface with water vapour from the mould. The porosity in the cast metal is the result of the sum of these internal and external reactions, resulting in a minimum at approximately 0.015% phosphorus for the case of this particular sample of alloy.

A similar reaction occurs in grey iron in the presence of 0.005–0.02% aluminium or 0.04% titanium. The reaction is characterised by subsurface pores that have a shiny internal surface covered with a continuous graphite film. (The

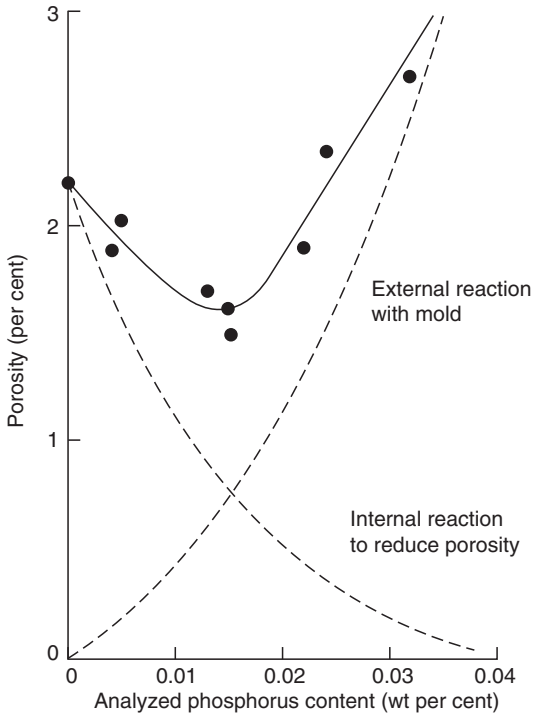

FIGURE 7.49

Effect of phosphorus on the porosity in 75 mm thick plates of leaded gunmetal LG2 cast at 1100°C.

Data from Townsend (1984).

graphite film is present simply because the free surface provided by the pore allows the graphite to accommodate its volume expansion on precipitation most easily. Similarly, these pores are often seen to be filled with a frozen droplet of iron, again simply because the pore is an available volume into which liquid can be exuded during the period when the graphite expansion is occurring. Such droplets would be expected to be more common in casting made in rigid moulds, where the expansion could not be easily accommodated by the expansion of the mould.)

Carter et al. (1979) describes the analogous problem caused by the presence of magnesium in **ductile iron**. Clearly, this double effect of the addition of a strong deoxidiser, resulting in an optimum concentration of the addition, is a general phenomenon.

In much of the work on *subsurface* pores in **irons and steels**, the phenomenon is called *surface* pinhole porosity. This is almost certainly the result of the loss of the surface of the casting by a combination of oxidation and/or severe grit blasting, allowing the pores to be broken into, or simply uncovered. The *surface pinholes* almost certainly originated as *subsurface pinholes*.

In the case of low-carbon equivalent grey irons, it is found that small surface pinholes occur that have an internal surface lined with iron oxide, and whose surrounding metal is decarburised, as witnessed by a reduction in the carbide content of the metal. Although Dawson et al. (1965) and others make out a case for these defects to be the result of a

reaction with slag, it seems more reasonable to suppose that once again the pores were originally subsurface, but the high oxygen content of the metal promoted early nucleation, with the result that the pores were extremely close to the surface of the casting. The thin skin of metal quickly oxidised, opening the pore to the air at an early stage, and allowing plenty of time for oxidation and decarburisation whilst the casting was still at a high temperature. Tests to check whether the pores have been connected to the atmosphere do not appear to have ever been carried out.

Dawson reports that an addition of 0.02% aluminium usually eliminates the problem. This relatively high addition of aluminium is probably to be expected because the oxygen in solution in these low-carbon equivalent irons will be higher than that found in normal grey irons. However, if even higher levels of aluminium were added, the problem would be expected to return because of the increased rate of reaction with moisture in the mould, following the example in Figure 7.49.

Oxygen and carbon are important when CO is the major contributing gas, although, of course, in cast irons, where carbon is present in excess, the CO pressure is effectively controlled solely by the amount of oxygen present. This deduction is nicely confirmed for malleable cast irons by the Italian workers Molaroni and Pozzesi (1963), who found a strong correlation between their proposed '*oxidation index', I,* defined as:

$$I = \mathrm{C} + 4\mathrm{Mn} + 1.5\mathrm{Si} - 0.42\mathrm{FeO} - 5.3$$

where the symbols for the elements carbon C, manganese Mn, etc., represent the weight percentage of the alloying elements in the iron. Compositions of irons that gave a positive index were largely free from pores, whereas those with an increasingly negative index were, on average, more highly porous.

In steels, there are several gases that can be important in different circumstances. The most important are CO (Eqn 6.5), N_2 (Eqn 6.7) and H_2 (Eqn 1.3). Because, at the melting point of iron, hydrogen has a solubility in the liquid of approximately 245 mlkg^{-1} and in the solid of 69 mlkg^{-1} (extrapolating slightly from Brandes and Brook 1992), its partition coefficient is $69/245 = 0.28$, with the result that it is concentrated ahead of the solidification front by a factor of $1.0/0.28 = 3.55$. It therefore makes a modest contribution to the gas pressure for nucleation of pores in iron alloys.

Nitrogen seems to have a similar importance in nucleation. Its solubility at the melting point of iron is 0.0129 wt% in the solid and 0.044 wt% in the liquid (Brandes, 1983) giving a partition coefficient 0.29, and a concentration effect for nitrogen ahead of the freezing front of approximately 3.4 times. This situation has already been discussed in Section 4.6.3 on metal-mould reactions, and is discussed further in the following section.

Because $k = 0.05$ for oxygen in iron, and $k = 0.2$ for carbon in iron, the concentration factors are 20 and 5, respectively, so that when combined, the equilibrium CO pressure at the solidification front is $20 \times 5 = 100$ times higher than in the bulk melt (The distribution coefficients refer to bcc delta-iron; those for fcc gamma-iron would be nearer to unity, implying much less concentration ahead of the solidification front for solidification to austenite). Because of the multiplying factor 100, oxygen in solution in the iron is the major contributing gas in the nucleation of CO gas pores during the solidification of many irons and steels.

Nitrogen porosity

There has been a massive effort to understand the metal-mould reactions in which nitrogen is released. This gives problems in both iron and steel castings as subsurface pores. A review for steel castings is given by Middleton (1970).

Subsurface porosity is common for steels cast into moulds bonded with urea formaldehyde resin (Middleton, 1970), or bonded with other amines that release ammonia, NH_3, on heating. These include hexamine in Croning shell moulds (Middleton and Canwood, 1967). The ammonia breaks down at casting temperatures to release both nitrogen and hydrogen.

The nitrogen problem in ferrous castings has resulted in the production of a whole new class of sand binders known as 'low nitrogen' binders. However, later work (Graham et al., 1987) investigating the relation between total nitrogen content of the binder and the subsurface porosity and fissures in iron castings found no direct correlation. However, Graham did find a good correlation with the ammonia content of the binder. Ammonia is released during the pyrolysis of

important components of many binders, such as urea, amines (including hexamine used in shell moulds) and ammonium salts. The ammonia in turn will decompose at high temperature as follows

$$NH_3 \Leftrightarrow N + 3H$$

thus nascent nitrogen and nascent hydrogen are released (the word *nascent* meaning *in the act of being born,* implying high reactivity of the atomic forms of these elements rather than their molecular forms). Both will contribute to the formation of pores in the metal. Both nitrogen and hydrogen will have a similar influence in the nucleation of a pore, concentrating reasonably strongly ahead of the freezing front. For the subsequent growth, however, hydrogen will be the major influence because of its much faster rate of diffusion. That both gases are released simultaneously by ammonia explains the extreme effectiveness of ammonia in creating porosity. Nitrogen alone would not have been particularly effective. Even if it may have been successful in nucleating pores, without the additional help from hydrogen any subsequent growth would have been limited. Hydrogen is supplied by gas in solution in the liquid metal, and any fresh supply through the surface from a surface reaction.

It seems that ammonia can build up in greensand systems as the clays and carbons absorb the decomposition products of cores. Lee (1987) confirms that an ammoniacal nitrogen test on the moulding sand was found to be a useful indicator of the pore-forming potential of the sand, even though the test was not a measure of total nitrogen.

The action of gases working in combination is illustrated by the work of Naro (1974) in his work on phenolic urethane-isocyanate binders. He showed that, from a range of irons, ductile iron (high carbon and low oxygen) was least susceptible and low-carbon equivalent irons (high oxygen) were most susceptible to porosity from the binder. Once again, it seems logical that the oxygen remaining in solution in the iron plays a key role encouraging nucleation, contributes modestly to both nucleation and growth, whereas hydrogen overwhelmingly dominates growth.

Barriers to diffusion

In some unusual conditions, hydrogen appears to be prevented, or at least inhibited, from diffusing into some metals.

For magnesium alloys, potassium borofluoride (KBF_4) has been known for many years to be an effective suppressant of metal/mould reactions for Mg alloys. In fact, if not added to the sand moulds of some Mg castings, both mould and casting will be consumed by fire—the ultimate metal/mould reaction! However, Al-5Mg and Al-10Mg casting alloys, and even Al-7Si-0.4Mg alloy, also benefit from KBF_4 or K_2TiF_6 additions to suppress reactions with the mould. We might speculate that liquid oxyfluorides, produced by the dissolution of the alumina film in the flux, assist to seal the surface of the liquid metal.

Naro (1974) confirms the widely reported fact that the addition of 0.25% iron oxide to phenolic urethane-isocyanate–bonded sands reduces subsurface pores in a wide range of cast irons. This is a curious fact and difficult to explain at this time. One suggestion is that the oxide creates a surface flux, possibly an iron silicate. This glassy liquid phase is likely to reduce the rate at which gases can diffuse into the casting.

The rate of uptake of nitrogen in stainless steel is inhibited by the presence of silicon in the steel that, at certain oxidation potentials, forms SiO_2 on the surface in preference to Cr_2O_3 (Kirner et al., 1988).

Even when the surface film consists only of a layer or so of adsorbed surface-active atoms, the presence of the layer reduces the rate at which gases can transfer across the surface. This happens, for instance, in the case of carbon steels: sulphur and other surface-active impurities hinder the rate at which nitrogen can be transferred. An excellent review of this phenomenon is given by Hua and Parlee (1982).

However, the precise mechanisms and effectiveness of many of these inhibition reactions are not clear at this time.

7.3 POROSITY DIAGNOSIS

7.3.1 GAS POROSITY

To be able to take effective action to cure a porosity problem, clearly it has to be correctly identified. Table 7.3 is designed to assist with diagnosis of the wide variety of types of gas pores. Some care is needed where gas and shrinkage effects overlap, but these situations can usually be identified with some certainty.

Table 7.3 Porosity Diagnosis Summary

	Intrinsic (Metallurgical Defects)		Extrinsic (Entrained Casting Defects)	
	Gas from Solution in Melt	**Gas from Mould Reaction**	**Entrained Air Bubbles**	**Core Blows**
Spatial distribution	1−2 mm subsurface clear from pores. Bulk of casting has a uniform distribution of pores	1−2 mm under surface	Clustered above ingates	Uniform depth under cope
Size (mm)	0.05−0.5	0.05−0.5	1−5	5−500
Features	Associated with bifilms in suspension in melt	Associated with bifilms in suspension in melt	Associated with oxides (solid oxides include bifilms + bubble trails) (liquid oxides include slags)	Connected by thick bubble trail to originating core
Examples	Figures 7.41, 7.43	Figure 7.41		Figures 7.35, 7.36, 10.10 and 10.11

7.3.2 SHRINKAGE POROSITY

The various forms of shrinkage cavity are summarised in Figure 7.50. Without exception, all the morphologies are dictated by (1) the *geometry* of the casting and (2) *gravity*. These two key features allow shrinkage-dominated porosity to be clearly differentiated from other sources of porosity. The various forms that shrinkage porosity can take include the following.

a. Centreline porosity is formed in a skin-freezing alloy that has suffered an inadequate supply of liquid from the feeder. The geometry dictates that the pore is closely parallel to the thermal axis of the casting.
b. Sponge porosity. Formed in a long freezing range alloy, with adequate temperature gradient, but inadequate feed liquid from the feeder (e.g. Figure 7.8).
c. Layer porosity; the result of inadequate interdendritic feeding in a poor temperature gradient. The nucleation of internal porosity indicates a poor cleanness of the liquid metal. Geometry dictates that the pores are closely at right angles to the thermal axis of the casting.
d. Surface-initiated porosity generated in a long freezing range alloy in conditions of poor temperature gradient, but adequate cleanness of the melt.
e. Surface sink (external shrinkage porosity) formed in conditions of no liquid available from the feeder, but good cleanness of melt, in a relatively skin-freezing alloy, resulting in good solid feeding. Gravity dictates that the sink is usually sited on the cope surface of the casting.

Notice that the shrinkage pores are always influenced by the geometry of the casting, whether sometimes parallel to the axis of the casting as in centreline shrinkage, or (perhaps seemingly perversely) sometimes at right angles to the axis of the casting, as in layer porosity. Fortunately, the other major influence to the distribution of shrinkage porosity, gravity, is kinder to our intuition, acting only downwards.

If the porosity is clearly *not* strongly influenced by the shape of the casting and by gravity (for instance, porosity in random locations or well away from the thermal axis of the casting as in Figure 7.31(d)), we can conclude it is *not* shrinkage porosity. Very often, in fact most often, it will be porosity associated with masses of bifilms and bubble damage. This is common variety of porosity that only 'appears' to be shrinkage porosity.

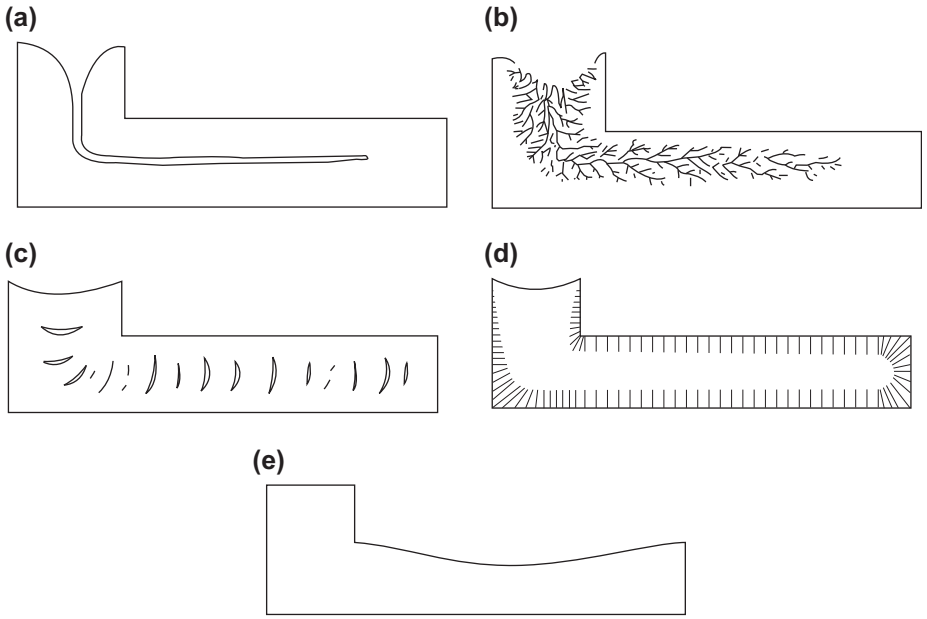

FIGURE 7.50

Summary of the various types of shrinkage porosity.

The casting engineer needs to keep at the forefront of the mind that in *most* cases the pores are *not* shrinkage pores. Nearly all porosity I see identified on micrographs and labelled 'shrinkage' are actually oxides. It is useful to repeat here the valuable mantra learned earlier, learning to say not 'it is shrinkage' but 'it *appears* to be shrinkage', bearing in mind that the pores are in nearly every case clusters of oxides together with entrained air, or bubble trails, introduced during the turbulence of the pour. These unwelcome features disappear if the filling system design is good.

Readers might find helpful the short summary of the different types of porosity and how they might be identified presented in Table 7.3.